Francis Bernardeau

La structuration des galaxies, théorie

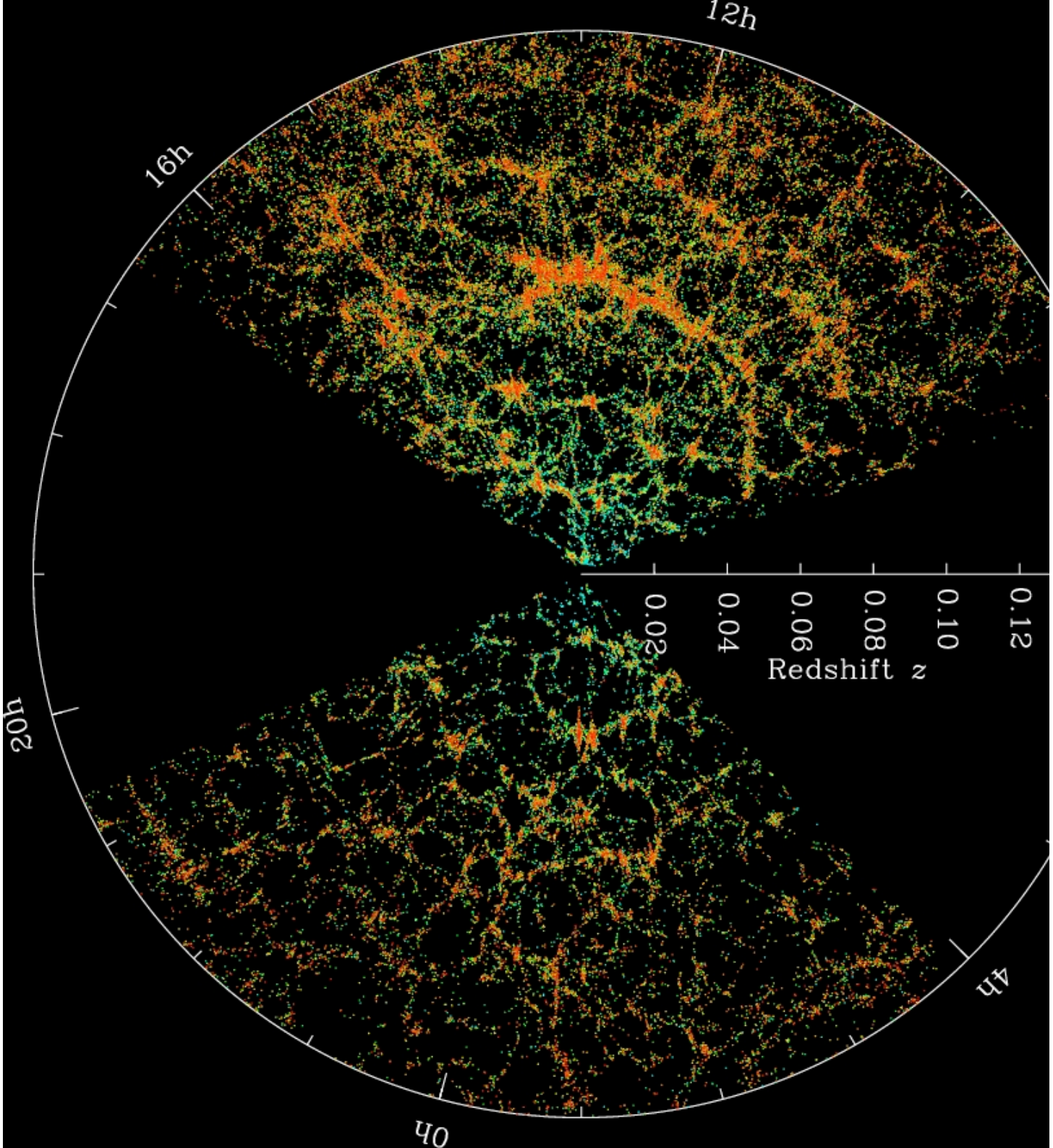

Introduction

Table des matières

Bibliographie

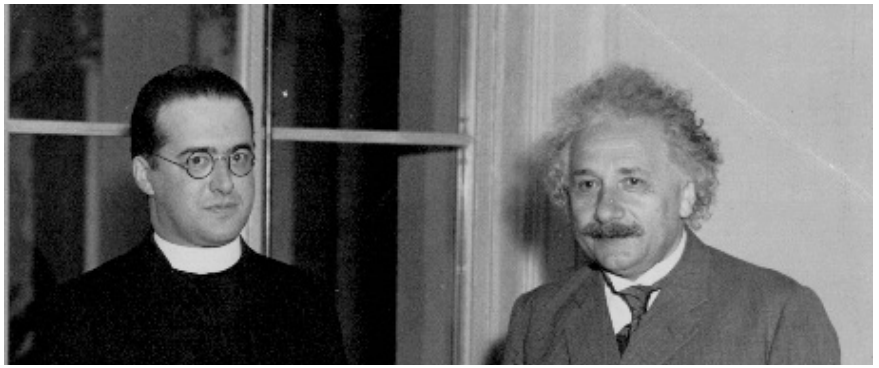

- P.J.E. Peebles, *The Large Scale Structure of the Universe, 1980*

- S. Dodelson, *Modern Cosmology, 2003*
- J.-Ph. Uzan et P. Peter, *Cosmologie Primordiale, 2006*
- F. Bernardeau, *Cosmologie, des fondements théoriques aux observations, 2007*

- *Articles de revue/cours*
  - *F. Bernardeau, S. Colombi, E. Gaztanaga, and R. Scoccimarro, « Large-scale structure of the Universe and cosmological perturbation theory », Phys. Rep 2002*
  - *F. Bernardeau, « The evolution of the large-scale structure of the universe: beyond the linear regime », Les Houches 2013*
  - *??, Les Houches 2013*

Observing the LSS of the universe

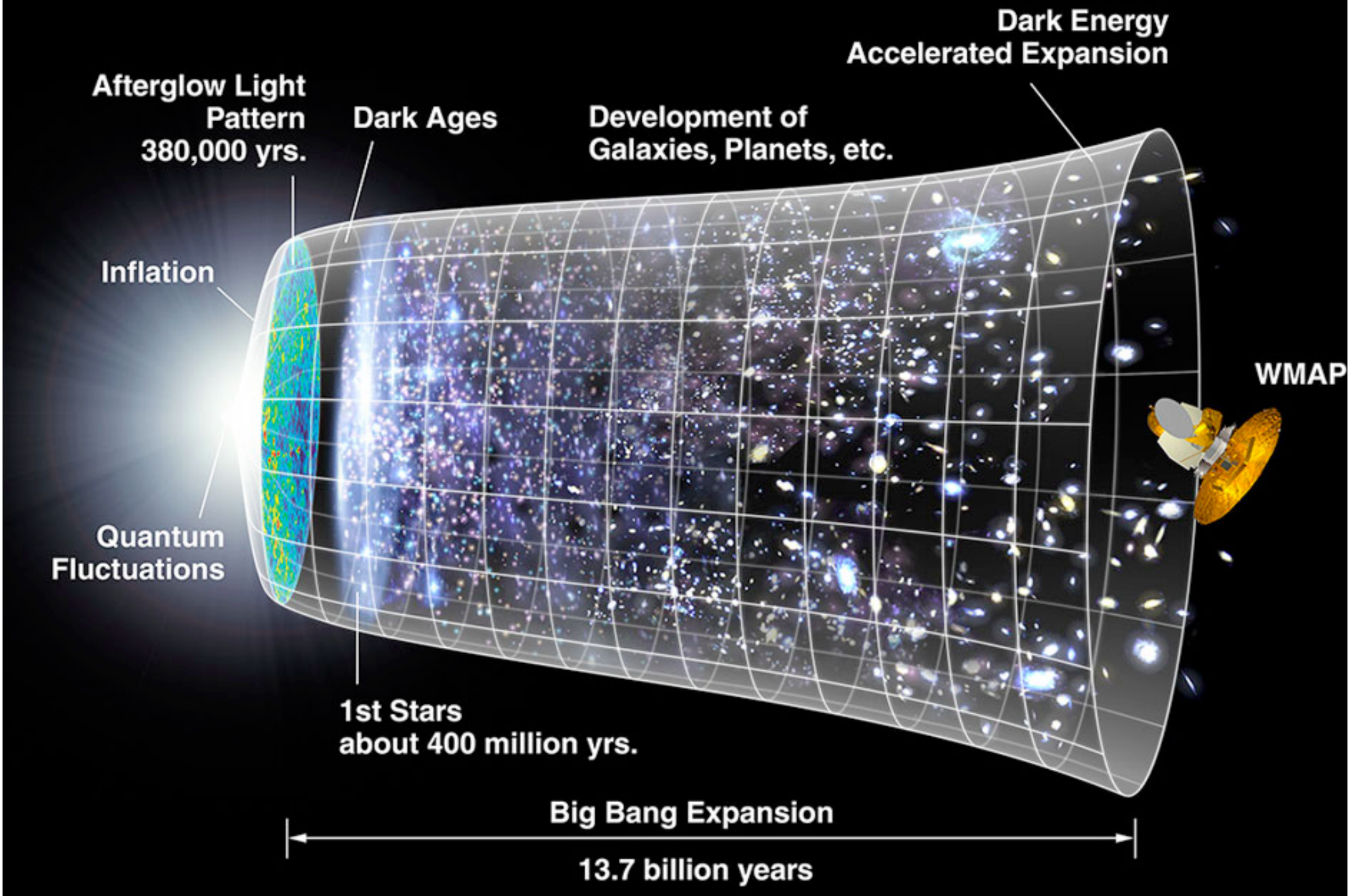

The CMB sky, temperature and polarization

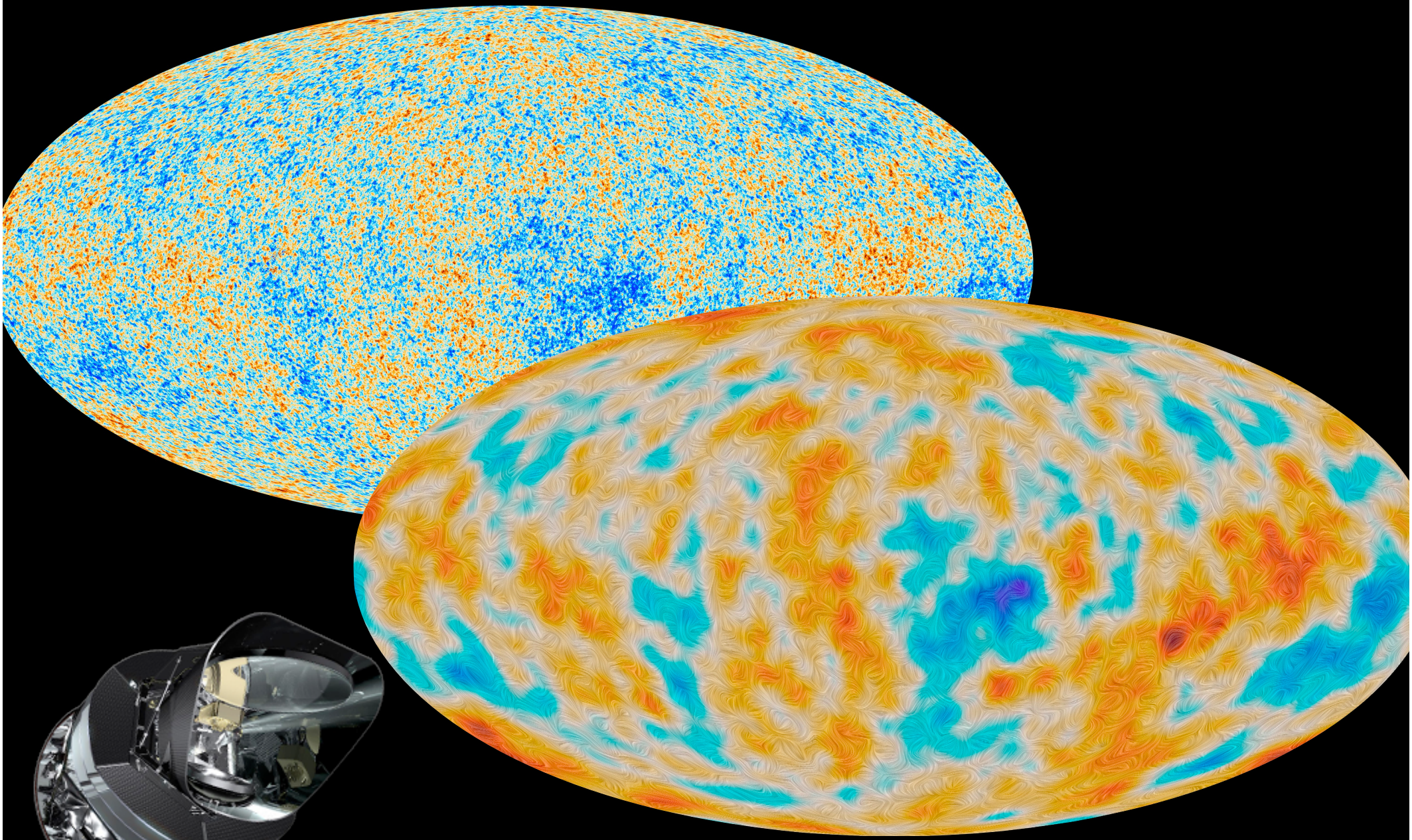

A linear sky at 10^{-5} precision

The linear sky

$$ {}_s a_{\ell m} = \int \mathrm{d}k \; {}_s\mathcal{T}_{\ell m}(k) \; \phi_{\mathrm{adiab}}(k) + \ldots $$

harmonic modes (for temperature and polarization)

transfer functions: it contains the microphysics - Boltzmann & GR

metric fluctuations as it emerges from inflation

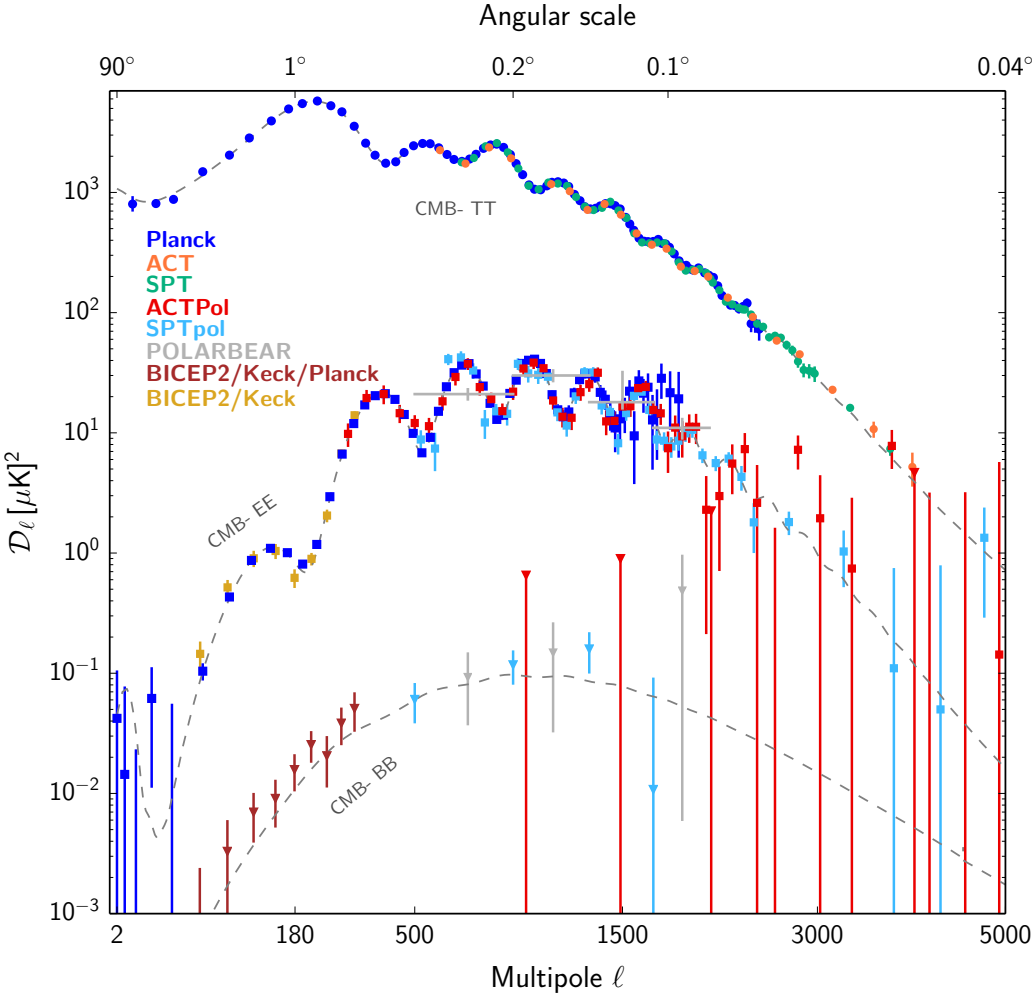

$$ \left\langle {}_s a_{\ell m} \, {}_s a_{\ell' m'} \right\rangle = \delta_{\ell \ell'} \delta_{m m'} \, {}_s C_\ell $$

CMB angular power spectra determinations as of mid-2015 (from Planck Collaboration et al. 2015 and Calabrese 2016). This corresponds to the determination (with S/N > 1) of 1 114 000 modes measured with *TT*, 96 000 with *EE* (60 000 with *TE*, not shown), and tens of modes in *BB* (and weak constraints on *T B* and *E B*) .

The development of cosmological instabilities across time and scale

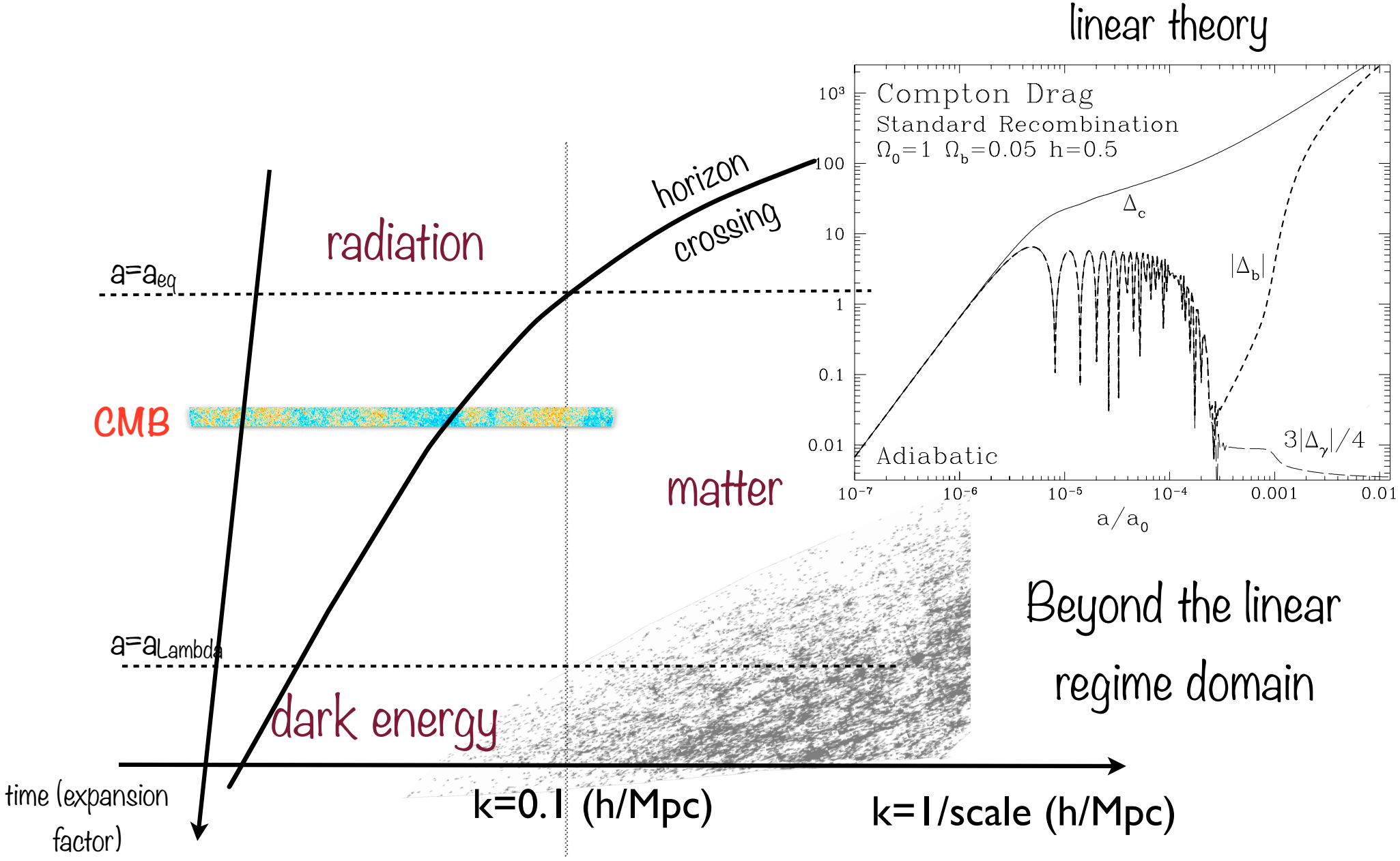

Entering the nonlinear regime

Modes are now full functionals of the initial modes. At best they can expended with respect to initial metric fluctuations

$$\delta_\rho(\vec{k}) = \int \mathrm{d}^3\vec{q}\,\mathcal{T}(\vec{k},\vec{q})\,\phi_{\rm adiab}(\vec{q}) + \int \mathrm{d}^3\vec{q}_1\mathrm{d}^3\vec{q}_2\,\mathcal{T}(\vec{k},\vec{q}_1,\vec{q}_2)\,\phi_{\rm adiab}(\vec{q}_1)\phi_{\rm adiab}(\vec{q}_2) + \ldots$$

A theorist work program

- **identify relevant observables (power spectra and beyond)**
- **controlled predictions of identified observables**
- controlled predictions of covariances between such observables (modes are not independent)
- *theoretical* error structure.

A self-gravitating expanding dust fluid

The Vlasov equation

So let us start assuming that the universe is full of dust like particles with the same mass, m.
The first step of the calculation is to introduce the phase space density function, $f(\mathbf{x}, \mathbf{p})\,\mathrm{d}^3\mathbf{x}\,\mathrm{d}^3\mathbf{p}$, which is the number of particles per volume element $\mathrm{d}^3\mathbf{x}\,\mathrm{d}^3\mathbf{p}$ where the position $\mathbf{x}$ of the particles is expressed in comoving coordinates and the particle conjugate momentum $\mathbf{p}$ reads

$$\mathbf{p} = \mathbf{u}\, m\, a, \tag{1}$$

where a is the expansion factor, $\mathbf{u}$ is the peculiar velocity, i.e. the difference of the physical velocity of the Hubble expansion.

The Vlasov equation

Then the conservation of the particles together with the Liouville theorem when the the two-body interactions can be neglected implies that the total time derivative of f vanishes so that

$$\frac{\mathrm{d}f}{\mathrm{d}t} = \frac{\partial}{\partial t} f(\mathbf{x}, \mathbf{p}, t) + \frac{\mathrm{d}\mathbf{x}}{\mathrm{d}t} \frac{\partial}{\partial \mathbf{x}} f(\mathbf{x}, \mathbf{p}, t) + \frac{\mathrm{d}\mathbf{p}}{\mathrm{d}t} \frac{\partial}{\partial \mathbf{p}} f(\mathbf{x}, \mathbf{p}, t) = 0. \quad (2)$$

This is the Vlasov equation.

The Vlasov equation

The time variation of the position can be expressed in terms of $\mathbf{p}$ and one gets

$$\frac{\mathrm{d}\mathbf{x}}{\mathrm{d}t} = \frac{\mathbf{p}}{m\,a^2}. \tag{3}$$

The time variation of the momentum in general can be obtained from the geodesic equation. Assuming the metric perturbations are small and for scales much below the Hubble scale we have

$$\frac{\mathrm{d}\mathbf{p}}{\mathrm{d}t} = -m\nabla_{\mathbf{x}}\Phi(\mathbf{x}, t) \tag{4}$$

where Φ is the potential. We recall that in the context of metric perturbation in an expanding universe the potential $\Phi(\mathbf{x})$ is sourced by the density contrast (of all species). In our context we simply have

$$\Delta\Phi(\mathbf{x}) = \frac{4\pi G m}{a}\left(\int f(\mathbf{x}, \mathbf{p}, t)\mathrm{d}^3\mathbf{p} - \overline{n}\right) \tag{5}$$

where $\overline{n}$ is the spatial average of $\int f(\mathbf{x}, \mathbf{p}, t)\mathrm{d}^3\mathbf{p}$.

The Vlasov equation

We then have

$$\frac{\partial}{\partial t} f(\mathbf{x}, \mathbf{p}, t) + \frac{\mathbf{p}}{m\, a^2} \frac{\partial}{\partial \mathbf{x}} f(\mathbf{x}, \mathbf{p}, t) - m \nabla_{\mathbf{x}} \Phi(\mathbf{x}, t) \frac{\partial}{\partial \mathbf{p}} f(\mathbf{x}, \mathbf{p}, t) = 0. \quad (6)$$

The system (6, 5) forms the *Vlasov-Poisson* equation. This is precisely the set of equations the N-body simulations attempt to solve.

The motion equations

We can now derive the basic conservation equations we are going to use from the first 2 moments of the Vlasov equation. Let us define the density field per volume $\mathrm{d}^3\mathbf{r}$ as

$$\rho(\mathbf{x}, t) = \frac{m}{a^3} \int \mathrm{d}^3\mathbf{p}\, f(\mathbf{x}, \mathbf{p}). \tag{7}$$

It can be decomposed in an homogeneous form and an inhomogeneous form,

$$\rho(\mathbf{x}, t) = \overline{\rho}(t)(1 + \delta(\mathbf{x}, t)). \tag{8}$$

Note that $\overline{\rho}(t)$ the spatial averaged of $\rho(\mathbf{x}, t)$ should behave like $a(t)^{-3}$ for non relativistic species.

The motion equations

One should then define the higher order moment of the phase space distribution: the mean velocity flow is defined as (for each component),

$$u_i(\mathbf{x}, t) = \frac{1}{\int \mathrm{d}^3\mathbf{p}\, f(\mathbf{x}, \mathbf{p}, t)} \int \mathrm{d}^3\mathbf{p}\, \frac{p_i}{ma} f(\mathbf{x}, \mathbf{p}, t), \tag{9}$$

and the second moment defines the velocity dispersion $\sigma_{ij}(\mathbf{x}, t)$,

$$u_i(\mathbf{x}, t)u_j(\mathbf{x}, t)+\sigma_{ij}(\mathbf{x}, t) = \frac{1}{\int \mathrm{d}^3\mathbf{p}\, f(\mathbf{x}, \mathbf{p}, t)} \int \mathrm{d}^3\mathbf{p}\, \frac{p_i}{ma}\, \frac{p_j}{ma}\, f(\mathbf{x}, \mathbf{p}, t). \tag{10}$$

The motion equations

The first two moments of the Vlasov equation give then the conservation and Euler equations, respectively

$$\frac{\partial \delta(\mathbf{x},t)}{\partial t} + \frac{1}{a}\left[(1+\delta(\mathbf{x},t))\mathbf{u}_i(\mathbf{x},t)\right]_{,i} = 0 \tag{11}$$

and

$$\frac{\partial \mathbf{u}_i(\mathbf{x},t)}{\partial t} + \frac{\dot{a}}{a}\mathbf{u}_i(\mathbf{x},t) + \frac{1}{a}\mathbf{u}_j(\mathbf{x},t)\,\mathbf{u}_i(\mathbf{x},t)_{,j} = -\frac{1}{a}\Phi(\mathbf{x},t)_{,i} - \frac{\left(\rho(\mathbf{x},t)\,\sigma_{ij}(\mathbf{x},t)\right)_{,j}}{\rho(\mathbf{x},t)\,a}. \tag{12}$$

The first term of the right hand side of eqn (12) is the gravitational force, the second is due to the pressure force which in general can be anisotropic. In the context we are interested in, it actually vanishes until the formation of the first caustics.

Single flow approximation

The early stages of the gravitational instabilities are indeed characterized, assuming the matter is non-relativistic, by a negligible velocity dispersion when it is compared to the velocity flows, i.e. much smaller than the velocity gradients induced by the density fluctuations of the scales of interest. This is the *single flow approximation*. It simply states that one can assume

$$f(\mathbf{x}, \mathbf{p}, t) = \frac{a^3\, \rho(\mathbf{x}, t)}{m}\, \delta^{(3)}[\mathbf{p} - m\, a\, \mathbf{u}(\mathbf{x}, t)], \tag{13}$$

to a good approximation. This approximation will naturally break at the time of shell crossings when different flows – pulled toward one-another by gravity – cross. The Vlasov-Poisson equation in the single flow regime is the system that will be studied throughout these lecture notes, from linear to non nonlinear regime.

Single flow approximation

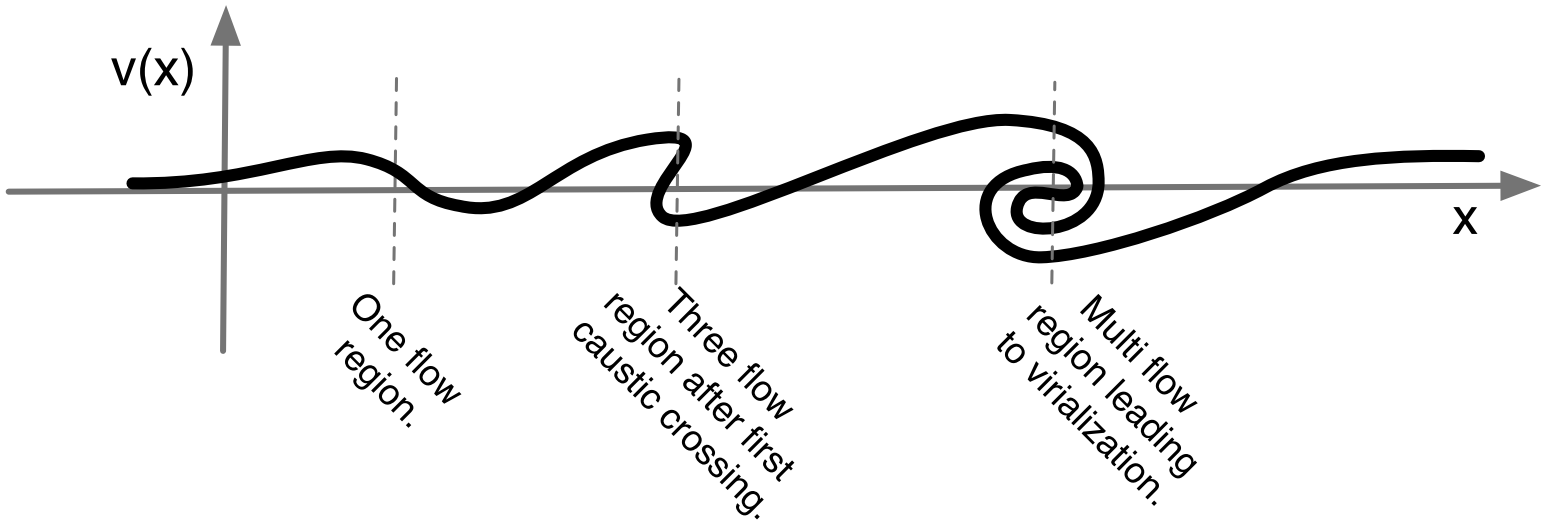

Figure: Schematic description of phase space after the first shell crossings and emergence of multi-flow regions. The figure is for 1D dynamics. From left to right, one can see regions with growing number of flows after dark matter caustic crossings.

The curl modes

In the single flow regime, one can note that the source term of the Euler equation is potential, implying that it cannot generate any curl mode in the velocity field. More precisely, one can decompose any three-dimensional field in a gradient part and a curl part

$$\mathbf{u}_i(\mathbf{x}) = \psi(\mathbf{x})_{,i} + \mathbf{w}_i(\mathbf{x}) \tag{14}$$

where $\mathbf{w}_{i,i} = 0$. Defining the local vorticity as

$$\omega_k(\mathbf{x}) = \epsilon^{ijk}\mathbf{u}_{i,j}(\mathbf{x}) \tag{15}$$

where ϵ^{ijk} is the totally anti-symmetric Levi-Civita tensor one can easily show that

$$\omega_k(\mathbf{x}) = \epsilon^{ijk}\mathbf{w}_{i,j}(\mathbf{x}). \tag{16}$$

The curl modes

And applying the operator $\epsilon^{ijk}\nabla_j$ to the Euler equation one gets (see [**?**])

$$\frac{\partial}{\partial t}\omega_k + \frac{\dot{a}}{a}\omega_k - \epsilon^{ijk}\epsilon^{lmi}\left(\mathbf{u}_l\,\omega_m\right)_{,j} = 0. \tag{17}$$

This equation actually expresses the fact that the vorticity is conserved throughout the expansion. In the linear regime that is when the last term of this equation is dropped it simply means that the vorticity scales like $1/a$. In the subsequent stage of the dynamics the vorticity can only grow in contracting regions but it is still somehow conserved, it cannot be created out of potential modes only. That will be the case until shell crossing where the anisotropic velocity dispersion can then induce vorticity. This has been explicitly demonstrated in various studies [**?**, **?**, **?**]. As a consequence, in the following, curl modes in the vector flied will always be neglected.

The linear theory

We now proceed to explore the linear regime of the Vlasov-Poisson system. One objective is to make contact with earlier stages of the gravitational dynamics and the second is to introduce the notion of Green function we will use in the following.

The linear modes

The linearization of the motion equation is obtained when one assumes that the terms $[\delta(\mathbf{x},t))\mathbf{u}_i(\mathbf{x},t)]_{,i}$ and $\mathbf{u}_j(\mathbf{x},t)\,\mathbf{u}_i(\mathbf{x},t)_{,j}$ in respectively the continuity and the Euler equation vanish. This is obtained when both the density contrast and the velocity gradients in units of H are negligible. The linearized system is obtained in terms of the velocity divergence

$$\theta(\mathbf{x},t) = \frac{1}{aH}u_{i,i} \tag{18}$$

so that the system now reads

$$\frac{\partial}{\partial t}\delta(\mathbf{x},t) + H\theta(\mathbf{x},t) = 0 \tag{19}$$

$$\frac{\partial}{\partial t}\theta(\mathbf{x},t) + 2H\theta + \frac{\dot{H}}{H}\theta(\mathbf{x},t) = -\frac{3}{2}H\Omega_m(t)\delta(\mathbf{x},t) \tag{20}$$

after taking the divergence of the Euler equation. We have introduced here the Hubble parameter $H = \dot{a}/a$ and used the Friedman equation $H^2 = 8\pi/3\ G\rho_c(t)$ together with the definition of $\Omega_m = \overline{\rho}(t)/\rho_c(t)$.

The linear modes

The resolution of this system is now simple. It can be obtained after eliminating the velocity divergence and one gets a second order dynamical equation,

$$\frac{\partial^2}{\partial\, t^2}\delta(\mathbf{x},t) + 2\,H\frac{\partial}{\partial\, t}\delta(\mathbf{x},t) - \frac{3}{2}\,H^2\,\Omega_m\,\delta(\mathbf{x},t) = 0, \tag{21}$$

for the density contrast. It is to be noted that the spatial coordinates are here just labels: there is no operator acting of the physical coordinates. This is quite a unique feature in the growth of instabilities in a pressureless fluid. That implies in particular that the linear growth rate of the fluctuations will be independent on scale. The time dependence of the linear solution is given by the two solutions of

$$\ddot{D} + 2\,H\,\dot{D} - \frac{3}{2}\,H^2\,\Omega_m\,D = 0, \tag{22}$$

one of which is decaying and the other is growing with time.

The linear modes, Einstein de Sitter case

For an Einstein de-Sitter (EdS) background (a universe with no curvature and with a critical matter density) the solutions read

$$D_+^{\rm EdS}(t) \propto t^{2/3}, \quad D_-^{\rm EdS}(t) \propto 1/t, \tag{23}$$

that is $D_+^{\rm EdS}(t)$ is proportional to the expansion factor. This result gives the time scale of the growth of structure. This is what permits a direct comparison between the amplitude of the metric perturbations at recombination and the density perturbation in the local universe. Note that it implies that the potential, for the corresponding mode, is constant (see the Poisson equation).

The linear modes, general solutions

Il n'existe pas de solution générale à (22) qui soit valable pour tout modèle cosmologique. Cependant si on admet que le contenu de l'univers à bas redshift correspond à un mélange de matière, d'une énergie du vide correspondant à une simple constante cosmologique, en présence éventuellement d'un terme de courbure, alors la constante de Hubble prend la forme,

$$H = H_0 \sqrt{\Omega_{\rm m}^{(0)} a^{-3} + (1 - \Omega_{\rm m}^{(0)} - \Omega_{\sim}^{(0)}) a^{-2} + \Omega_\Lambda}, \qquad (24)$$

et est solution de (22). C'est la solution décroissante. La solution croissante peut facilement être obtenue par méthode de variation des constantes. On obtient ainsi, sous les hypothèses mentionnées plus haut,

$$D_-(t) \propto H(t), \qquad (25)$$

$$D_+(t) \propto H(t) \int \frac{{\rm d}t}{(aH)^2}. \qquad (26)$$

The linear theory

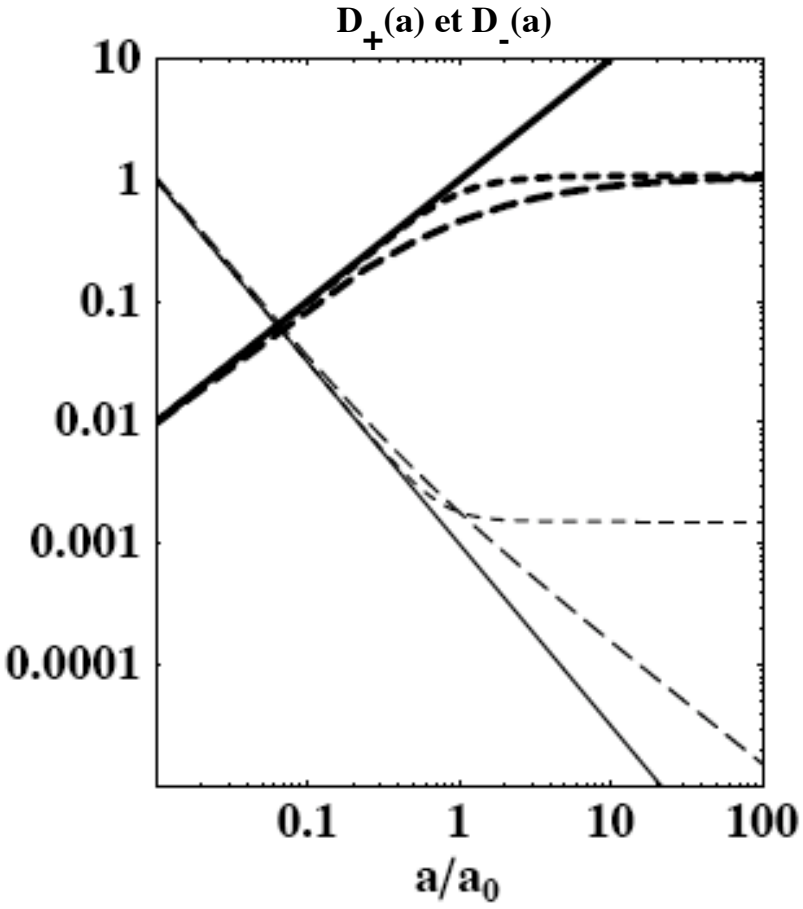

Figure: Comportement des taux de croissance (lignes épaisses) et de décroissance (lignes fines) des instabilités gravitationnelles pour un univers Einstein-de Sitter (lignes continues), un univers avec $\Omega_{\rm m}^{(0)} = 0.3,\ \Omega_\Lambda = 0$ (lignes pointillées longues) et un univers avec $\Omega_{\rm m}^{(0)} = 0.3,\ \Omega_\Lambda^{(0)} = 0.7$ (lignes pointillées courtes).

The linear theory

Si on se restreint à des cosmologies sans constante cosmologique, $\Omega_\Lambda = 0$, D_+ peut s'exprimer analytiquement en fonction de a,

$$D_+(a) \propto 1 + \frac{3\Omega_{\rm m}^{(0)}}{a - a\Omega_{\rm m}^{(0)}} + 3\sqrt{\frac{(a(\Omega_{\rm m}^{(0)} - 1) - \Omega_{\rm m}^{(0)})\Omega_{\rm m}^{(0)^2}}{a^3(\Omega_{\rm m}^{(0)} - 1)^3}} \times \log\left(\sqrt{a\left(\frac{1}{\Omega_{\rm m}^{(0)}} - 1\right) + 1} - \sqrt{a\left(\frac{1}{\Omega_{\rm m}^{(0)}} - 1\right)}\right)$$

The linear theory

Pour un contenu en énergie matière arbitraire, il faut résoudre bien sûr l'équation (22). Les résultats d'une telle intégration sont montrés sur la figure 2. Une forme plus simple existe cependant dans le cas d'univers plat avec constante cosmologique. Dans ce cas la dépendance temporelle de D_+ est donnée par

$$D_+(t) = {}_2F_1\left(1, \frac{1}{3}; \frac{11}{6}; -\sinh^2\left(\frac{3\alpha t}{2}\right)\right) \sinh^{\frac{2}{3}}\left(\frac{3\alpha t}{2}\right), \quad (27)$$

et le facteur f prend la forme

$$f = 1 - \frac{6}{11} \frac{{}_2F_1\left(2, \frac{4}{3}; \frac{17}{6}; -\sinh^2\left(\frac{3\alpha t}{2}\right)\right) \sinh^2\left(\frac{3\alpha t}{2}\right)}{{}_2F_1\left(1, \frac{1}{3}; \frac{11}{6}; -\sinh^2\left(\frac{3\alpha t}{2}\right)\right)} \quad (28)$$

avec $\alpha = \sqrt{\Lambda/3}$.

La relation densité-vitesse

Pour être complet, il faut bien sûr expliciter la relation entre le contraste de densité et la divergence du champ de vitesse. L'équation de continuité peut se réécrire,

$$a\frac{\partial}{\partial a}\delta + \theta = 0. \tag{29}$$

Le champ θ s'écrit donc,

$$\theta(t,\mathbf{x}) = \frac{\partial \log D_+}{\partial \log a}\delta_+(t,\mathbf{x}) + \frac{\partial \log D_-}{\partial \log a}\delta_-(t,\mathbf{x}) \tag{30}$$

où $\delta_\pm(t,\mathbf{x}) = D_\pm(t)\delta_\pm(\mathbf{x})$. Pour un univers Einstein-de Sitter, cette relation devient

$$\theta(t,\mathbf{x}) = \delta_+(t,\mathbf{x}) - \frac{3}{2}\delta_-(t,\mathbf{x}). \tag{31}$$

La relation densité-vitesse

Poursuivons l'examen de la relation densité-vitesse. Si on se limite au terme croissant le facteur de proportionnalité entre θ et δ est donc la dérivée logarithmique de D_+ avec le facteur d'expansion,

$$f \equiv \frac{\mathrm{d}\log D_+}{\mathrm{d}\log a}. \tag{34}$$

Ce facteur vaut 1 pour un univers Einstein de Sitter. On peut bien sûr le calculer analytiquement ou numériquement selon les cas. Par exemple pour un univers plat avec constante cosmologique une bonne paramétrisation de f est,

$$f(\Omega_\mathrm{m}) = \Omega^{5/9} \approx \Omega^{0.55}; \tag{35}$$

et pour un univers sans constante cosmologique,

$$f(\Omega_\mathrm{m}) = \Omega^{3/5}. \tag{36}$$

La figure (4) compare les résultats exacts à ces formes approchées. On voit que l'écart est tout au plus de quelques pour-cents.

La relation densité-vitesse

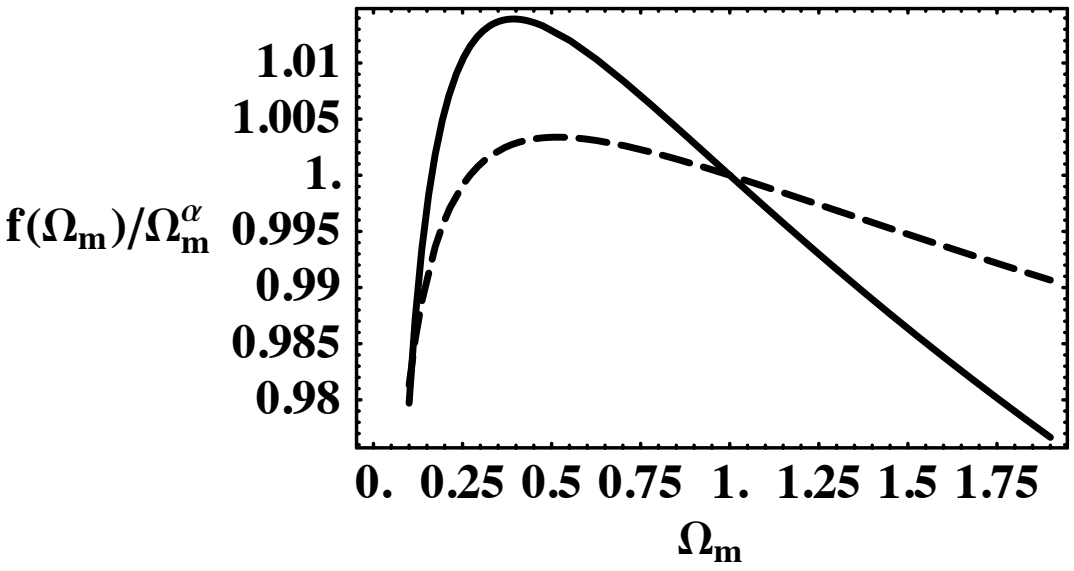

Figure: Facteur f, équation (34), divisé par sa valeur estimée, équations (35-36), en fonction de $\Omega_{\rm m}$ pour un espace sans constante cosmologique (ligne continue) ou pour un espace plat (tirets).

Linear theory: the Green functions

The previous results show that the linear density field can be written in general

$$\delta(\mathbf{x}, t) = \delta_+(\mathbf{x}) D_+(t) + \delta_-(\mathbf{x}) D_-(t) \tag{37}$$

and

$$\theta(\mathbf{x}, t) = -\frac{\mathrm{d}}{\mathrm{d}\log a} D_+ \ \delta_+(\mathbf{x}) - \frac{\mathrm{d}}{\mathrm{d}\log a} D_- \delta_-(\mathbf{x}). \tag{38}$$

The actual growing and decaying modes can then be obtained by inverting this system. For instance for an Einstein de Sitter background one gets

$$\delta_+(\mathbf{x}) D_+(t) = \frac{D_+(t)}{D_+(t_0)} \left[\frac{3}{5} \delta(\mathbf{x}, t_0) - \frac{2}{5} \theta(\mathbf{x}, t_0) \right], \tag{39}$$

$$\delta_-(\mathbf{x}) D_-(t) = \frac{D_-(t)}{D_-(t_0)} \left[\frac{2}{5} \delta(\mathbf{x}, t_0) + \frac{2}{5} \theta(\mathbf{x}, t_0) \right], \tag{40}$$

and similar results for the velocity divergence.

Linear theory: the Green functions

Following [**?**], this result can be encapsulated in a simple form after one introduces the doublet $\Psi_a(\mathbf{k}, \tau)$,

$$\Psi_a(\mathbf{k}, \tau) \equiv \Big(\delta(\mathbf{x}, t),\ -\theta(\mathbf{x}, t)\Big), \tag{41}$$

where a is an index whose value is either 1 (for the density component) or 2 (for the velocity component).

Linear theory: the Green functions

The linear growth solution can now be written

$$\Psi_a(\mathbf{x}, t) = g_a{}^b(t, t_0)\Psi_b(\mathbf{x}, t_0) \tag{42}$$

where g_a^b is the Green function of the system. It is usually written with the following time variable,

$$\eta = \log D_+ \tag{43}$$

(not to be mistaken with the conformal time). For an Einstein de Sitter universe, we have explicitly,

$$g_a{}^b(\eta, \eta_0) = \frac{e^{\eta-\eta_0}}{5}\begin{bmatrix} 3 & 2 \\ 3 & 2 \end{bmatrix} + \frac{e^{-\frac{3}{2}(\eta-\eta_0)}}{5}\begin{bmatrix} 2 & -2 \\ -3 & 3 \end{bmatrix}. \tag{44}$$

We will see in the following that, provided the doublet Ψ_a is properly defined, this form remains practically unchanged for any background.

Linear theory: The general background case

For a general background, it is fruitful to extent the definition of the doublet to,

$$\Psi_a(\mathbf{x},\eta) \equiv \left(\delta(\mathbf{x},\eta),\ -\frac{1}{f_+}\theta(\mathbf{x},\eta)\right), \tag{45}$$

where

$$f_+ = \frac{\mathrm{d}\log D_+}{\mathrm{d}\log a} \tag{46}$$

Defining $\hat{\theta} = -\theta(\mathbf{x},\eta)/f_+$ and for the time variable η, the linearized motion equations indeed read

$$\frac{\partial}{\partial\eta}\delta(\mathbf{x},\eta) - \hat{\theta}(\mathbf{x},\eta) = 0 \tag{47}$$

$$\frac{\partial}{\partial\eta}\hat{\theta}(\mathbf{x},\eta) \left(\frac{3}{2}\frac{\Omega_m}{f_+^2} - 1\right)\hat{\theta} - \frac{3}{2}\frac{\Omega_m}{f_+^2}\delta(\mathbf{x},\eta) = 0, \tag{48}$$

Cosmic fields as statistical objects

The origin of stochasticity

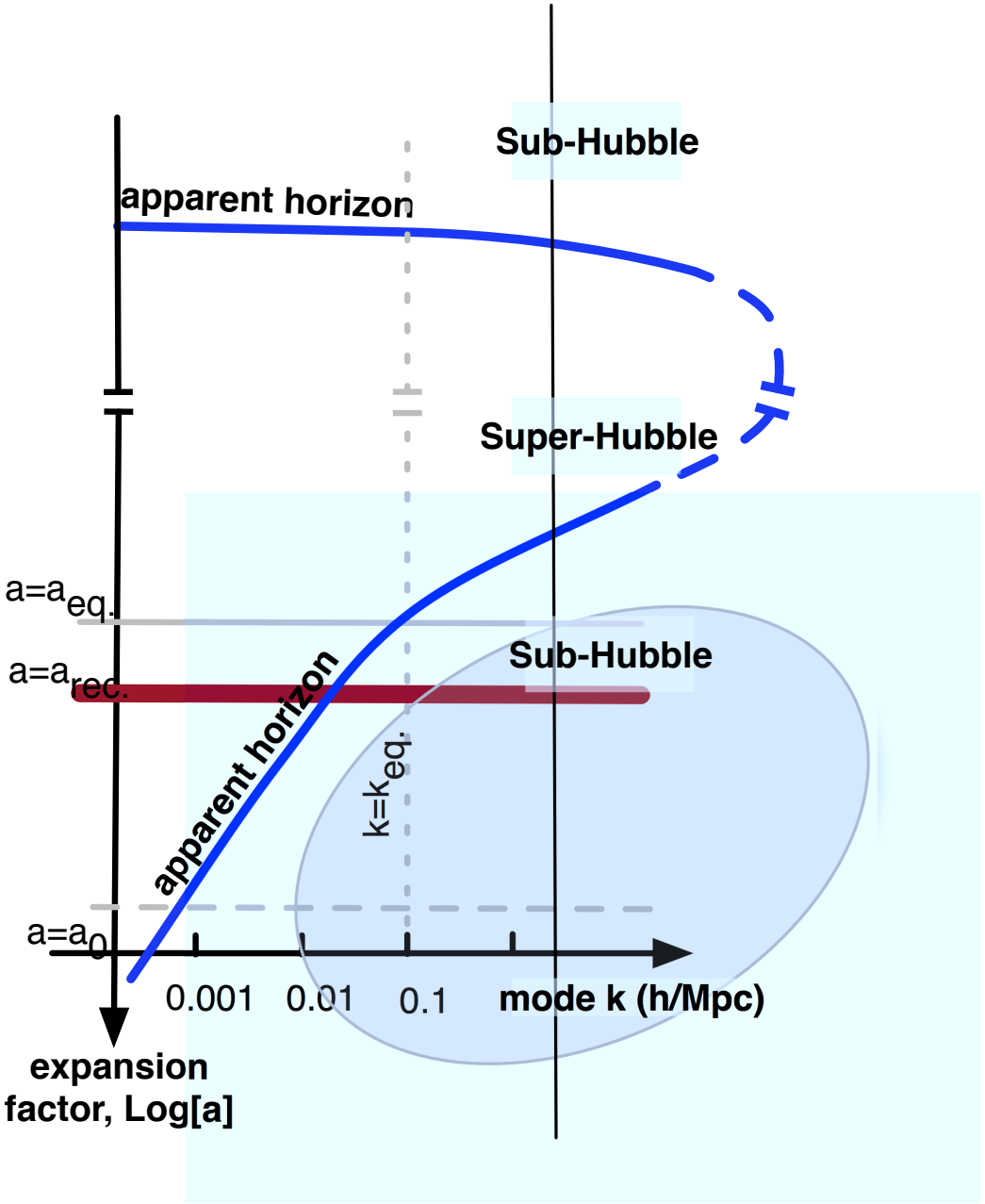

Figure: Development of linear metric perturbation across scale and time.

The origin of stochasticity

In models of inflation the stochastic properties of the fields originate from quantum fluctuations of a scalar field, the inflaton. This field has quantum fluctuations that can be decomposed in Fourier modes using the creation and annihilation operators $a^\dagger_{\mathbf{k}}$ and $a_{\mathbf{k}}$ for a wave mode $\mathbf{k}$,

$$\delta\varphi = \int \mathrm{d}^3\mathbf{k} \left[a_{\mathbf{k}}\, \psi_k(t)\, \exp(\mathrm{i}\mathbf{k}.\mathbf{x}) + a^\dagger_{\mathbf{k}}\, \psi^*_k(t)\, \exp(-\mathrm{i}\mathbf{k}.\mathbf{x}) \right]. \quad (55)$$

The operators obey the standard commutation relation,

$$[a_{\mathbf{k}}, a^\dagger_{-\mathbf{k}'}] = \delta_D(\mathbf{k} + \mathbf{k}'), \quad (56)$$

and the mode functions $\psi_k(t)$ are obtained from the Klein-Gordon equation for φ in an expanding Universe.

The origin of stochasticity

We give here its expression for a de-Sitter metric (i.e. when the spatial sections are flat and H is constant),

$$\psi_k(t) = \frac{H}{(2\,k)^{1/2}\,k}\left(\mathrm{i} + \frac{k}{a\,H}\right)\,\exp\left[\frac{\mathrm{i}\,k}{a\,H}\right], \qquad (57)$$

where a and H are respectively the expansion factor and the Hubble constant that are determined by the overall content of the Universe through the Friedmann equations.
When the modes exit the Hubble radius, $k/(aH) \ll 1$, one can see from eqn (57) that the dominant mode reads,

$$\varphi_{\mathbf{k}} \approx \frac{iH}{\sqrt{2}k^{3/2}}\left(a_{\mathbf{k}} + a^{\dagger}_{-\mathbf{k}}\right), \quad \delta\varphi = \int \mathrm{d}^3\mathbf{k}\,\varphi_{\mathbf{k}}\,e^{\mathrm{i}\,\mathbf{k}.\mathbf{x}}. \qquad (58)$$

Therefore these modes are all proportional to $a_{\mathbf{k}} + a^{\dagger}_{-\mathbf{k}}$.

The origin of stochasticity

One important consequence of this is that the quantum nature of the fluctuations has disappeared [**?**, **?**]: any combinations of $\varphi_{\mathbf{k}}$ commute with each other. The field φ can then be seen as a classic stochastic field where *ensemble averages identify with vacuum expectation values*,

$$\langle ... \rangle \equiv \langle 0 | ... | 0 \rangle. \tag{59}$$

The origin of stochasticity

After the inflationary phase the modes re-enter the Hubble radius. They leave imprints of their energy fluctuations in the gravitational potential, the statistical properties of which can therefore be deduced from eqns (56, 58). All subsequent stochasticity that appears in the cosmic fields can thus be expressed in terms of the random variable $\varphi_{\mathbf{k}}$. The linear theory calculation precisely tells us how each mode, in each fluid component, grows across time, i.e. it provides us with the so-called transfer functions, $T_a(\mathbf{k}, \eta, \eta_0)$, defined as

$$\delta_a(\mathbf{k}, \eta) = T_a(\mathbf{k}, \eta, \eta_0)\delta\varphi(\mathbf{k}, \eta_0) \tag{60}$$

where η_0 is a time which corresponds to an arbitrarily early time.

Statistical homogeneity and isotropy

In the following the density contrast will be decomposed in Fourier modes that, for a flat universe, are defined such as

$$\delta(\mathbf{x}) = \int \frac{\mathrm{d}^3\mathbf{k}}{(2\pi)^{3/2}}\, \delta(\mathbf{k})\, \exp(\mathrm{i}\mathbf{k}\cdot\mathbf{x}) \tag{61}$$

or equivalently

$$\delta(\mathbf{k}) = \int \frac{\mathrm{d}^3\mathbf{x}}{(2\pi)^{3/2}}\, \delta(\mathbf{x})\, \exp(-\mathrm{i}\mathbf{k}\cdot\mathbf{x}). \tag{62}$$

The observable quantities of interest are actually the statistical properties of such a field, whether it is represented in real space or in Fourier space.

Statistical homogeneity and isotropy

The *Cosmological Principle*, e.g. that the assumption that the Universe is statically isotropic and homogeneous, implies that real space correlators are homogeneous and isotropic which for instance implies that $\left\langle \delta(\mathbf{x})\delta(\mathbf{x}+\mathbf{r})\right\rangle$ is a function of the separation r only. This defines the two-point correlation function,

$$\xi(r) = \left\langle \delta(\mathbf{x})\delta(\mathbf{x}+\mathbf{r})\right\rangle. \tag{63}$$

In Fourier space, the two point correlator of the Fourier modes then takes the form,

$$\begin{aligned}
\left\langle \delta(\mathbf{k})\delta(\mathbf{k}')\right\rangle &= \int \frac{\mathrm{d}^3\mathbf{x}}{(2\pi)^{3/2}}\frac{\mathrm{d}^3\mathbf{r}}{(2\pi)^{3/2}}\,\xi(r)\,\exp[-\mathrm{i}(\mathbf{k}+\mathbf{k}')\cdot\mathbf{x} - \mathrm{i}\mathbf{k}'\cdot\mathbf{r}] \\
&= \delta_{\mathrm{Dirac}}(\mathbf{k}+\mathbf{k}')\int \mathrm{d}^3\mathbf{r}\,\xi(r)\,\exp(\mathrm{i}\mathbf{k}\cdot\mathbf{r}) \\
&\equiv \delta_{\mathrm{Dirac}}(\mathbf{k}+\mathbf{k}')\,P(k),
\end{aligned} \tag{64}$$

where $P(k)$ is the *power spectrum* of the density field, e.g. the cross-correlation matrix is symmetric in Fourier space.

Power spectrum

$$\langle \delta_{\mathbf{k}} \delta_{\mathbf{k}'} \rangle = \delta_{\mathrm{Dirac}}(\mathbf{k} + \mathbf{k}')\, P(k)$$

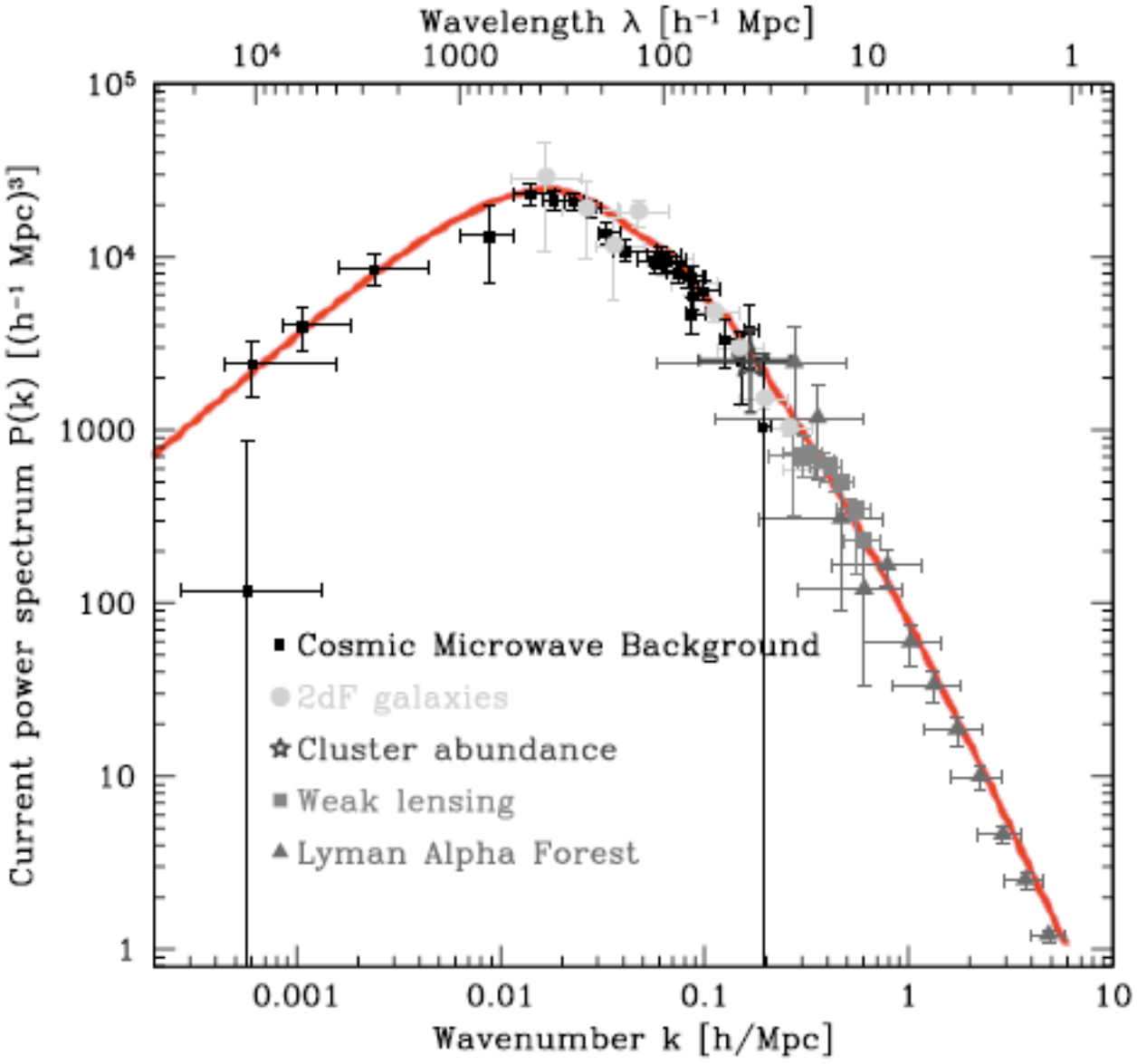

Statistical homogeneity and isotropy

All these relations apply to the observed fields. However in case of the primordial fluctuations, the field $\delta\varphi(\mathbf{k})$ corresponds to a free field from a quantum mechanical point of view. That makes it eventually a Gaussian classical field. As such it obeys the Wick theorem. The latter tells us that higher order correlators can then be entirely constructed from the power spectrum (from pair associations) through the relations,

$$\begin{aligned} \left\langle \delta\varphi(\mathbf{k}_1)\dots\delta\varphi(\mathbf{k}_{2p+1})\right\rangle &= 0 \qquad (65)\\ \left\langle \delta\varphi(\mathbf{k}_1)\dots\delta\varphi(\mathbf{k}_{2p})\right\rangle &= \sum_{\text{pair associations}} \prod_{p \text{ pairs (i,j)}} \left\langle \delta\varphi(\mathbf{k}_i)\delta\varphi(\mathbf{k}_j)\right\rangle. \end{aligned}$$

These relations apply as well to any linear combinations of the primordial field, and therefore to any field computed in the linear regime.

Moments and cumulants

In the nonlinear regime however, fields also exhibit higher order non-trivial correlation functions that cannot be reconstructed from the two-point order correlators. They are defined as the *connected* part (denoted with subscript c) of the joint ensemble average of fields in an arbitrarily number of locations. Formally, for the density field, it reads,

$$\begin{aligned}\langle \delta(\mathbf{x}_1), \ldots, \delta(\mathbf{x}_N) \rangle &= \langle \delta(\mathbf{x}_1), \ldots, \delta(\mathbf{x}_N) \rangle_c \\ &+ \sum_{\mathcal{S} \in \mathcal{P}(\{\mathbf{x}_1, \ldots, \mathbf{x}_n\})} \prod_{s_i \in \mathcal{S}} \langle \delta(\mathbf{x}_{s_i(1)}), \ldots, \delta(\mathbf{x}_{s_i(\#s_i)}) \rangle_c, \end{aligned} \tag{66}$$

where the sum is made over the proper partitions (any partition except the set itself) of $\{\mathbf{x}_1, \ldots, \mathbf{x}_N\}$ and s_i is thus a subset of $\{\mathbf{x}_1, \ldots, \mathbf{x}_N\}$ contained in partition $\mathcal{S}$. When the average of $\delta(\mathbf{x})$ is defined as zero, only partitions that contain no singlets contribute.

Moments and cumulants

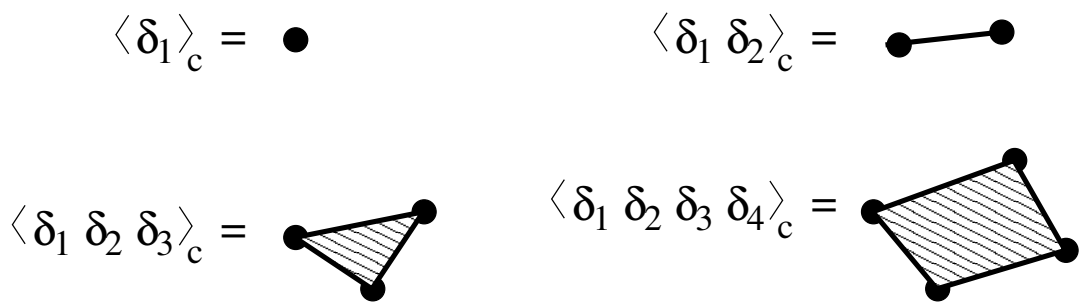

Figure: Representation of the connected part of the moments.

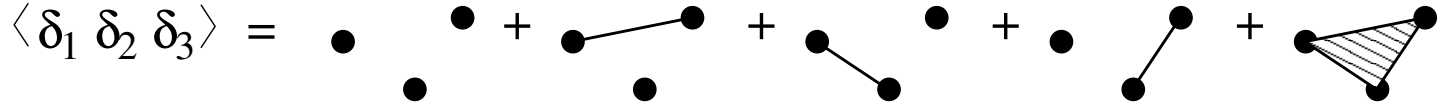

Figure: Writing of the three-point moment in terms of connected parts.

Moments and cumulants

The decomposition in connected and non-connected parts can be easily visualized. It means that any ensemble average can be decomposed in a product of connected parts. They are defined for instance in Fig. 6. The tree-point moment is "written" in Fig. 7. Because of homogeneity of space $\langle \delta(\mathbf{k}_1) \dots \delta(\mathbf{k}_N) \rangle_c$ is always proportional to $\delta_D(\mathbf{k}_1 + \dots + \mathbf{k}_N)$. Then we can define $P_N(\mathbf{k}_1, \dots, \mathbf{k}_N)$ with

$$\langle \delta(\mathbf{k}_1) \dots \delta(\mathbf{k}_N) \rangle_c = \delta_D(\mathbf{k}_1 + \dots + \mathbf{k}_N)\, P_N(\mathbf{k}_1, \dots, \mathbf{k}_N). \qquad (67)$$

One case of particular interest is for $n = 3$, the bispectrum, which is usually denoted by $B(\mathbf{k}_1, \mathbf{k}_2, \mathbf{k}_3)$. Note that it depends on 2 wave modes only, and it depends on 3 independent variables characterizing the triangle formed by the 3 wave modes (for instance 2 lengths and 1 angle).

Moment and cumulant generating functions

It is convenient to define a function from which all moments can be generated, namely the *moment generating function*. It can be defined[2] for any number of random variables. Here we give its definition for the local density field. It is defined by

$$\mathcal{M}(t) \equiv \sum_{p=0}^{\infty} \frac{\langle \rho^p \rangle}{p!} t^p = \langle \exp(t\delta) \rangle. \tag{68}$$

The moments can obviously obtained by subsequent derivatives of this function at the origin $t = 0$. A cumulant generating function can similarly be defined by

$$\mathcal{C}(t) \equiv \sum_{p=2}^{\infty} \frac{\langle \rho^p \rangle_c}{p!} t^p. \tag{69}$$

[2] It is to be noted however that the existence of moments – which itself is not guaranteed for any stochastic process – does not ensure the existence of their generating function as the series defined in (68) can have a vanishing converging radius. Such a case is encountered for a lognormal distribution for instance and it implies that the moments of such a stochastic process do not uniquely define the probability distribution function.

Moment and cumulant generating functions

A fundamental result is that the cumulant generating function is given by the logarithm of the moment generation function

$$\mathcal{M}(t) = \exp[\mathcal{C}(t)]. \tag{70}$$

In case of a Gaussian probability distribution function, this is straightforward to check since $\langle \exp(t\delta) \rangle = \exp(\sigma^2 t^2/2)$.

Into the nonlinear universe

Linear theory: The general background case

For a general background, the doublet is defined as,

$$\Psi_a(\mathbf{x},\eta) \equiv \left(\delta(\mathbf{x},\eta),\ -\frac{1}{f_+}\theta(\mathbf{x},\eta)\right), \tag{45}$$

where

$$f_+ = \frac{\mathrm{d}\log D_+}{\mathrm{d}\log a} \tag{46}$$

Defining $\hat{\theta} = -\theta(\mathbf{x},\eta)/f_+$ and for the time variable $\eta = \log D_+$, the linearized motion equations indeed read

$$\frac{\partial}{\partial\eta}\delta(\mathbf{x},\eta) - \hat{\theta}(\mathbf{x},\eta) = 0 \tag{47}$$

$$\frac{\partial}{\partial\eta}\hat{\theta}(\mathbf{x},\eta) + \left(\frac{3}{2}\frac{\Omega_m}{f_+^2} - 1\right)\hat{\theta} - \frac{3}{2}\frac{\Omega_m}{f_+^2}\delta(\mathbf{x},\eta) = 0, \tag{48}$$

Linear theory: The general background case

It can be rewritten as

$$\frac{\partial}{\partial \eta}\Psi_a(\mathbf{x},\eta) + \Omega_a{}^b(\eta)\Psi_b(\mathbf{x},\eta) = 0, \tag{49}$$

with

$$\Omega_a{}^b(\eta) = \begin{pmatrix} 0 & -1 \\ -\frac{3}{2}\frac{\Omega_m}{f_+^2} & \frac{3}{2}\frac{\Omega_m}{f_+^2} - 1 \end{pmatrix}. \tag{50}$$

A field representation of the nonlinear motion equations

Inserting the non-linear terms one eventually gets,

$$\frac{\partial}{\partial \eta}\Psi_a(\mathbf{k},\eta) + \Omega_a{}^b(\eta)\Psi_b(\mathbf{k},\eta) \;=\; \gamma_a{}^{bc}(\mathbf{k}_1,\mathbf{k}_2)\;\Psi_b(\mathbf{k}_1,\eta)\;\Psi_c(\mathbf{k}_2,\eta), \tag{73}$$

where $\Omega_a{}^b(\eta)$ is defined in eqn (50) and where (and that will be the case henceforth) we use the convention that repeated Fourier arguments are integrated over and the Einstein convention on repeated indices, and where the *symmetrized vertex* matrix $\gamma_a{}^{bc}$ describes the non linear interactions between different Fourier modes.

A field representation of the nonlinear motion equations

The components of ${\gamma_a}^{bc}$ are given by

$$
\begin{aligned}
{\gamma_2}^{22}(\mathbf{k}_1,\mathbf{k}_2) &= \delta_{\rm Dirac}(\mathbf{k}-\mathbf{k}_1-\mathbf{k}_2)\,\frac{|\mathbf{k}_1+\mathbf{k}_2|^2(\mathbf{k}_1\cdot\mathbf{k}_2)}{2k_1^2k_2^2},\\
{\gamma_1}^{21}(\mathbf{k}_1,\mathbf{k}_2) &= \delta_{\rm Dirac}(\mathbf{k}-\mathbf{k}_1-\mathbf{k}_2)\,\frac{(\mathbf{k}_1+\mathbf{k}_2)\cdot\mathbf{k}_1}{2k_1^2},
\end{aligned}
\qquad (74)
$$

${\gamma_a}^{bc}(\mathbf{k}_1,\mathbf{k}_2)={\gamma_a}^{cb}(\mathbf{k}_2,\mathbf{k}_1)$, and $\gamma=0$ otherwise, where $\delta_{\rm Dirac}$ denotes the Dirac distribution function. The matrix ${\gamma_a}^{bc}$ is independent on time (and on the background evolution) and encodes all the non-linear couplings of the system.

A field representation of the nonlinear motion equations

One can then take advantage of the knowledge of the Green function of this system to write a formal solution of eqn (73) as

$$\Psi_a(\mathbf{k},\eta) = g_a{}^b(\eta)\,\Psi_b(\mathbf{k},\eta_0) + \\ + \int_{\eta_0}^{\eta} \mathrm{d}\eta'\; g_a{}^b(\eta,\eta')\;\gamma_b{}^{cd}(\mathbf{k}_1,\mathbf{k}_2)\Psi_c(\mathbf{k}_1,\eta')\Psi_d(\mathbf{k}_2,\eta'), \qquad (75)$$

where $\Psi_a(\mathbf{k},\eta_0)$ denotes the initial conditions.
In the following calculations we will be using the value of the $\Omega_a{}^b$ matrix to be that of the Einstein de Sitter background that is effectively assuming that D_- scales like $D_+^{-3/2}$. This is known to be a very good approximation even in the context of a $\Lambda-$CDM universe.

Diagrammatic representations

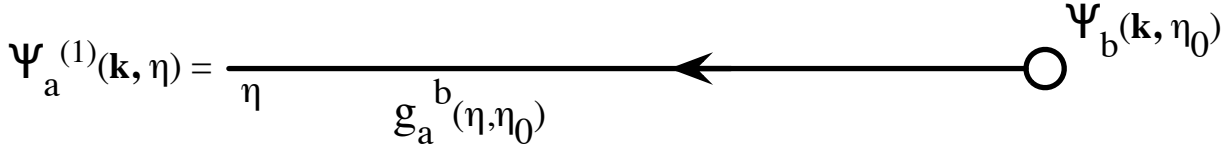

Figure: Diagrammatic representation of the linear propagator. Ψ_b represents the initial conditions and $g_a^{\ b}$ is the time dependent propagator. This diagram value is the linear solution of the motion equation.

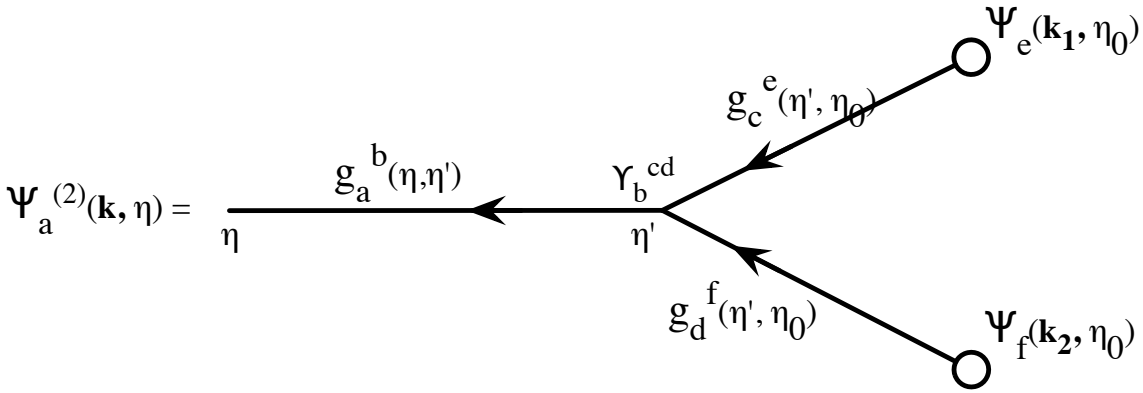

Figure: Diagrammatic representation of the fields at second order. This diagram value is given by eqn (75) when one replaces Ψ_c and Ψ_d in the second term of the right hand side by their linear expressions. In the diagram, each time one encounters a vertex, a time integration and a Dirac function in the wave modes is implicitly assumed.

Diagrammatic representations

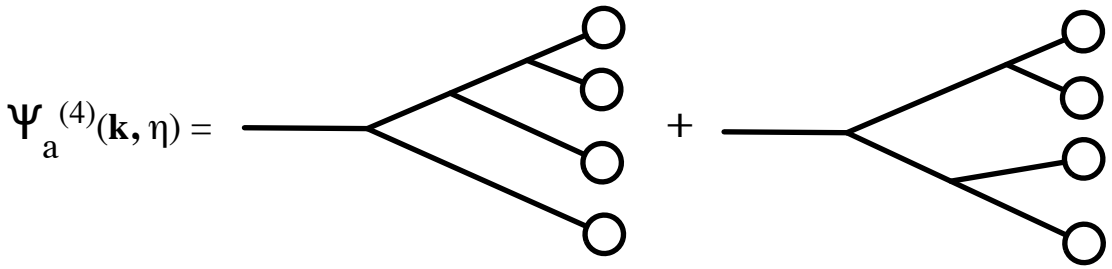

Figure: Diagrammatic representation of the fields at fourth order. Three different diagrams are found to contribute.

One of a nice feature of eqn (75) is that it admits simple diagrammatic representations in a way very similar to Feynman diagrams.

A field representation of the nonlinear motion equations

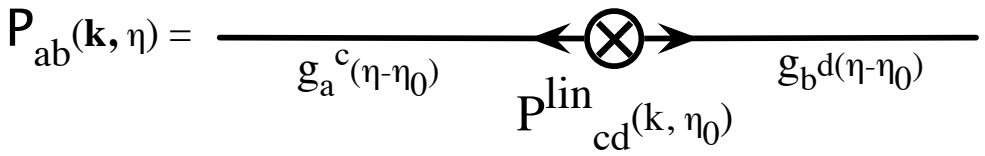

Figure: Diagrammatic representation of the power spectrum at linear order. The symbol $\otimes$ represents the linear power spectrum in the (adiabatic) growing mode.

A field representation of the nonlinear motion equations

Relevant statistical quantities are obtained however once ensemble average are taken. Assuming Gaussian initial conditions, one then can apply the Wick theorem to all the factors representing the initial field values that appear in diagrams (or product of diagrams) of interest. In practice, at least for these notes, the diagrams will all be computed assuming the initial conditions correspond effectively to the adiabatic linear growing mode. The simplest of such diagram is presented on Fig. 11. It corresponds to the ensemble average of $\langle \Psi_a(\mathbf{k}, \eta)\Psi_b(\mathbf{k}, \eta)\rangle$ and it makes intervene the linear power spectrum represented by $\otimes$. The previous construction can obviously be extended to any number of fields. The next diagrams will inevitably make intervene loops (in their diagram representation). One idea we will pursue here is to take advantage of such expansions to explore the density spectrum at 1-loop order and 2-loop order, also called at Next-to Leading Order and Next to Next to Leading Order (respectively NLO and NNLO).

A field representation of the nonlinear motion equations

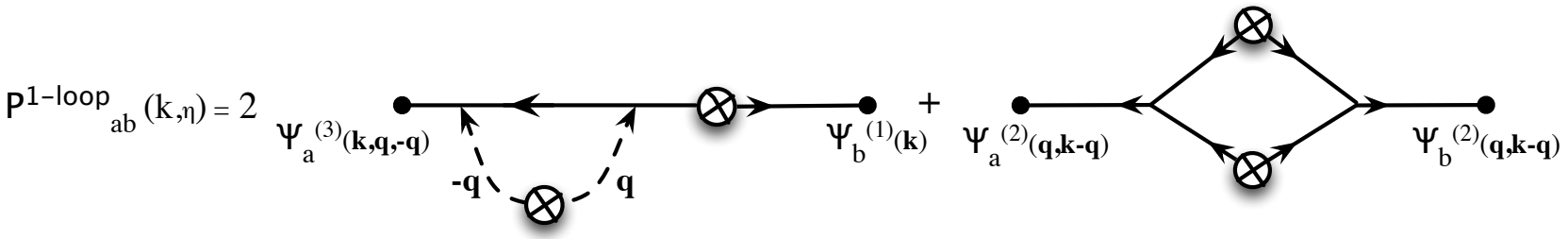

Figure: Diagrammatic representation of the 2 terms contributing to the power spectrum at one-loop order.

The 2 diagrams contributing to the power spectrum at NLO are shown on Fig. 12. The first calculation of such contributions were done in the 90's.

Scaling of solutions

It is interesting to compute the way subsequent orders in perturbation theory scale with the linear solution. As the vertices and the time integrations are both dimensionless operations, one can easily show that the $p-$th order expression of the density field is of the order of the power p of the linear density field. In other words, there are kernels functions $F_a^{(n)}$ such that

$$\begin{aligned}\Psi_a^{(p)}(\mathbf{k},\eta) &= \int \frac{\mathrm{d}\mathbf{k}_1}{(2\pi)^{3/2}} \cdots \frac{\mathrm{d}\mathbf{k}_p}{(2\pi)^{3/2}} \delta_{\mathrm{Dirac}}(\mathbf{k}-\mathbf{k}_{1\ldots p}) \\ &\times \mathcal{F}_a^{(p)}(\mathbf{k}_1,\ldots,\mathbf{k}_p;\eta)\delta_+(\mathbf{k}_1,\eta)\ldots\delta_+(\mathbf{k}_p,\eta) \quad (76)\end{aligned}$$

where $\delta_+(\mathbf{k}_i,\eta)$ is the linear growing mode for wave modes $\mathbf{k}_i$, $\mathbf{k}_{1\ldots p} = \mathbf{k}_1 + \cdots + \mathbf{k}_p$ and where $\mathcal{F}_a^{(p)}(\mathbf{k}_1,\ldots,\mathbf{k}_p;\eta)$ are dimensionless functions of the wave modes and are a priori time dependent.

Scaling of solutions

For an Einstein-de Sitter background, the functions $\mathcal{F}_a^{(p)}(\mathbf{k}_1, \ldots, \mathbf{k}_p; \eta)$ are actually time independent and in general depends only very weakly on time (and henceforth on the cosmological parameters.) The functions $\mathcal{F}_a^{(p)}$ are usually noted F_p and G_p for respectively $a = 1$ and $a = 2$. For instance it is easy to show that

$$F_2(\mathbf{k}_1, \mathbf{k}_2) = \frac{5}{7} + \frac{1}{2}\frac{\mathbf{k}_1 \cdot \mathbf{k}_2}{k_1^2} + \frac{1}{2}\frac{\mathbf{k}_1 \cdot \mathbf{k}_2}{k_2^2} + \frac{2}{7}\frac{(\mathbf{k}_1 \cdot \mathbf{k}_2)^2}{k_1^2\, k_2^2} \tag{77}$$

for an Einstein-de Sitter universe. For an arbitrary background the coefficient $5/7$ and $2/7$ are slightly altered but only very weakly.

Scaling of solutions

It can be noted that this kernel is very general and is actually directly observable. Indeed for Gaussian initial conditions the first non-vanishing contribution to the bi-spectrum is obtained when one, and only one, factor is written at second order in the initial field,

$$\langle \delta(\mathbf{k}_1)\delta(\mathbf{k}_2)\delta(\mathbf{k}_3)\rangle_c = \langle \delta^{(1)}(\mathbf{k}_1)\delta^{(1)}(\mathbf{k}_2)\delta^{(2)}(\mathbf{k}_3)\rangle_c + \text{sym.} \qquad (78)$$

and it is easy to show that it eventually reads

$$\begin{aligned} \langle \delta(\mathbf{k}_1)\delta(\mathbf{k}_2)\delta(\mathbf{k}_3)\rangle_c &= \delta_{\mathrm{Dirac}}(\mathbf{k}_1+\mathbf{k}_2+\mathbf{k}_3) \\ &\times \left[2\,F_2(\mathbf{k}_1,\mathbf{k}_2)P^{\mathrm{lin.}}(k_1)P^{\mathrm{lin.}}(k_2) + \text{sym.}\right] \end{aligned} \qquad (79)$$

where sym. refers to 2 extra terms obtained by circular changes of the indices. The important consequence of this form is that the bispectrum therefore scales like the square of the power spectrum.

Scaling of solutions

In particular the reduced bispectrum defined as

$$Q(\mathbf{k}_1, \mathbf{k}_2, \mathbf{k}_3) = \frac{B(\mathbf{k}_1, \mathbf{k}_2, \mathbf{k}_3)}{P(k_1)P(k_2) + P(k_2)P(k_3) + P(k_3)P(k_1)} \tag{80}$$

is expected to have a time independent amplitude at early time.

Scaling of solutions

More generally, the connected p-point correlators at lowest order in perturbation theory scale like the power $p-1$ of the 2-point correlators: it comes from the fact that in order to connect p points using the Wick theorem one needs at least $p-1$ lines connecting a product of $2(p-1)$ fields taken at linear order. For instance the local $p-$order cumulant of the local density contrast $\langle \delta^p \rangle_c$ scales like,

$$\langle \delta^p \rangle_c \sim \langle \delta^2 \rangle^{p-1}. \tag{81}$$

In the last sections of these notes, more detailed presentation of these relations will be given.

Scaling of solutions

Other consequences of these scaling results concern the p-loop corrections to the power spectrum. Indeed one expects to have

$$P^{\mathrm{p-loop}}(k) \sim P^{\mathrm{lin.}}(k) \left[\int \frac{\mathrm{d}q}{q}\, q^3 P(q)\right]^p . \tag{82}$$

At least that would be the case if the linear power spectrum peaked at wave modes about k. This is not necessarily the case. In the following we explore the mode coupling structure, i.e. how modes q are contributing to the corrective terms to the power spectrum depending on whether they are much smaller (infrared domain) or much larger (ultra-violet domain) than k.

Time flow equations

Although in this presentation we will focus on the diagrammatic representation of the motion equations, and their integral form, there exists an alternative set of differential equations that gives the time dependence of the multi-point spectra. These equations form a hierarchy and we will give here the first two. The evolution equation (73) indeed allows to compute the time derivative of products such as $\Psi_a(\mathbf{k},\eta)\Psi_b(\mathbf{k}',\eta)$ or $\Psi_a(\mathbf{k}_1,\eta)\Psi_b(\mathbf{k}_2,\eta)\Psi_c(\mathbf{k}_3,\eta)$.

Time flow equations

After taking their ensemble averages, it leads respectively to the following equations,

$$\frac{\partial}{\partial\eta}P_{ab}(\mathbf{k},\eta)+\Omega_a^c(\mathbf{k}\,,\eta)P_{cb}(\mathbf{k},\eta)+(a\leftrightarrow b)= \tag{83}$$
$$+\int d^3q\,\left[\gamma_a^{cd}(-\mathbf{q},\mathbf{q}-\mathbf{k})\,B_{bcd}(\mathbf{k},\,-\mathbf{q},\,\mathbf{q}-\mathbf{k};\eta)+(a\leftrightarrow b)\right],$$

and

$$\frac{\partial}{\partial\eta}B_{abc}(\mathbf{k},\,-\mathbf{q},\,\mathbf{q}-\mathbf{k};\eta)$$
$$+\Omega_a^d(\mathbf{k}\,,\eta)B_{dbc}(\mathbf{k},\,-\mathbf{q},\,\mathbf{q}-\mathbf{k};\eta)+(a\leftrightarrow b,c)= \tag{84}$$
$$2\left[\gamma_a^{de}(-\mathbf{q},\mathbf{q}-\mathbf{k})P_{db}(\mathbf{q}\,,\eta)P_{ec}(\mathbf{k}-\mathbf{q},\eta)+(a\leftrightarrow b,c)\right],$$

where in the latter equation the connected parts of the four-point correlators have been dropped.

LSS at NLO and NNLO

- Not a quantum field theory problem...

- The system is not invariant over time translation: it is actually an unstable (non-equilibrium) system, where perturbations grow with time (as ~ power-law). The late time behavior is not known.

- Loop corrections are not due to virtual particle productions but to mode couplings effects, modes being set in the initial conditions.

- Vertices have a non-trivial k-dependence but which is entirely due to the conservation equation and is independent of the energy content of the universe. Only $2 \rightarrow 1$ vertices exist (quadratic couplings). This is not the case generically for modified gravity models (like f(R), ...)

- Due to the shape of CDM spectrum, there are no strict UV divergences (nor IR). Loops are all finite (no need for "renormalization" per se) although UV contributions are not well controlled.

- More closely related to hydrodynamical turbulence

A symmetry: the extended Galilean invariance

Also known in the context of the Navier-Stokes equations for an incompressible fluid (Pope 2000)

More explicitly the motion equations are invariant under the following transformations,

$$x_i \to x_i - s_i(\eta), \quad u_i \to u_i + \frac{\mathrm{d}}{\mathrm{d}\eta} s_i(\eta),$$

then motion equations are unchanged and propagator becomes,

$$g_a{}^b(\eta, \eta') \to g_a{}^b(\eta, \eta') \exp\left(\mathrm{i}\mathbf{k}.[\mathbf{s}(\eta) - \mathbf{s}(\eta')]\right)$$

Richer than mere Galilean invariance !

As a consequence, there are Ward identities

$$\lim_{q \to 0} B(\mathbf{q}, \mathbf{k}, -\mathbf{k} - \mathbf{q}; \eta, \eta', \eta'') \quad =$$

$$-\frac{\mathbf{q}.\mathbf{k}}{q^2} P^{\mathrm{lin.}}(q; \eta, \eta) \, P^{\mathrm{lin.}}(k; \eta', \eta'') \left(e^{\eta' - \eta} - e^{\eta'' - \eta}\right)$$

Kehagias and Riotto 2013; Peloso and Pietroni 2013; Creminelli et al. 2013

The infrared domain and the eikonal approximation

On of the reason for exploring the mode coupling structure is that the vertices ${\gamma_a}^{bc}(\mathbf{k}_1, \mathbf{k}_2)$ can be large when the ratio k_1/k_2 (or its inverse) gets large. We will see that it corresponds to contributions coming from the infrared (IR) domain.

The IR behavior for the 1-loop corrections to the power spectrum

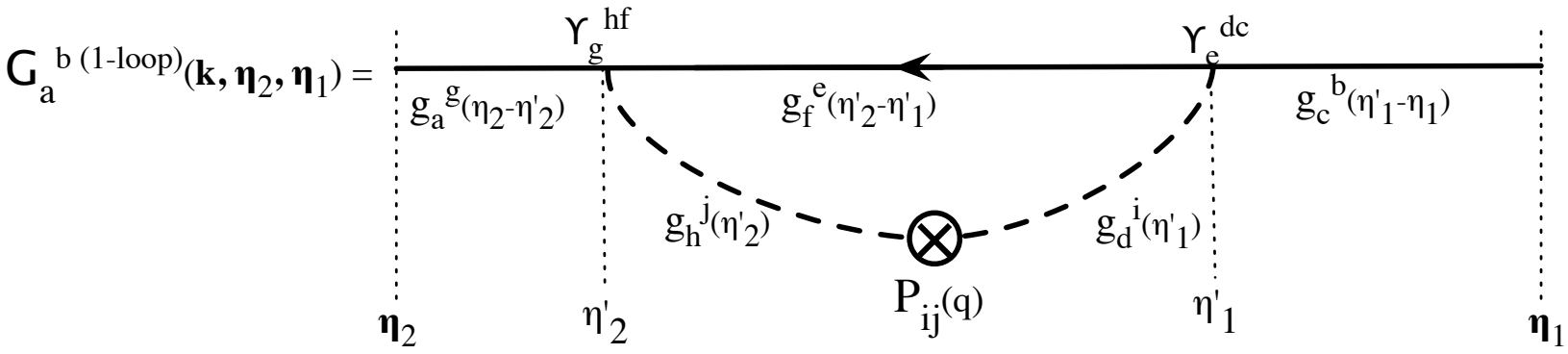

Figure: The one-loop correction diagram to the propagator.

Let us first consider the one-loop correction to the power spectrum. We want to compute the amplitude of the one-loop correction when the wave mode that circulates in the loop **q** is much smaller than the mode of interest, **k**.

The IR behavior for the 1-loop corrections to the power spectrum

Let us consider more specially the left diagram appearing on Fig. 12 which is partly reproduced in more detail on Fig. 13. In this approximation the incoming modes from the loop are either $\mathbf{q}$ or $-\mathbf{q}$. As one assumes $q \ll k$, the modes on the horizontal line is always $\mathbf{k}$. We can then compute the expression of each of the vertices. The one on the right (at time η_1') then reads,

$$\gamma_e{}^{dc} \approx \frac{1}{2}\frac{\mathbf{q}.\mathbf{k}}{q^2}\ \delta_e^c\ \delta_2^d\ \delta_{\mathrm{Dirac}}(\mathbf{k}-\mathbf{k}_1). \tag{85}$$

The IR behavior for the 1-loop corrections to the power spectrum

Anticipating the next paragraph we can call this the eikonal limit of the vertex. We note two key properties: it is diagonal in the c and e indices (of the main line) and it selects only the second component of the incoming waves. The value of the other vertex can be similarly evaluated,

$$\gamma_g^{hf} \approx -\frac{1}{2}\frac{\mathbf{q}.(\mathbf{k}+\mathbf{q})}{q^2}\,\delta_g^f\,\delta_2^h\,\delta_{\mathrm{Dirac}}(\mathbf{k}-\mathbf{k}_1) \approx -\frac{1}{2}\frac{\mathbf{q}.\mathbf{k}}{q^2}\,\delta_g^f\,\delta_2^h\,\delta_{\mathrm{Dirac}}(\mathbf{k}-\mathbf{k}_1). \tag{86}$$

The actual computation of the diagram then requires to

- sum over all internal indices;
- integrate the intermediate time variables, η_1' and η_2', over adequate intervals;
- integrate over the angle between $\mathbf{q}$ and $\mathbf{k}$.

The IR behavior for the 1-loop corrections to the power spectrum

The first step is now easy to perform and relies on generic properties of Green functions; the algebraic structure along the **k**-line indeed reads

$$\begin{aligned} g_a{}^g(\eta_2-\eta_2')\,\delta_g^f\,g_f{}^e(\eta_2'-\eta_1')\,\delta_e^c\,g_c{}^b(\eta_1'-\eta_1) \\ &= g_a{}^f(\eta_2-\eta_2')\,g_f{}^c(\eta_2'-\eta_1')\,g_c{}^b(\eta_1'-\eta_1) \\ &= g_a{}^b(\eta_2-\eta_1). \end{aligned} \tag{87}$$

The integration over the relative angle between **q** and **k** can then be done straightforwardly:

$$\int \mathrm{d}^3\mathbf{q}\frac{(\mathbf{q}.\mathbf{k})^2}{q^4} = \frac{4\pi}{3}\int q^2\mathrm{d}q\frac{k^2}{q^2}. \tag{88}$$

The IR behavior for the 1-loop corrections to the power spectrum

We can now insert this result into the first diagram of Fig. 12. It leads to

$$P_{ab}^{1-loop,\#1}(k) = P_{ab}^{\mathrm{lin.}}(k)\left[1 - k^2\sigma_d^2\right] \tag{89}$$

with

$$\sigma_d^2(\eta) = \frac{4\pi}{3}\int \mathrm{d}q\,(e^{\eta} - e^{\eta_0})^2\; P_{22}^{\mathrm{lin.}}(q) \tag{90}$$

if the incoming velocity modes are the in linear growing mode. σ_d can easily be interpreted as the r.m.s. of the 1D displacement field.

The IR behavior for the 1-loop corrections to the power spectrum

A very similar calculation can be done for the second diagram of Fig. 12. Using the same approximation one gets

$$P_{ab}^{1-loop,\#2}(k) = P_{ab}^{\mathrm{lin.}}(k)\left[1 + k^2\sigma_d^2\right] \tag{91}$$

and the two contributions actually cancel[3]. This cancellation was first noted by [**?**] and by [**?**]. In the following we explicitly show how it can be extended to all orders in perturbation theory with the help of the so called eikonal approximation (introduced in [**?**]).

[3] The actual calculations should be done with care in particular for a correct determination of the symmetry factors.

Methods of Field Theory

Standard PT: a series expansion in field values *FB et al. 2002*

Renormalization Perturbation Theory *Crocce & Scoccimarro '05, 06*

Inspired by hydro turbulence resummation schemes, see L'vov & Procaccia '95

Time-flow (renormalization) equations *M. Pietroni '08* *Anselmi & Pietroni '12*

From the field evolution equation to the multi-spectra evolution equation

The closure theory (=Large N expansion)

Taruya & Hiramatsu, ApJ 2008, 2009 *Valageas P., A&A, 2007*

Motion equations for correlators are derived using the Direct-Interaction (DI) approximation in which one separates the field expression in a DI part and a Non-DI part. At leading order in Non-DI >> DI, one gets a closed set of equations,

The eikonal approximation *FB, Van de Rijt & Vernizzi 2012*

Effective Theory approaches *Pietroni et al '12, Carrasco et al. '12*

A series reorganization: the multipoint propagator expansion

The key ingredients : the (multipoint) propagators

Scoccimarro and Crocce PRD, 2005

Final density / velocity div.

$$G_{ab}(k,\eta)\ \delta_{\rm D}(\mathbf{k}-\mathbf{k}') \equiv \left\langle \frac{\delta\Psi_a(\mathbf{k},\eta)}{\delta\phi_b(\mathbf{k}')} \right\rangle$$

Initial Conditions

$$G_{ab}(k) =$$

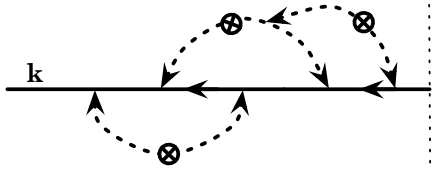

FB, Crocce, Scoccimarro, PRD, 2008

$$\Gamma^{(p)}_{ab_1\dots b_p}(\mathbf{k}_1,\dots,\mathbf{k}_p,\eta)\delta_{\rm D}(\mathbf{k}-\mathbf{k}_{1\dots p}) = \frac{1}{p!}\left\langle \frac{\delta^p\Psi_a(\mathbf{k},\eta)}{\delta\phi_{b_1}(\mathbf{k}_1)\dots\delta\phi_{b_p}(\mathbf{k}_p)} \right\rangle$$

$\Gamma^{(n)}(k,p_1,\dots,p_n)=$

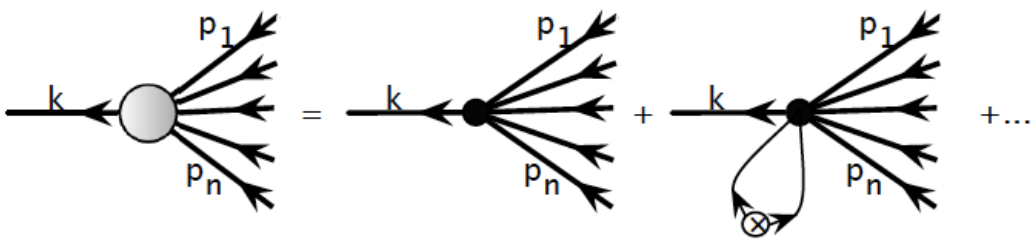

$$\Gamma^{(2)}_{abc}(\mathbf{k}_1,\mathbf{k}_2,\mathbf{k}_3) =$$

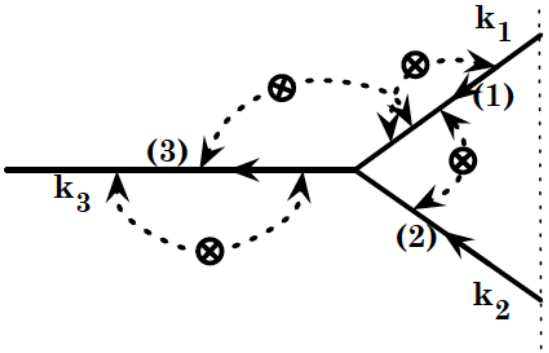

- This suggests another scheme: to use the n-point propagators as the building blocks

FB, Crocce, Scoccimarro, PRD, 2008

  - The reconstruction of the power spectrum :

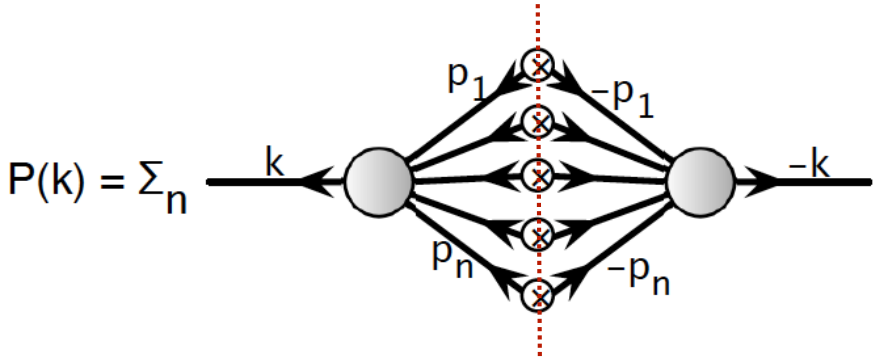

FIG. 3: Reconstruction of the power spectrum out of transfer functions. The crossed circles represent the initial spectrum. The sum runs over the number of internal co ing lines, e.g. the number of such circles. It is to be that each term of this sum is positive.

→ *Sum of positive terms*

  - Also provide the building blocks for higher order moments...

$B(k_1,k_2,k_3) = \Sigma_{r,s,t}$

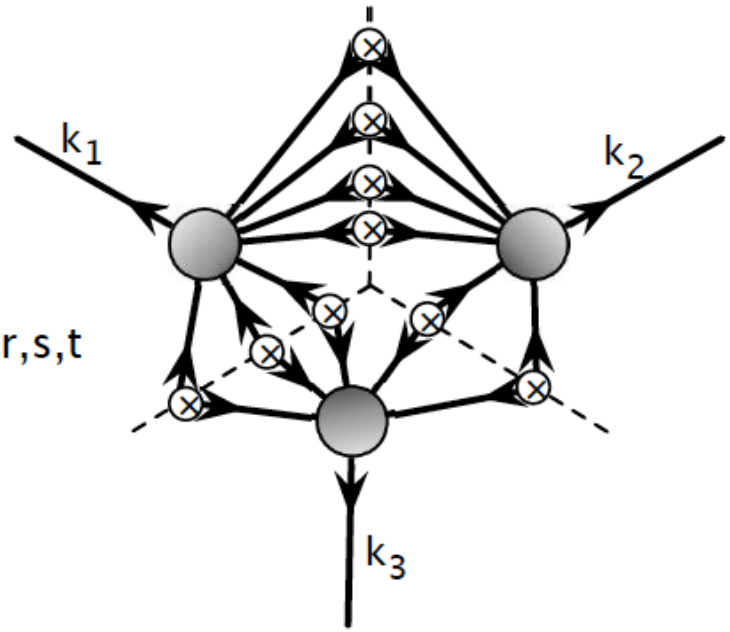

Γ-*expansion method*

- ***re-organisation(s) of the perturbation series***

- *Not a single way of doing (S)PT calculations*
  - *change of variables or fields : most dramatic is Eulerian to Lagrangian*
  - *re-organisation(s) of the perturbation series (for instance with multipoint propagators introduced in FB, Crocce, Scoccimarro, PRD, 2008)*
  - *PT can then come in many different flavors : SPT, RPT, TRG, RegPT, gRPT, MPT*

The RPT formulation

We are now in position to give the explicit form of the RPT proposition described by [**?**] [**?**]. It is based on the construction of the propagator $G_a{}^b(k,\eta)$ that encompasses both its full one-loop correction and the effect of the long-wave modes computed at all orders. The explicit form adopted in the original paper is too cumbersome to be re-derived here in detail but a form that shares its properties can easily be obtained. The impact of the long-wave modes can indeed be all incorporated with the help of the eikonal approximation where the "naked' Green function, $g_a{}^b(\eta,\eta')$, is transformed into the "dressed" one, $\xi_a{}^b(\eta,\eta')$. Then armed with the results from Section 73 we can first compute the ensemble average of $\xi_a{}^b(\mathbf{k},\eta)$ with respect to the long-wave modes.

The RPT formulation

When those modes are assumed to be in the linear regime and therefore to be Gaussian distributed, the use of the relation (70), leads to,

$$\langle \xi_a{}^b(\mathbf{k},\eta)\rangle = g_a{}^b(\eta,\eta')\,\exp\left[-\frac{1}{2}k^2\sigma_d^2(\eta,\eta')\right], \tag{113}$$

where $\sigma_d(\eta,\eta')$ is given by,

$$\sigma_d^2(\eta,\eta') = \frac{1}{3}\langle \mathbf{d}^2(\eta,\eta')\rangle = (e^{\eta}-e^{\eta'})^2 \int \frac{\mathrm{d}^3\mathbf{q}}{3q^2}\, P^{\mathrm{lin.}}(q). \tag{114}$$

The RPT formulation

This resummation result is the key result on which the RPT scheme is based. It is furthermore possible to include the full contribution of the one-loop contribution as given by the diagram of Fig. 13. Indeed this diagram itself can be computed within the eikonal framework and it leads to

$$G_a^{1-\mathrm{loop}\,b}(\mathbf{k},\eta,\eta') \to G_a^{1-\mathrm{loop}\,b}(\mathbf{k},\eta,\eta')\ \exp(\mathrm{i}\mathbf{k}.\mathbf{d}(\eta,\eta')) \qquad (115)$$

the ensemble average of which over the long-wave modes can also be taken. A possible global form in then the following [**?**],

$$\begin{aligned} G_a^{\mathrm{reg}\,b}(k,\eta_f,\eta_i) \;=\; & \Big[g_a{}^b(\eta,\eta') + \delta G_a^{1-\mathrm{loop}\,b}(k,\eta,\eta') \\ & + \frac{1}{2}k^2\sigma_d^2(\eta,\eta')g_a{}^b(\eta,\eta')\Big] \\ & \times \exp\left(-\frac{k^2\sigma_d^2(\eta,\eta')}{2}\right), \end{aligned} \qquad (116)$$

which has the expected behavior for both the large k and in the low k domains.

The two-point propagator at 1-loop and 2-loop orders

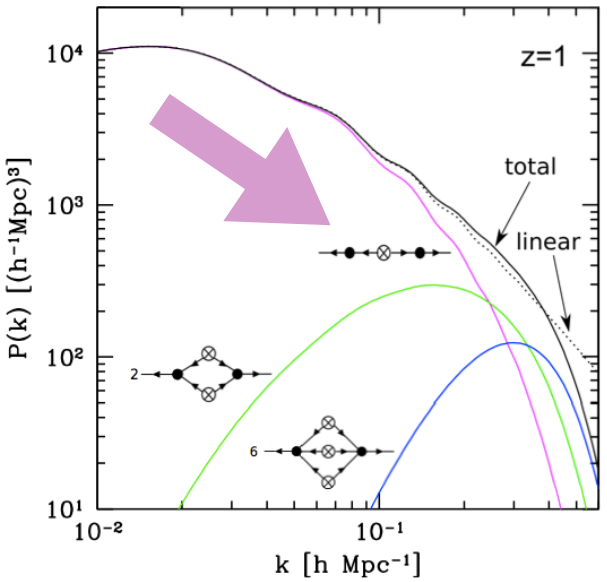

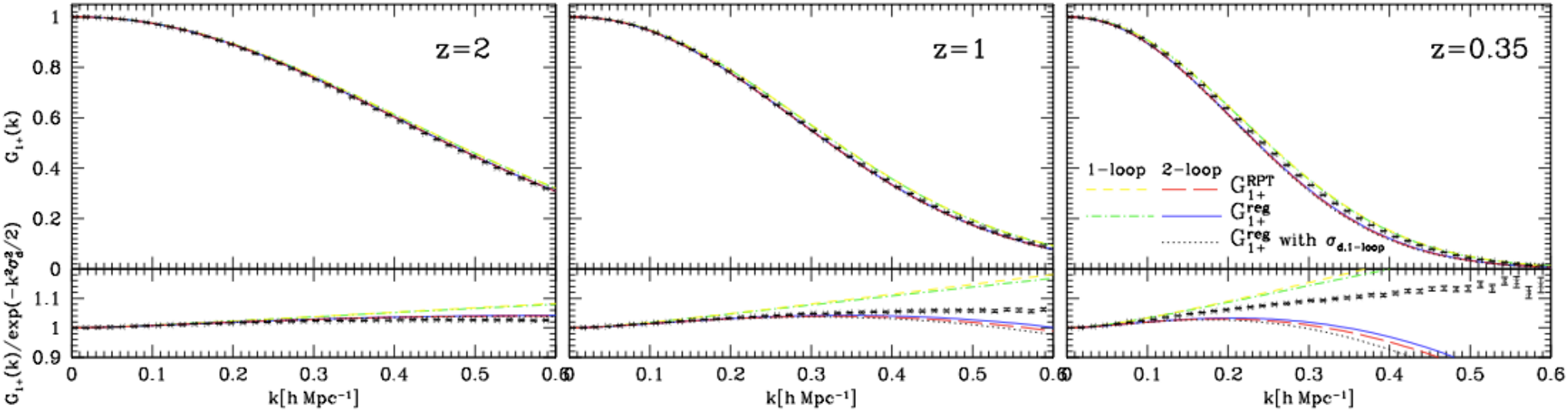

The RPT formulation

Other resummation schemes, MPTbreeze [**?**] and RegPT [**?**] proposed afterwards take full advantage[7] of the $\Gamma-$expansion presented in the previous section. It is based on a similar construction to (116) applied to the $p-$point propagator. More specifically the following form can be used,

$$\begin{aligned}\Gamma_a^{\mathrm{reg}\, b_1\ldots b_p}(\mathbf{k}_1,\ldots,\mathbf{k}_p,\eta,\eta') \;=\; & \\ & \Big[\Gamma_a^{\mathrm{tree} b_1\ldots b_p}(\mathbf{k}_1,\ldots,\mathbf{k}_p,\eta,\eta')+\delta\Gamma_a^{1-\mathrm{loop} b_1\ldots b_p}(\mathbf{k}_1,\ldots,\mathbf{k}_p,\eta,\eta') \\ & +\frac{1}{2}k^2\sigma_d^2(\eta,\eta')\Gamma_a^{\mathrm{tree}\;\; b_1\ldots b_p}(\mathbf{k}_1,\ldots,\mathbf{k}_p,\eta,\eta')\Big] \\ & \exp\left(-\frac{k^2\sigma_d^2(\eta,\eta')}{2}\right) \end{aligned} \tag{117}$$

where $k=|\mathbf{k}_1+\cdots+\mathbf{k}_p|$.

[7] They also have the advantage to be faster to compute.

Comparison with numerical simulations at tree and one-loop order for the 3-point propagator

FB, Crocce, Scoccimarro '12

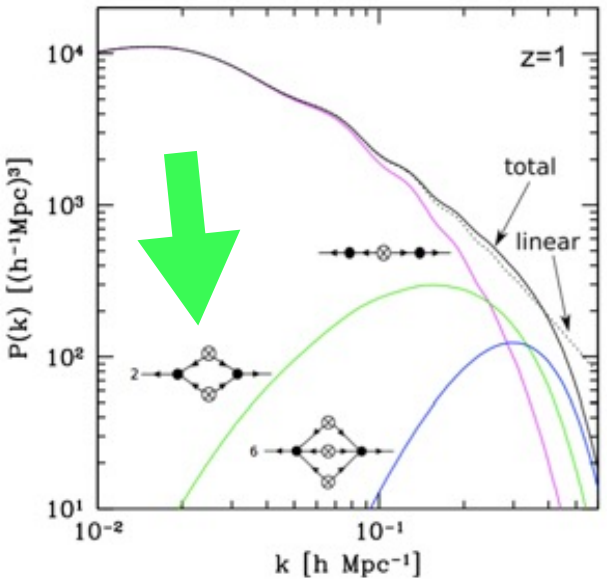

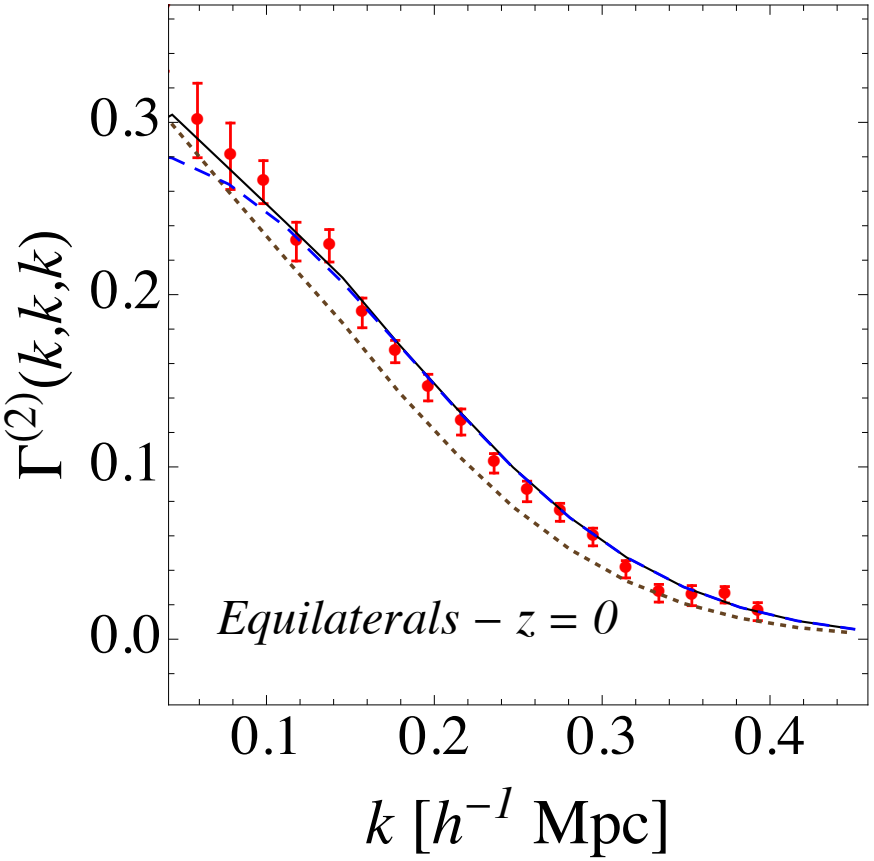

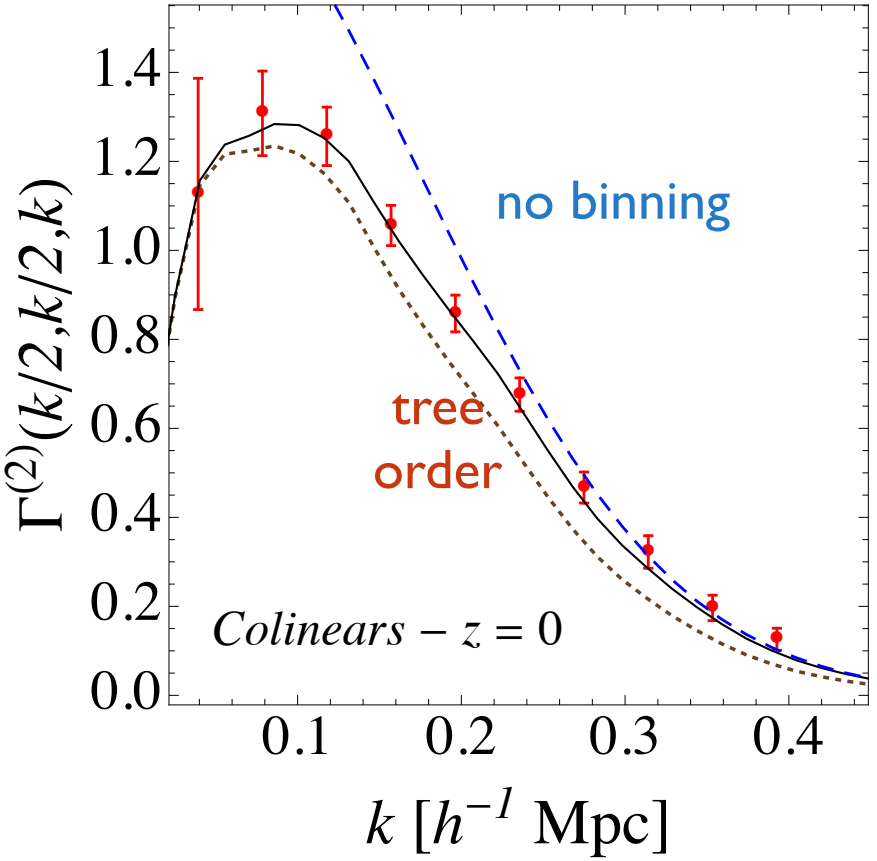

The performances of perturbation theory at NNLO

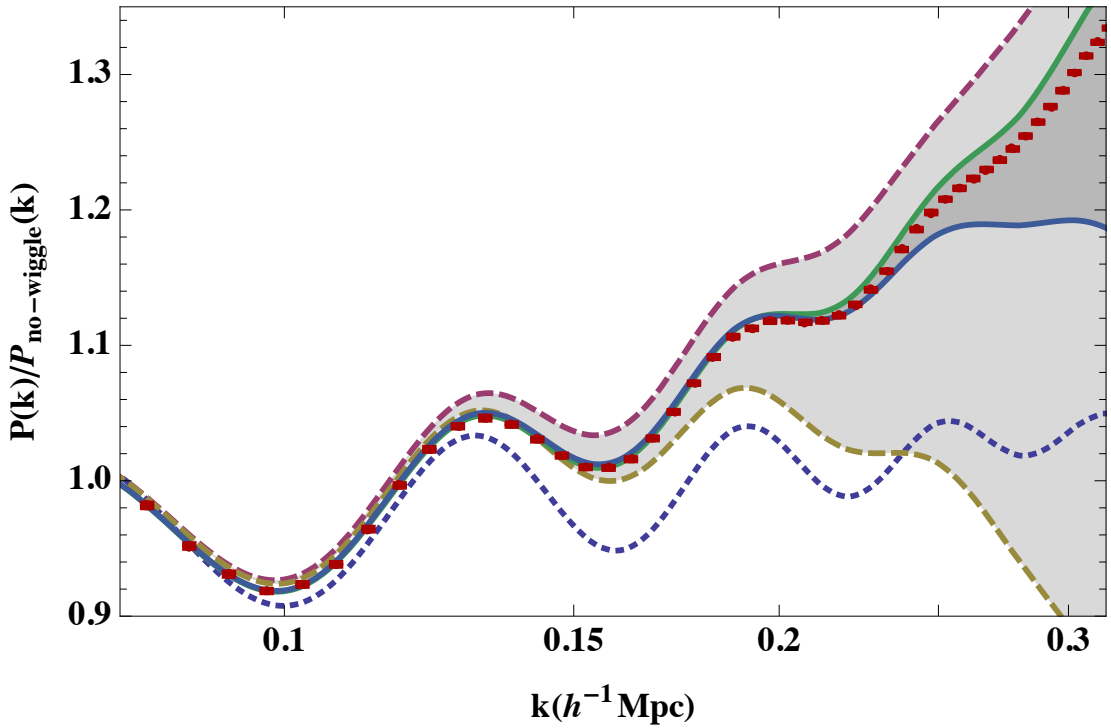

Figure: Comparison of PT results with $N-$body results for the power spectrum at $z = 1$. The dotted line is the linear prediction; the dashed lines are the standard PT and RegPT NLO predictions and the solid lines the NNLO predictions. The grey area show the departure between these predictions at one-loop order (light grey) and 2-loop order (darker grey).

Power spectra up to 1-loop and 2-loop order

Taruya , FB, Nishimichi, Codis '12 *Crocce, Scocimarro, FB, '12*

1st computation of 2-loop order effects in *Okamura, Taruya, Matsubara, '11*

- Public codes for fast computations of power spectra at 2-loop order are now available.

`http://maia.ice.cat/crocce/mptbreeze/`

`http://www-utap.phys.s.u-tokyo.ac.jp/~ataruya/regpt_code.html`

- Theoretical predictions are within 1% accuracy.

The RPT formulation

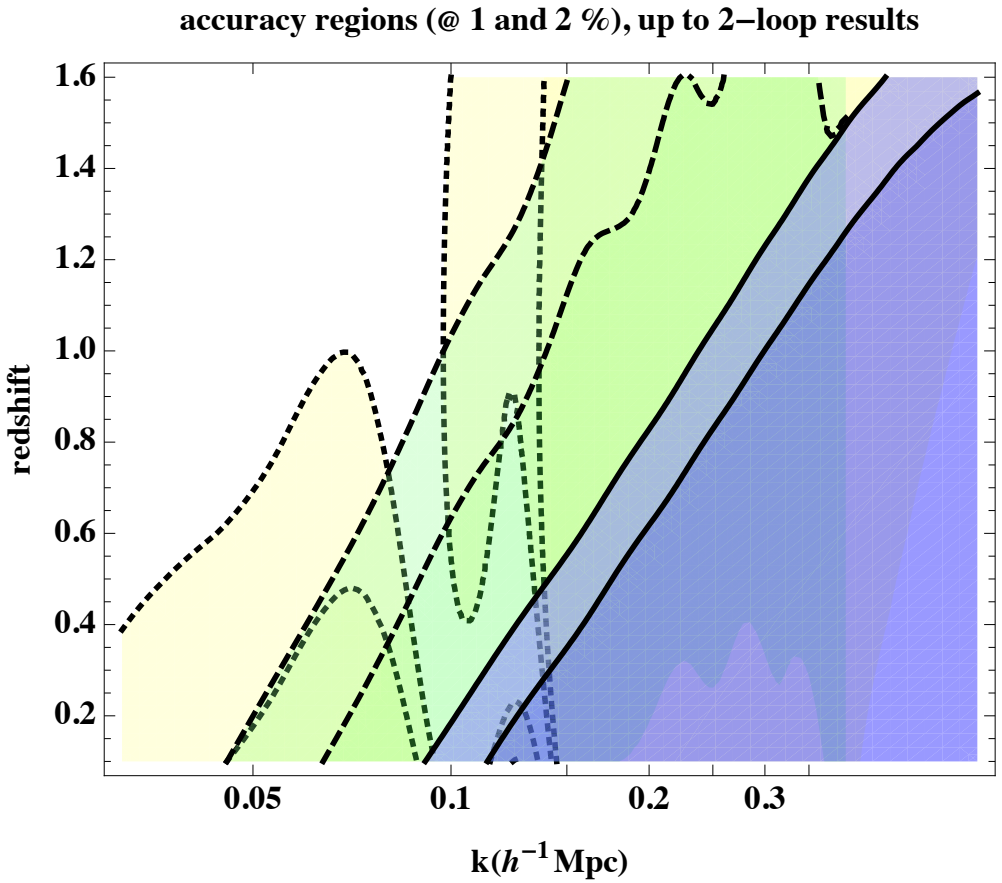

Figure: A tentative chart of the accuracy domain of the PT results with contour plots of the 1 and 2% accuracy region for the linear, NLO, and NNLO predictions for the power spectrum. The calculations have been made for the WMAP5 cosmological parameters.

Performances in real and redshift space

A. Taruya, T. Nishimichi, F. B. '13

The BAO wiggle in real space

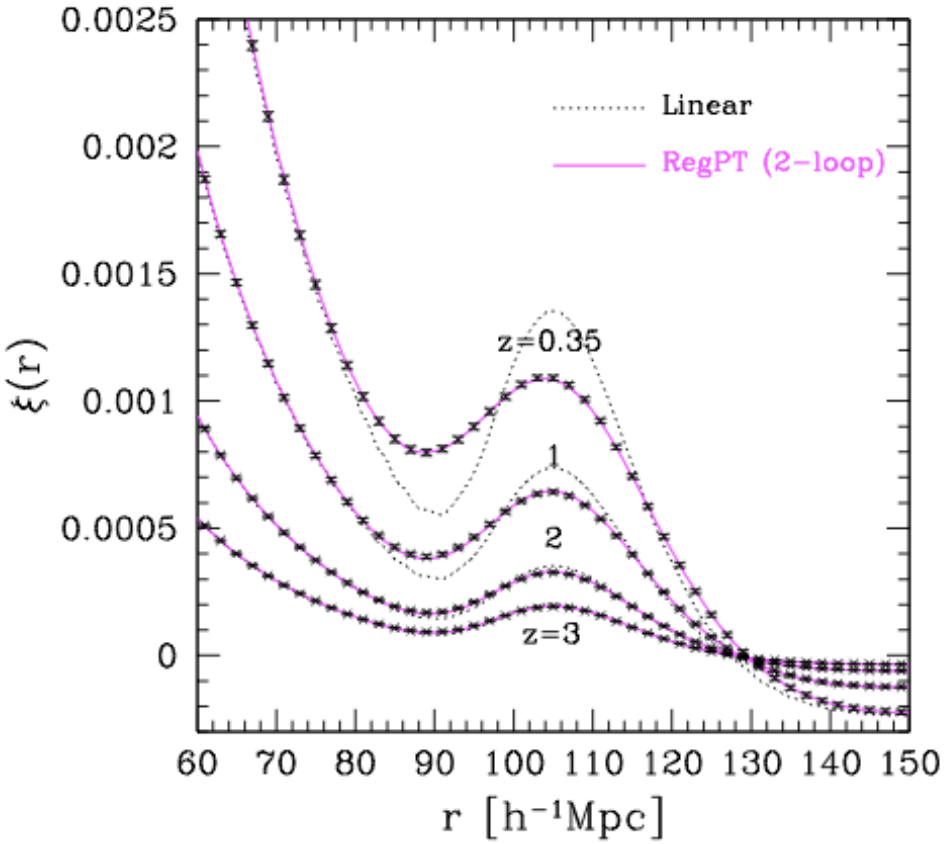

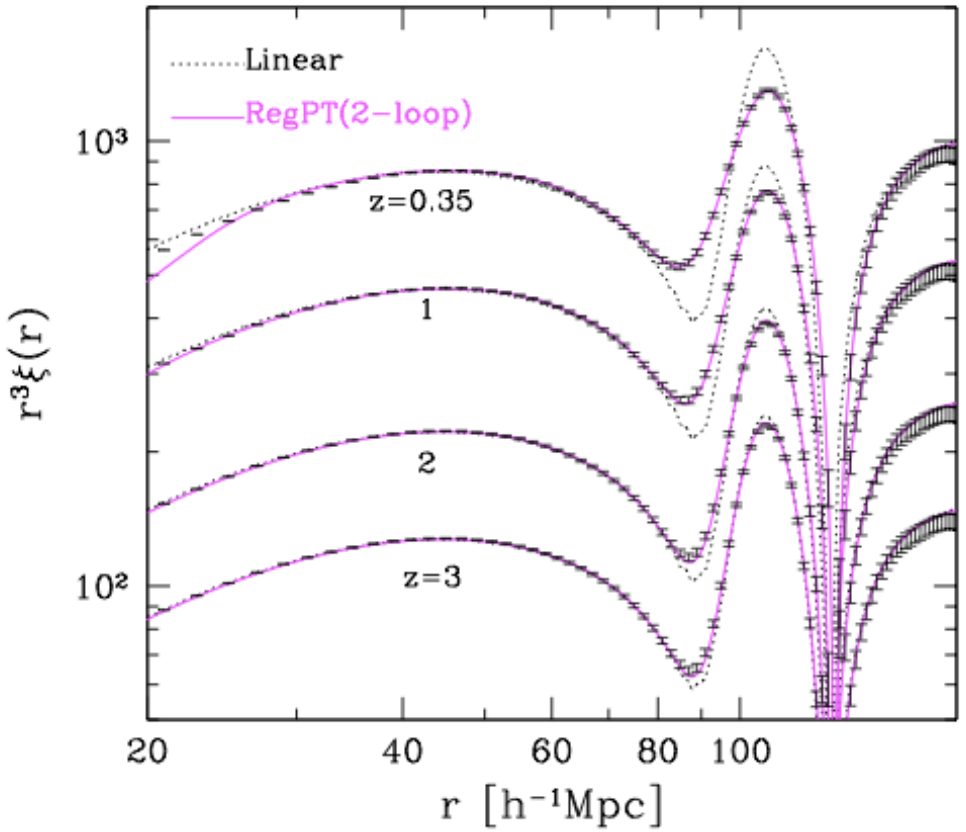

very good thanks to regularization

The BAO wiggle in z space

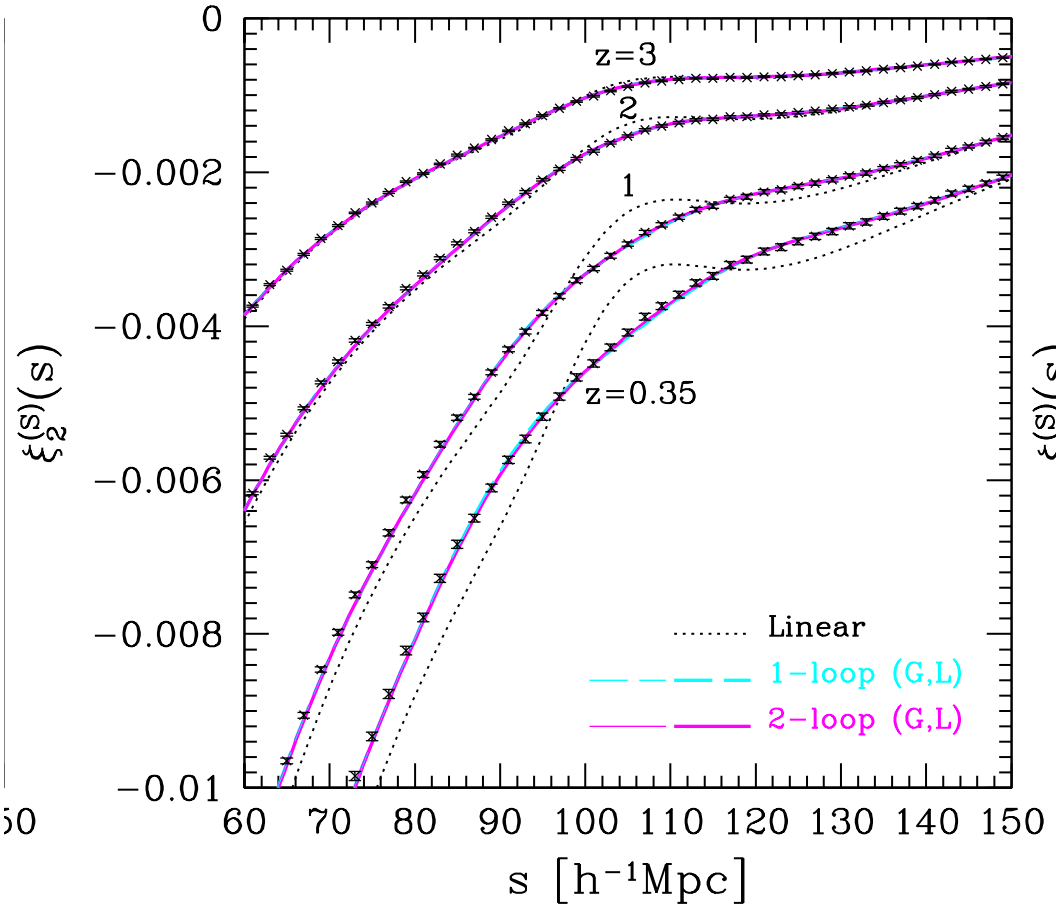

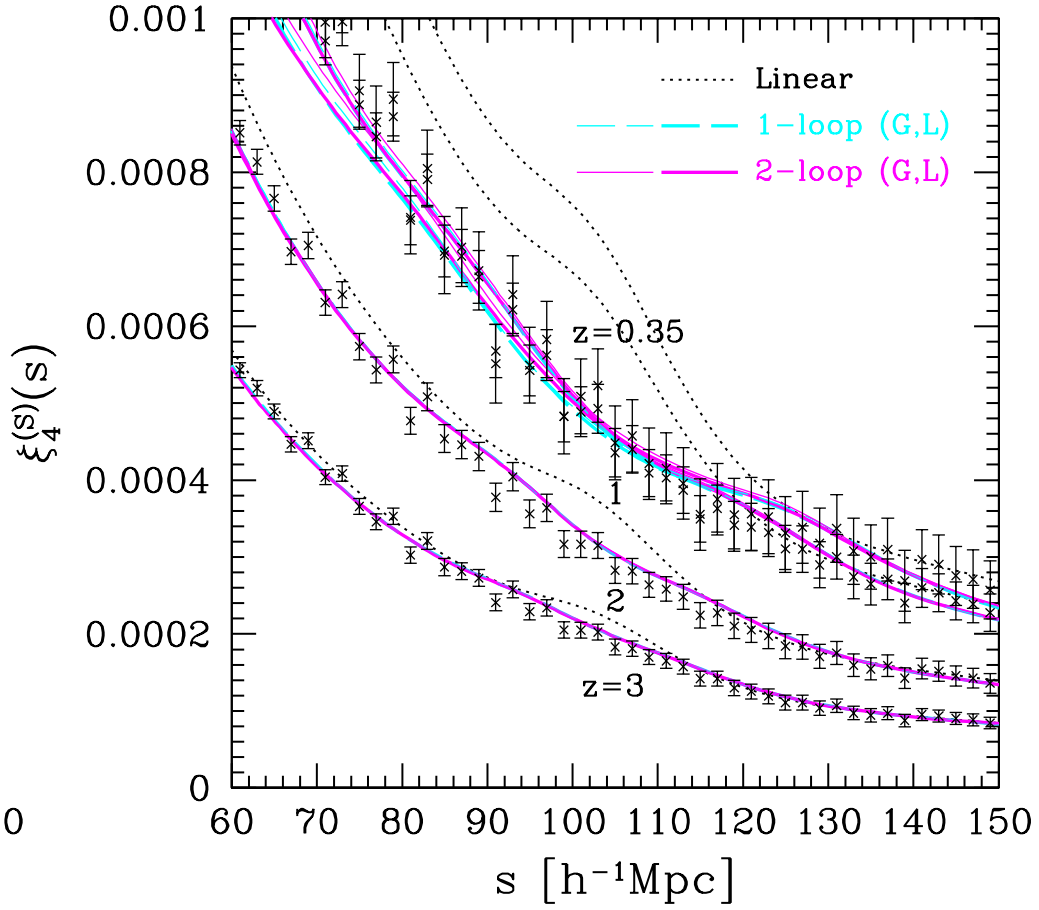

running RegPT :

- RegPT code available at (with Readme file)
  `http://www-utap.phys.s.u-tokyo.ac.jp/~ataruya/regpt_code.html`

```
fbernard@joola2(~/PTWhiz/RegPT)> ./RegPT RegPT.ini -direct
 ------------------------------------------------------------------------------
 :  RegPT up to 2 loop order for P(k) and Xi(r)                               :
 ------------------------------------------------------------------------------
 : Description of the online options:                                         :
 :  "-noverbose", to suppress verbose                                         :
 :  "-verbose" nn, to set verbose level at nn (default=1)                     :
 :                                                                            :
 :  "-path" aaa, access path to input and ouput files  (default =./)          :
 :  "-spectrum" bbb, prefix filename for input file, "bbb_spectrum.dat", that :
 :           contains 2 columns "k, P(k)", and output files,                  :
 :           "bbb_pk_RegPT.dat", "bbb_xi_RegPT.dat" and "bbb_st_PT.dat".      :
 :           Default for "bbb" is nil.                                        :
 :  "-camb" aaa, to use CAMB ouput "aaa_params.ini" for cosmological parameters:
 :           and "aaa_transfer_out.dat" for transfer functions (unless        :
 :           overridden by aaa_params.ini option content.). Output files will :
 :           be "aaa_xxx.dat".                                                :
 :                                                                            :
 :  "-sigma8" xxx, to specify value of sigma8, 0. to left it unchanged from   :
 :           file, (default=0.817)                                            :
 :  "-omegam" xxx, to specify the value of Omega_m (default=.279)             :
 :  "-omegab" xxx, to specify the value of Omega_b (default=.046)             :
 :  "-ns" xxx, to specify the value of ns (default=.96)                       :
 :  "-h" xxx, to specify the value of h (default=.70)                         :
 :    Note that spatial curvature is forced to be flat, i.e.                  :
 :    Omega_DE=1-Omega_m. ns, Omega_b, and h are only used to compute the     :
 :    no-wiggle power spectrum whereas Omega_m determines the growth rate.    :
 :                                                                            :
 :  "-direct1loop"  to use direct method for 1-loop ca                        :
 :  "-direct" to use fast AND direct method                                    :
 :  "-fast" to use fast method only (default choice)                           :
 :  "-datapath" xxx, to specify the path access to the data files of the      :
 :           fiducial models (default = "data/")                              :
 :  "-fiducial" aaa, to impose fiducial model, computer choice by default     :
 :  "-nz" nn z1 z2..., to specify the number of redshifts (default=1, z=0.5)  :
 :  "-xicompute", to compute 2-pt correlation functs (not done by default)    :
 :----------------------------------------------------------------------------:

    Execution log :

> linear matter power spectrum: testcamb/matterpower_zred1.dat
             kmin=8.56173665E-06
             kmax=1.00924969E+01
             ik_max=1399
> sigma8 in file: 0.503
             set to sigma8 = 0.850
> wave modes are  1.01% apart in testcamb/matterpower_zred1.dat
> output spacing is set such that k are 3% apart
             computation will be done every 3 input value
> selected fiducial model
  (from "wmap3", "M001", "M023"): M023
             sigma8_boost=  1.2756276704E+00
> Load matter power spectrum (fiducial model):
             data/matterpower_M023.dat
> Load RegPTmain data (for fiducial model):
             data/pkcorr_Gamma1_M023.dat
             data/pkcorr_Gamma2_M023.dat
```

Content of xxx_stfile.dat

wave-mode (k)

$P_{no\text{-}wiggle}(k)$

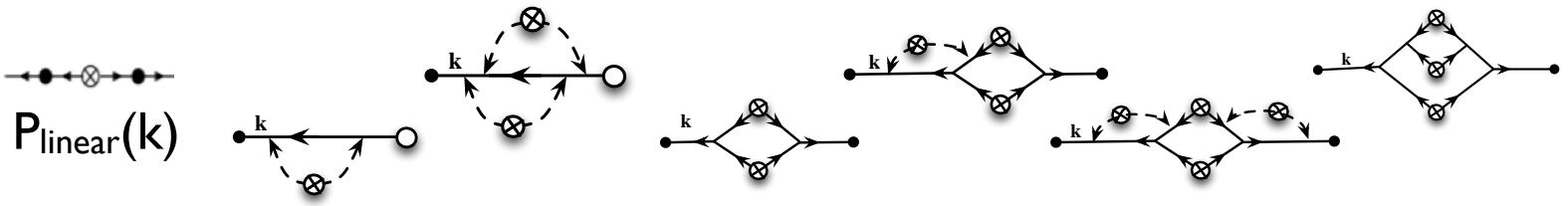

$P_{linear}(k)$

1.0144817830E-01	2.0387050508E+04	6.9105077219E+03	-2.2052776546E-01	-1.9951054829E-03	3.7251318142E+03	-1.6249293008E+03	1.7869663561E+02	9.2124530023E+02
1.0453771050E-01	1.9505944016E+04	6.6993885628E+03	-2.3529377049E-01	-2.9556933755E-04	3.7969911856E+03	-1.7676994171E+03	2.0738538436E+02	1.0108625940E+03
1.0772132870E-01	1.8652142157E+04	6.4432293741E+03	-2.5103577798E-01	1.7584438015E-03	3.8894975406E+03	-1.9326415613E+03	2.4188641911E+02	1.1086388409E+03
1.1100190130E-01	1.7825505895E+04	6.1361706425E+03	-2.6781719793E-01	4.2227480312E-03	3.9538724706E+03	-2.0968344743E+03	2.7998821833E+02	1.2115787174E+03
1.1438249050E-01	1.7025824509E+04	5.7839583922E+03	-2.8570607978E-01	7.1612796151E-03	4.0313439249E+03	-2.2814710789E+03	3.2496905433E+02	1.3244591153E+03
1.1786592750E-01	1.6252917128E+04	5.4003705122E+03	-3.0477302150E-01	1.0646798089E-02	4.1065888246E+03	-2.4796233542E+03	3.7669422095E+02	1.4430393697E+03
1.2145544590E-01	1.5506485545E+04	5.0043383250E+03	-3.2509475843E-01	1.4762671195E-02	4.1600263138E+03	-2.6795093896E+03	4.3408185335E+02	1.5721662740E+03
1.2515439090E-01	1.4786193442E+04	4.6192017592E+03	-3.4675293445E-01	1.9604087891E-02	4.2272664956E+03	-2.9036545448E+03	5.0147100732E+02	1.7076596671E+03
1.2896588440E-01	1.4091728788E+04	4.2701703361E+03	-3.6983235165E-01	2.5279152287E-02	4.2662915379E+03	-3.1245973459E+03	5.7522308434E+02	1.8570087787E+03
1.3289344310E-01	1.3422685934E+04	3.9771206600E+03	-3.9442483472E-01	3.1911466678E-02	4.3062942093E+03	-3.3622368200E+03	6.5969493814E+02	2.0209152392E+03
1.3694061340E-01	1.2778642298E+04	3.7473502327E+03	-4.2062750042E-01	3.9641749723E-02	4.3538282630E+03	-3.6235265268E+03	7.5766796109E+02	2.1834959809E+03
1.4111118020E-01	1.2159127249E+04	3.5746374213E+03	-4.4854442209E-01	4.8630549064E-02	4.3768090286E+03	-3.8832737890E+03	8.6545012026E+02	2.3640177982E+03
1.4540861550E-01	1.1563705373E+04	3.4439056830E+03	-4.7828332246E-01	5.9059669455E-02	4.4203347100E+03	-4.1810957228E+03	9.9321333427E+02	2.5592119900E+03
1.4983692770E-01	1.0991853663E+04	3.3347801115E+03	-5.0996164387E-01	7.1136986458E-02	4.4571019402E+03	-4.4953034726E+03	1.1384246660E+03	2.7709893437E+03
1.5440024440E-01	1.0443032778E+04	3.2234109534E+03	-5.4370437221E-01	8.5099157776E-02	4.4944771192E+03	-4.8341319990E+03	1.3053293633E+03	2.9827790614E+03
1.5910238030E-01	9.9167360798E+03	3.0886547266E+03	-5.7964109806E-01	1.0121393303E-01	4.5494361800E+03	-5.2183023909E+03	1.5023840700E+03	3.2182625320E+03
1.6394773130E-01	9.4123857344E+03	2.9213858841E+03	-6.1791313218E-01	1.1978726695E-01	4.5766381130E+03	-5.5986730768E+03	1.7188192548E+03	3.4657626643E+03
1.6894064840E-01	8.9294116499E+03	2.7270618431E+03	-6.5866930520E-01	1.4116630669E-01	4.6141463474E+03	-6.0188092334E+03	1.9699677033E+03	3.7190765031E+03
1.7408578100E-01	8.4672180140E+03	2.5210854718E+03	-7.0206919260E-01	1.6574628938E-01	4.6430632939E+03	-6.4567937799E+03	2.2526037862E+03	4.0123796817E+03
1.7938742040E-01	8.0252439294E+03	2.3245243042E+03	-7.4827799285E-01	1.9397353894E-01	4.6555031074E+03	-6.9006154663E+03	2.5656532352E+03	4.3144565313E+03
1.8485052880E-01	7.6028742905E+03	2.1573296675E+03	-7.9747577005E-01	2.2635746901E-01	4.6772728253E+03	-7.3876955834E+03	2.9265076403E+03	4.6246973079E+03
1.9048018750E-01	7.1994961167E+03	2.0279439046E+03	-8.4985372006E-01	2.6347647203E-01	4.6763723827E+03	-7.8708361546E+03	3.3220260432E+03	4.9579885986E+03
1.9628113510E-01	6.8145289649E+03	1.9304353935E+03	-9.0561020177E-01	3.0598337941E-01	4.6845462254E+03	-8.4015343259E+03	3.7780586087E+03	5.3111972647E+03
2.0225873590E-01	6.4473576013E+03	1.8503580606E+03	-9.6496050053E-01	3.5462211518E-01	4.7007870897E+03	-8.9838278428E+03	4.3044891354E+03	5.6603970786E+03
2.0841836930E-01	6.0973789836E+03	1.7702798548E+03	-1.0281320270E+00	4.1023551856E-01	4.7019103036E+03	-9.5771638980E+03	4.8901657900E+03	6.0567276107E+03
2.1476580200E-01	5.7639819366E+03	1.6766872304E+03	-1.0953687714E+00	4.7378169162E-01	4.7205338807E+03	-1.0246920139E+04	5.5753337934E+03	6.4694126622E+03

An alternative to the power spectra : response functions

Nishimichi, FB, Taruya, '14

$\delta P^{\rm lin}(q)$

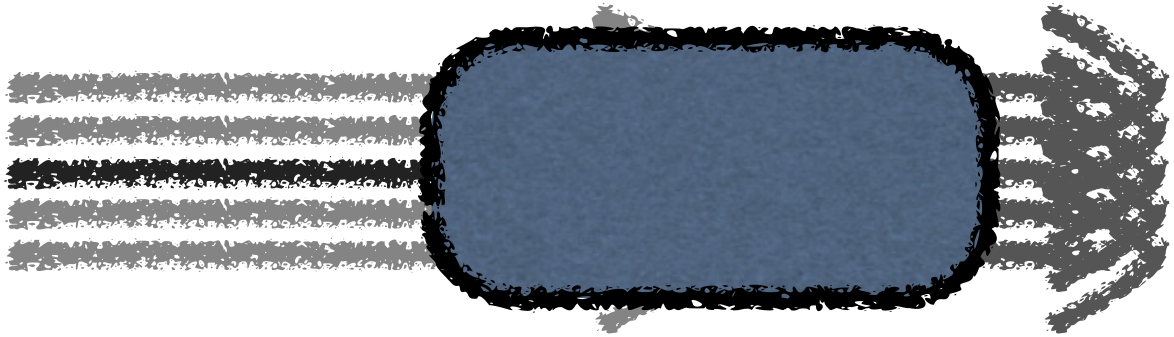

$\delta P^{\rm nl}(k)$

$$\mathcal{R}_{\mathcal{M}_1}(k,q) = q\ \frac{\delta P^{\rm nl}_{\mathcal{M}_1}(k)}{\delta P^{\rm lin}_{\mathcal{M}_1}(q)}$$

Of direct interest from P(k) predictions:

$$P^{\rm nl}_{\mathcal{M}_2}(k) \approx P^{\rm nl}_{\mathcal{M}_1}(k) + \int \frac{\mathrm{dq}}{q}\ \mathcal{R}_{\mathcal{M}_1}(k,q)\ \left[P^{\rm lin}_{\mathcal{M}_2}(q) - P^{\rm lin}_{\mathcal{M}_1}(q)\right]$$

How good can PTs be at predicting response functions ?

Kernels for the 2-point propagators at *p*-loop order

$$P_{\rm NL}^{\sharp-loop}(k) = \int \frac{{\rm d}q}{q}\; K^{\sharp-loop}(k,q)\; P_{\rm lin.}(q)$$

Convergence properties

1-loop

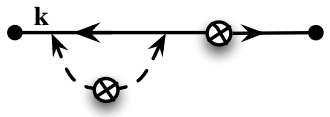

$n_s < -1$

2-loop

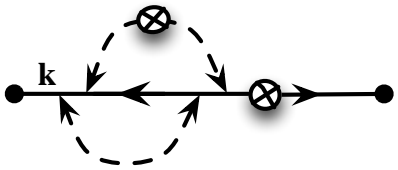

$n_s < -2$

3-loop

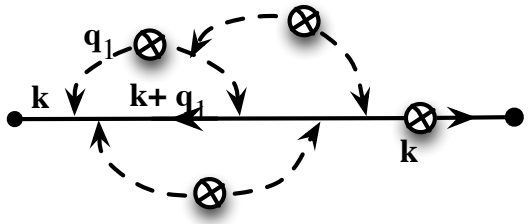

$n_s < -2.33$

see also Blas, Garny, Konstandin '13

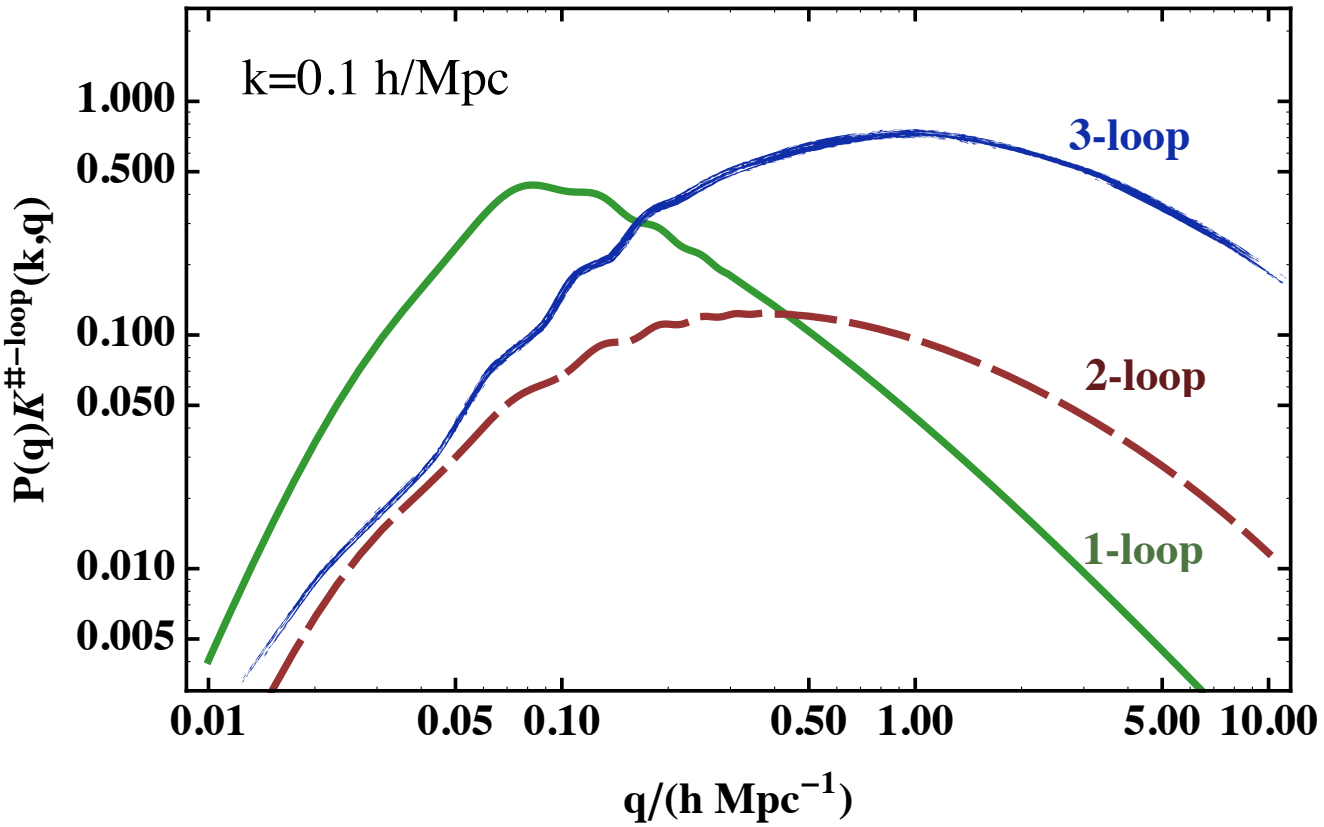

Should it be regularized or taken into account with Effective Theory approaches?

Pietroni et al. '11, Carrasco et al. '12

- UV shape of kernels is key to the validity of PT calculations and comparison with numerical simulations
- It comes from the IR behavior of coupling functions

$$\frac{\partial}{\partial\eta}\Phi_a(\mathbf{k},\eta)+\Omega_{ab}(\eta)\Phi_b(\mathbf{k},\eta)=\gamma_{abc}(\mathbf{k}_1,\mathbf{k}_2)\Phi_b(\mathbf{k}_1)\Phi_c(\mathbf{k}_2)$$

$$\gamma_{abc}(k_1,k_2)=\begin{pmatrix} \left\{0,\frac{(k_1+k_2).k_2}{2k_2.k_2}\right\} & \left\{\frac{(k_1+k_2).k_1}{2k_1.k_1},0\right\} \\ \{0,0\} & \left\{0,\frac{k_1.k_2(k_1+k_2).(k_1+k_2)}{2k_1.k_1k_2.k_2}\right\} \end{pmatrix}$$

$$\gamma_{abc}(\mathbf{q},\mathbf{k}-\mathbf{q}) \;\sim\; k^2/q^2$$

and power counting

$$\left[\frac{1}{q^2}\right]\left[q^3\;P_{\rm linear}(q)\right]^{\sharp\ \rm loops}$$

Response functions in Perturbation Theory calculations

FB, Taruya, Nishimichi, '12

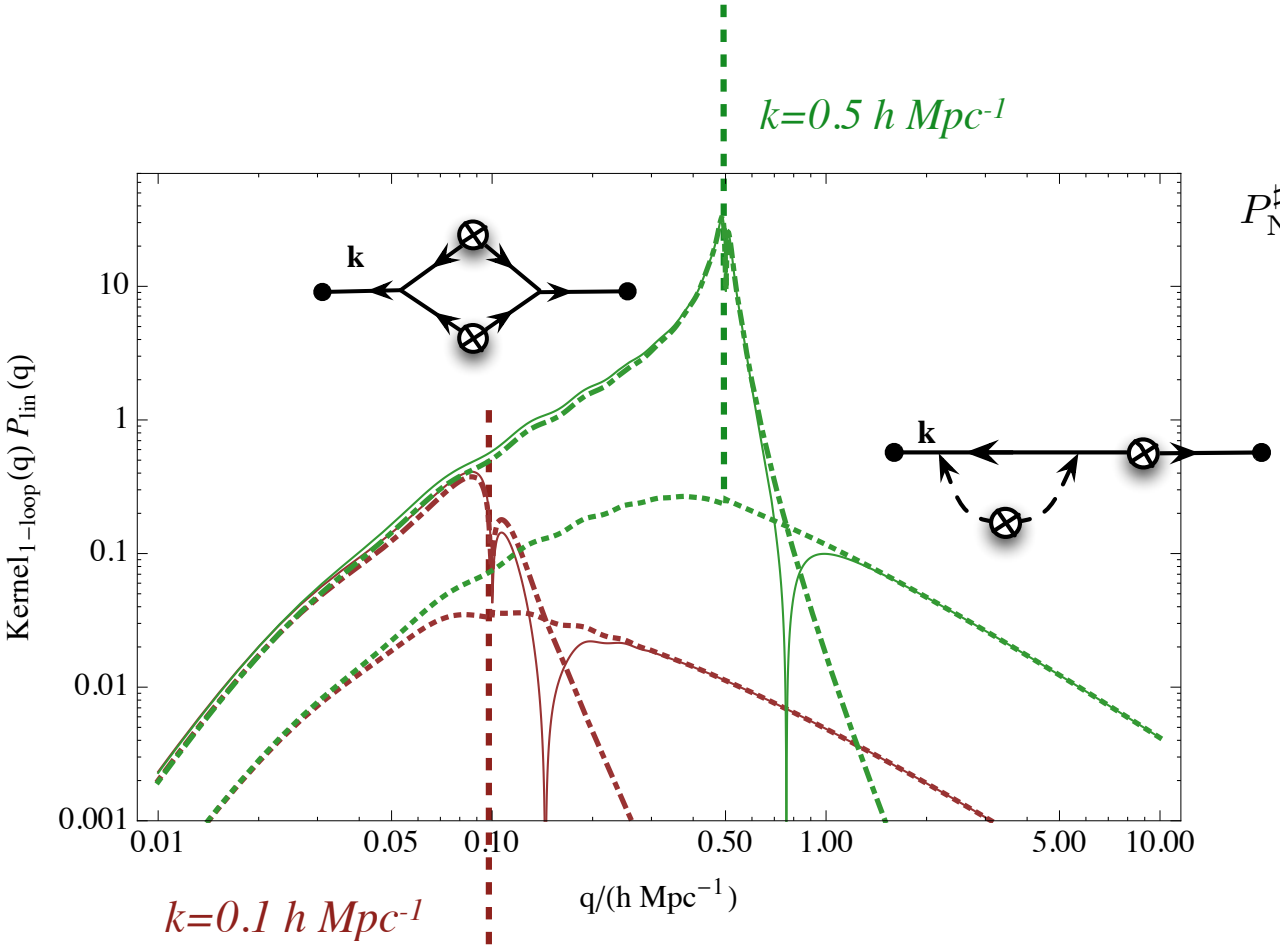

$$P_{\rm NL}^{\sharp-loop}(k) = \int \frac{{\rm d}q}{q}\; K^{\sharp-loop}(k,q)\; P_{\rm lin.}(q)$$

Expression of the density kernel for the propagator at 1-loop order

$$f(k,q) \;=\; \frac{3\left(2k^2+7q^2\right)\left(k^2-q^2\right)^3 \log\left[\frac{(k-q)^2}{(k+q)^2}\right] + 4\left(6k^7q - 79k^5q^3 + 50k^3q^5 - 21kq^7\right)}{2016k^3q^5}$$

First measurement of the response function

Nishimichi, FB, Taruya, '14

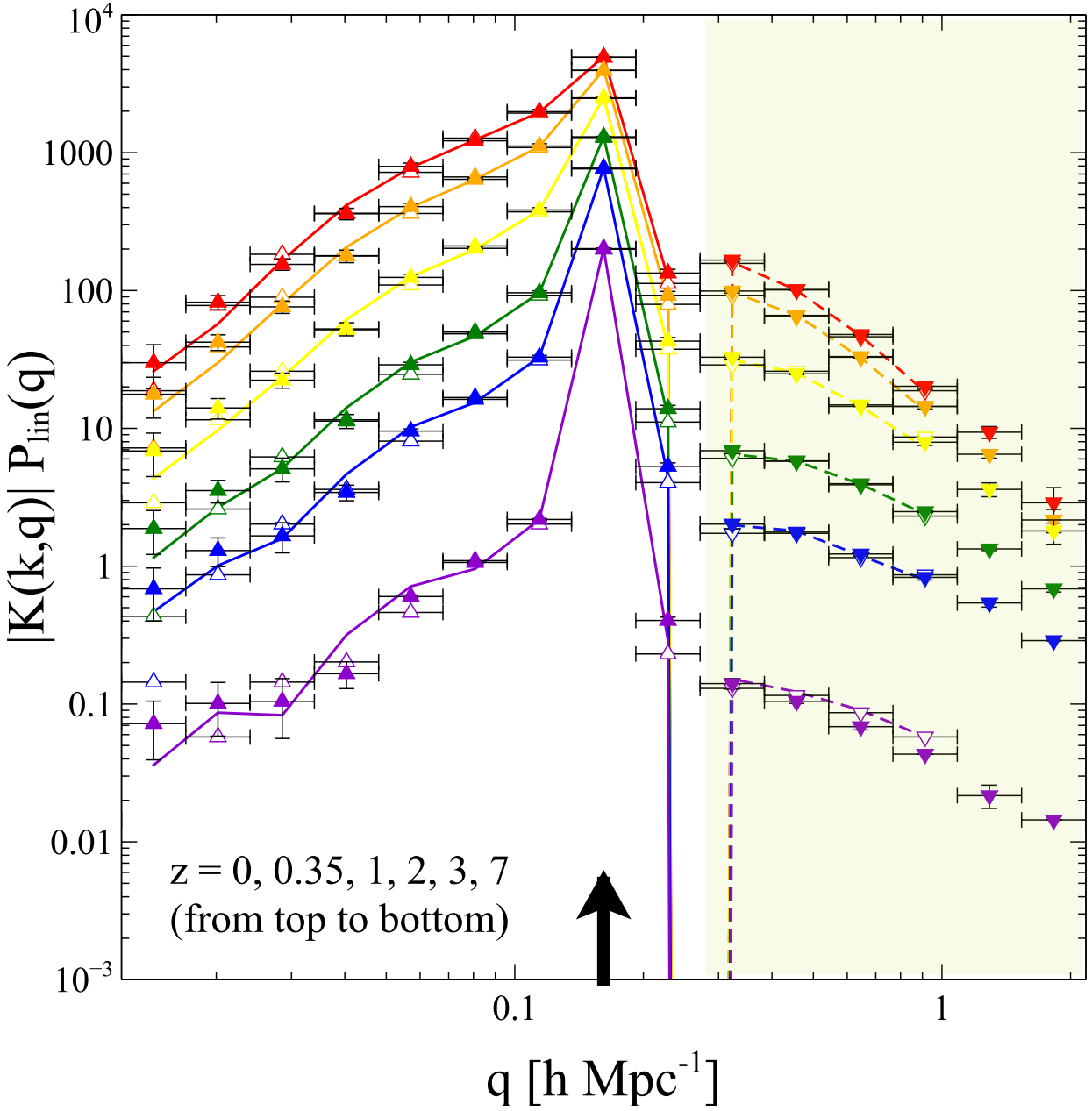

EFFECTIVE MODEL

- Calculation based on SPT
  - low-q is fine, automatically.
- 2-phenomenological regularizations
  - one, $\exp(-k^2\sigma_d^2)$ like RegPT
  - the other, $\exp(-q^2\sigma_d^2)$
- Cover a wide dynamic range seamlessly

data: 1400 sims.

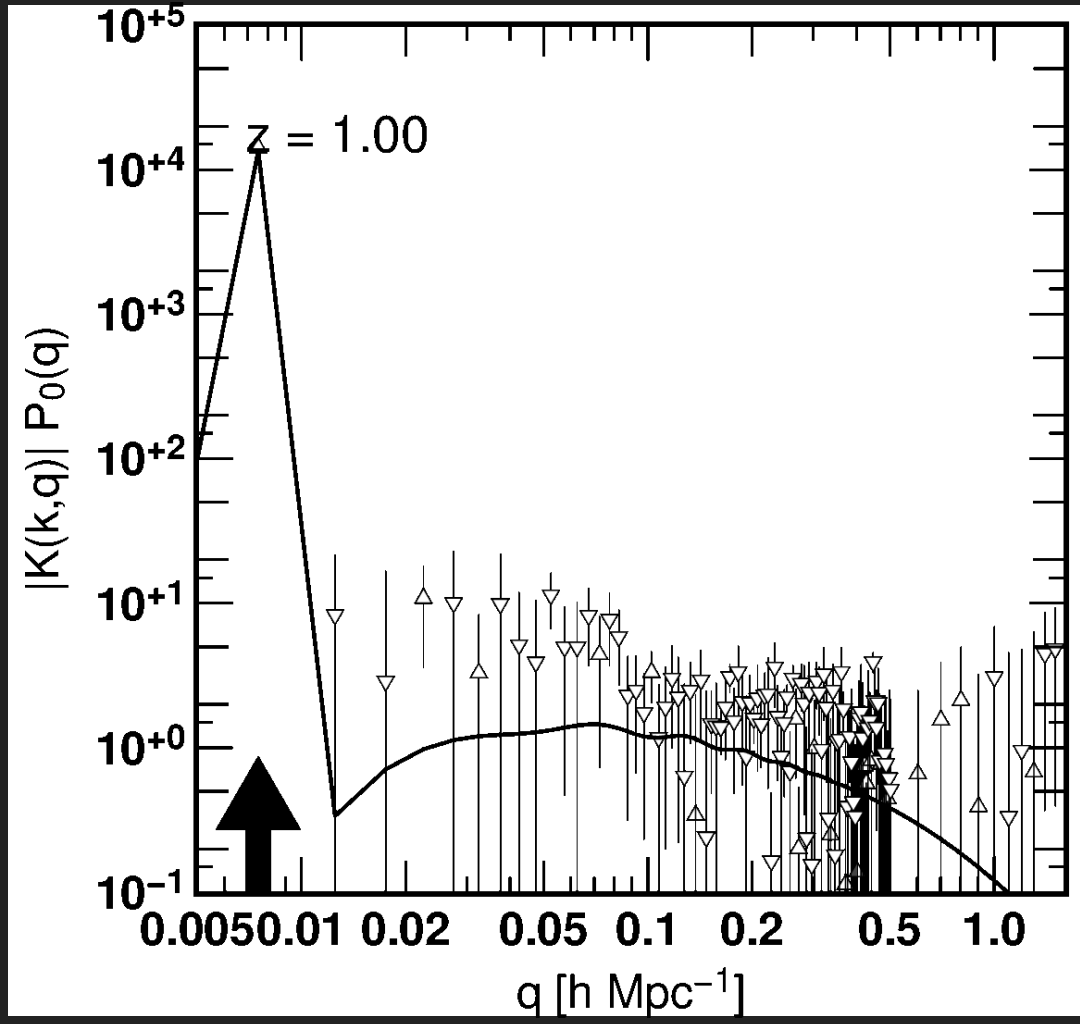

Comparison with 2-loop results

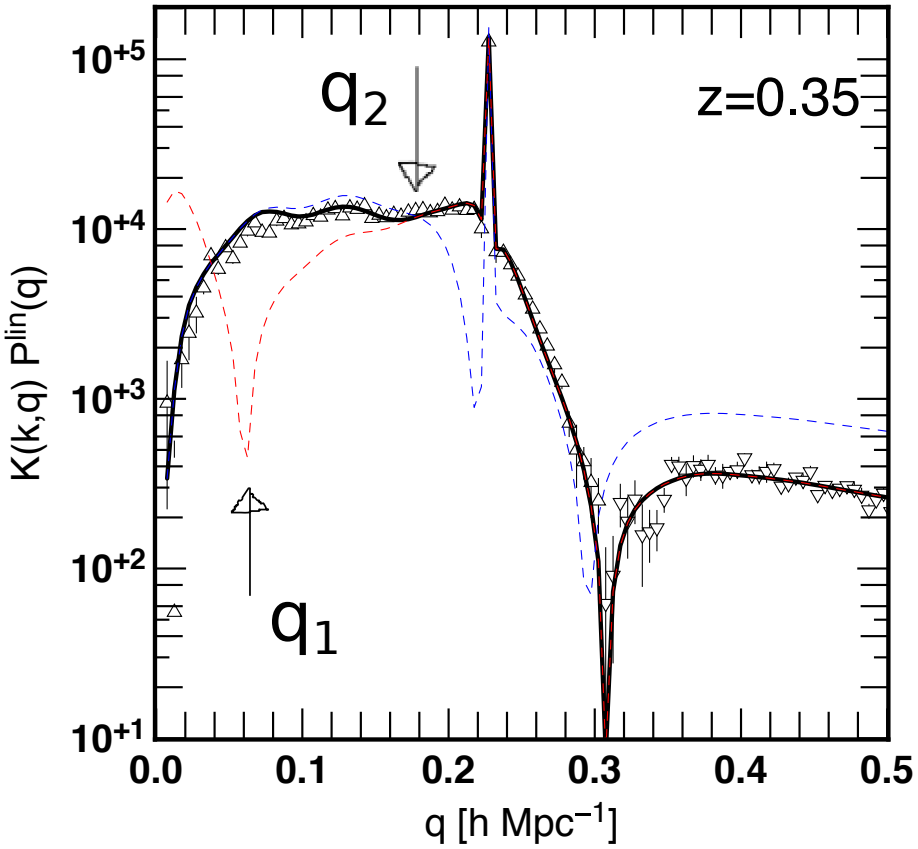

$$T^{\text{eff.}}(k,q) = \left[T^{1-\text{loop}}(k,q) + T^{2-\text{loop}}(k,q)\right] \frac{1}{1+(q/q_0)^2}$$

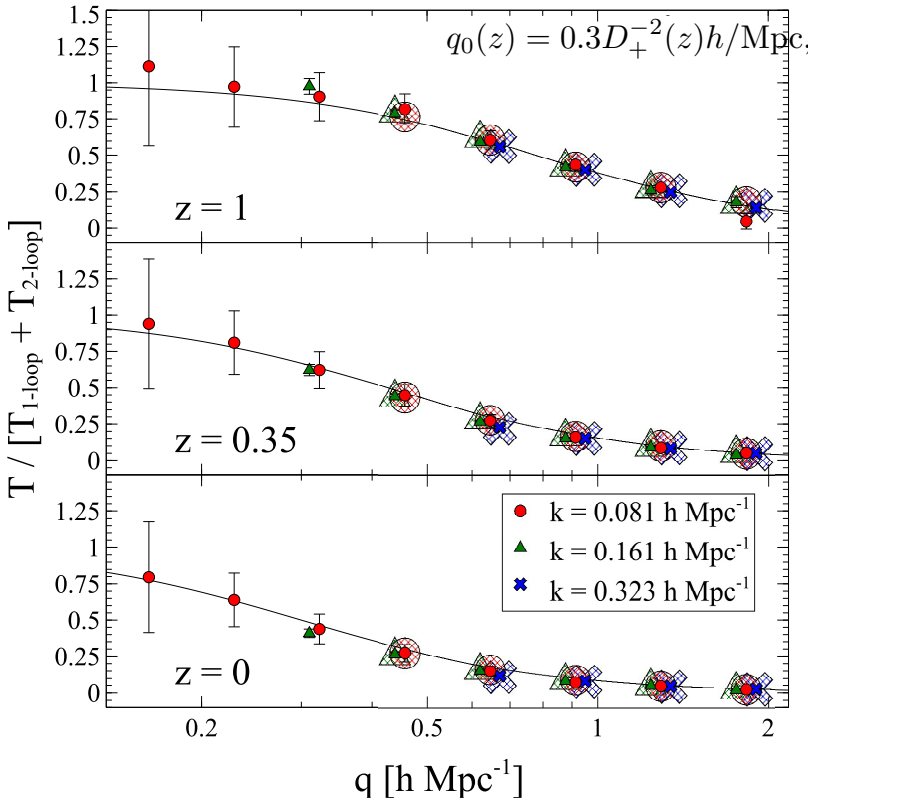

- From PT perspective, UV regularization is necessary. It expresses the fact that power spectra are intrinsically sensitive to small scale physics.

ANALYTICAL MODEL WITH HYBRID RESPONSE FUNCTION

from the definition of functional derivative

$$\Delta P_{\rm nl}(k) = \int {\rm d}\ln q\, K(k,q) \Delta P_{\rm lin}(q)$$

Simulation data for PLANCK cosmology as the fiducial model

- ✓ suppressed variance by "fixed-and-paired" method (Angulo, Pontzen'16)
- ✓ -0.4 < z < 5, 20 outputs
- ✓ alias correction by "interlacing" method (Sefusatti+'16)

→ Prediction for WMAP5 cosmology

TN et al. in prep

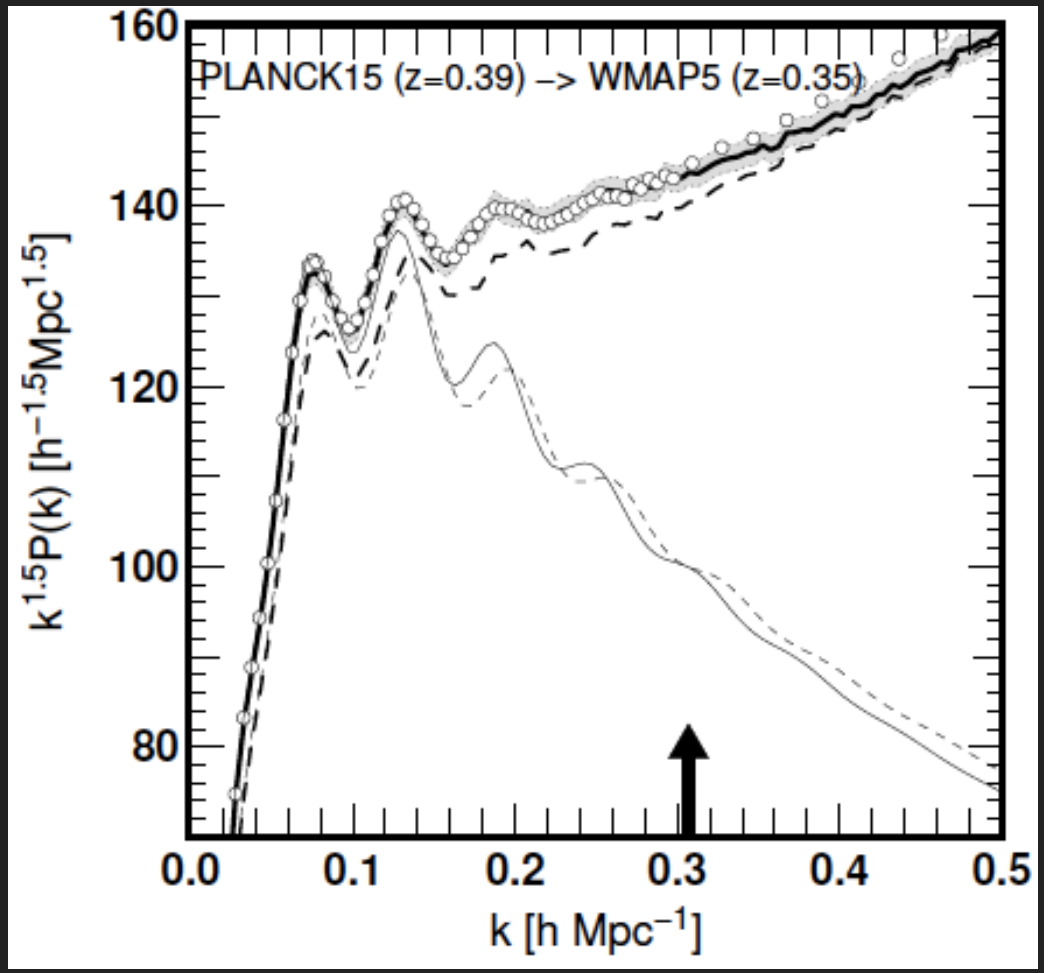

$$P_{\rm wmap5}(k) = P_{\rm planck15}(k) + \int {\rm d}\ln q\, K(k,q)[P_{\rm lin,wmap5}(q) - P_{\rm lin,planck15}(q)]$$

Lecture 1 and 2 : the easy parts

Lecture 3: a few steps from exact calculations to galaxy catalogues

- *Effective field theory corrective terms*
- *Galaxy biasing*
- *Redshift space distorsions*

By order of difficulty !

Recap : mode couplings from standard gravitational dynamics

Behavior of the response function

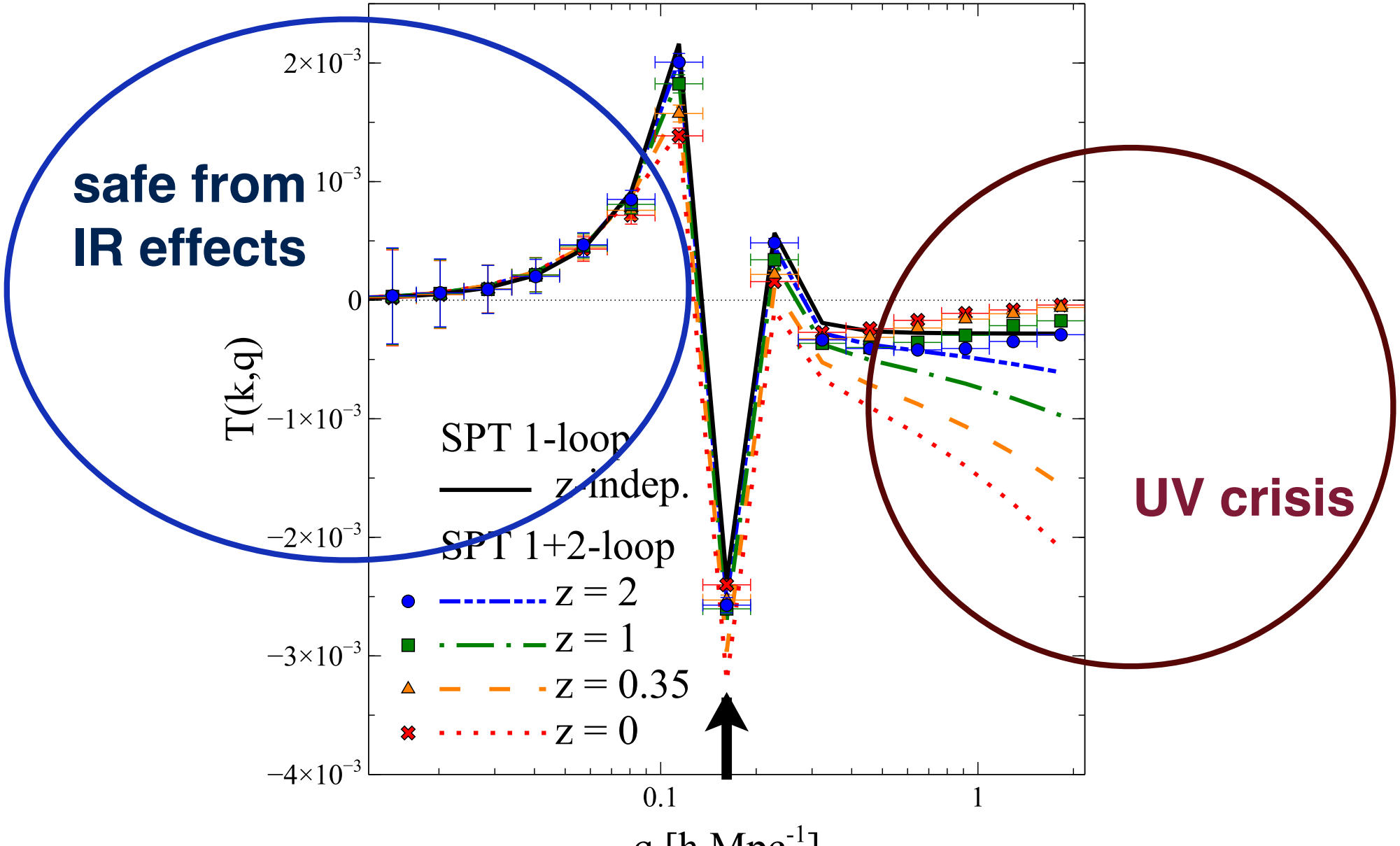

Going beyond: Effective Field Theory approaches

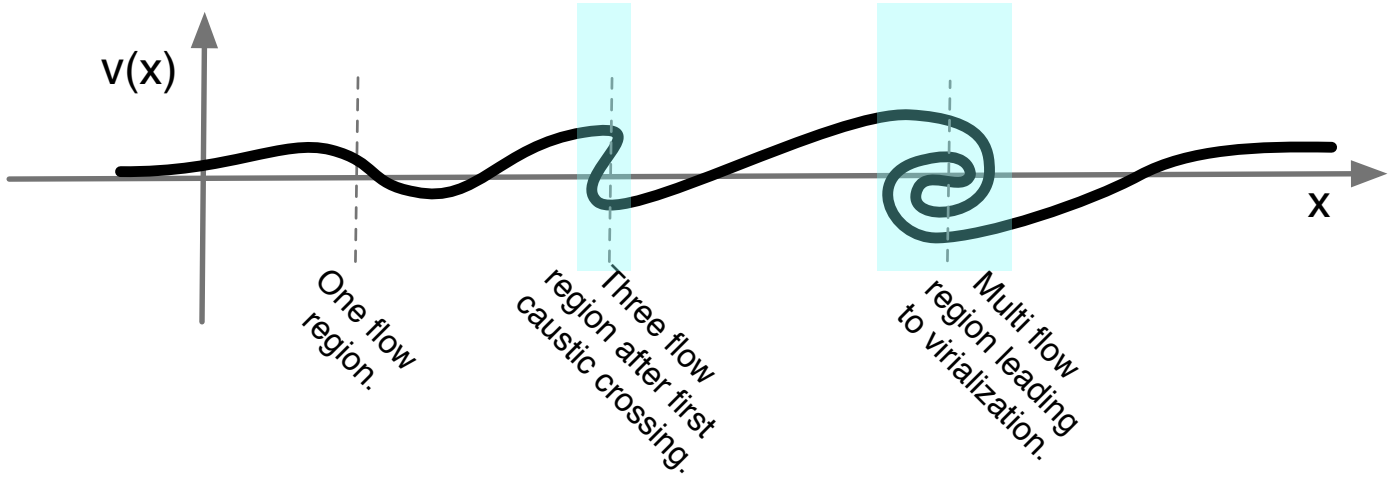

Describing the small scale physics, including shell crossings, with effective operators that respect symmetries of the problem (mass and momentum conservations) see for instance Carrasco et al. ’12.

Motion equation for the *long-wavelength* fields

filtered fields

$$\partial_\tau \delta + \partial_i[(1+\delta)v^i] = 0$$

$$\partial_\tau v^i + \mathcal{H} v^i + \partial^i \phi + v^j \partial_j v^i = -\frac{1}{a\rho}\partial_j \tau^{ij}$$

Extra source term that encodes the small scale physics

Counter-term for the velocity divergence

$$\tau_\theta \equiv -\partial_i \left[\frac{1}{a\rho} \partial_j \tau^{ij} \right]$$

Effective pressure term from

- coarse graining (filtering)
- small scale physics

At leading order (where d is free time dependent parameter)

$$\tau_\theta^{\rm det}\big|_{\rm LO} = -d^2 \triangle \delta_{(1)} = -d^2 \triangle\triangle \bar{\phi}_{(1)}$$

At next to leading order

$$\tau_\theta^{\rm det}\big|_{\rm NLO} = -d^2 \triangle [\delta_{(1)} + \delta_{(2)}] - e_1 \triangle \delta^2_{(1)} - e_2 \triangle (s_{ij(1)} s^{ij}_{(1)}) - e_3 \partial_i s^{ij}_{(1)} \partial_j \delta_{(1)}$$

$$s_{ij} = \left(\partial_i \partial_j - \frac{1}{3} \delta^{(\rm K)}_{ij} \triangle \right) \bar{\phi}$$

note that the time dependence of d should depend on order.

It leads to counter terms in the expression of power spectra

EFT is efficient is reproducing measured power spectra

$$\partial^2 \tau_{ij} \sim c_s\, k^2 \delta(k) + c_1\, k^2 [\delta^2](k) + c_4\, k^4 \delta(k)$$

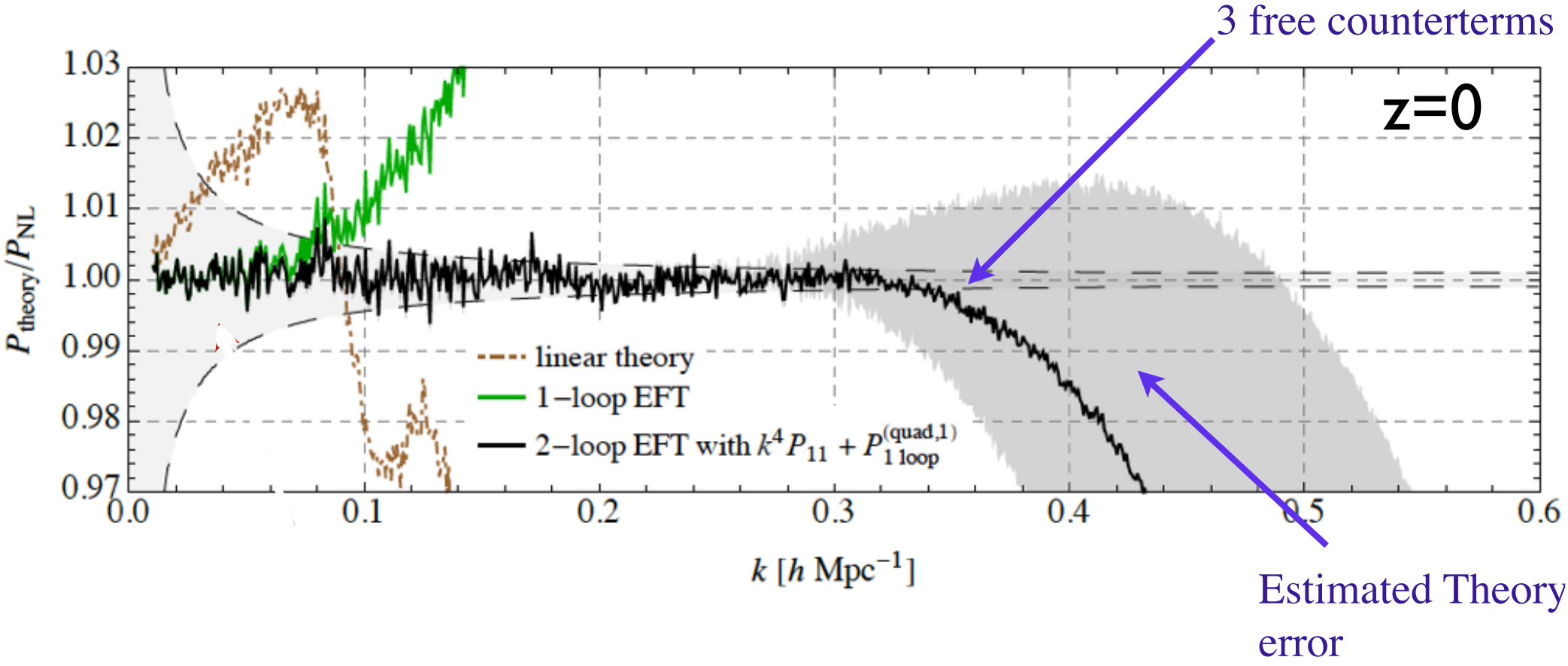

- k-reach pushed to $k \sim 0.34\, h\,\mathrm{Mpc}^{-1}$, cosmic variance $\sim 10^{-3}$
- Order by order improvement $\left(\frac{k}{k_{\rm NL}}\right)^L$

with Carrasco, Foreman and Green **JCAP1407**
with Zaldarriaga **JCAP1502**
with Foreman and Perrier **1507**
see also Baldauf, Shaan, Mercolli and Zaldarriaga **1507, 1507**

Sonder les grandes structures de l'Univers avec les galaxies

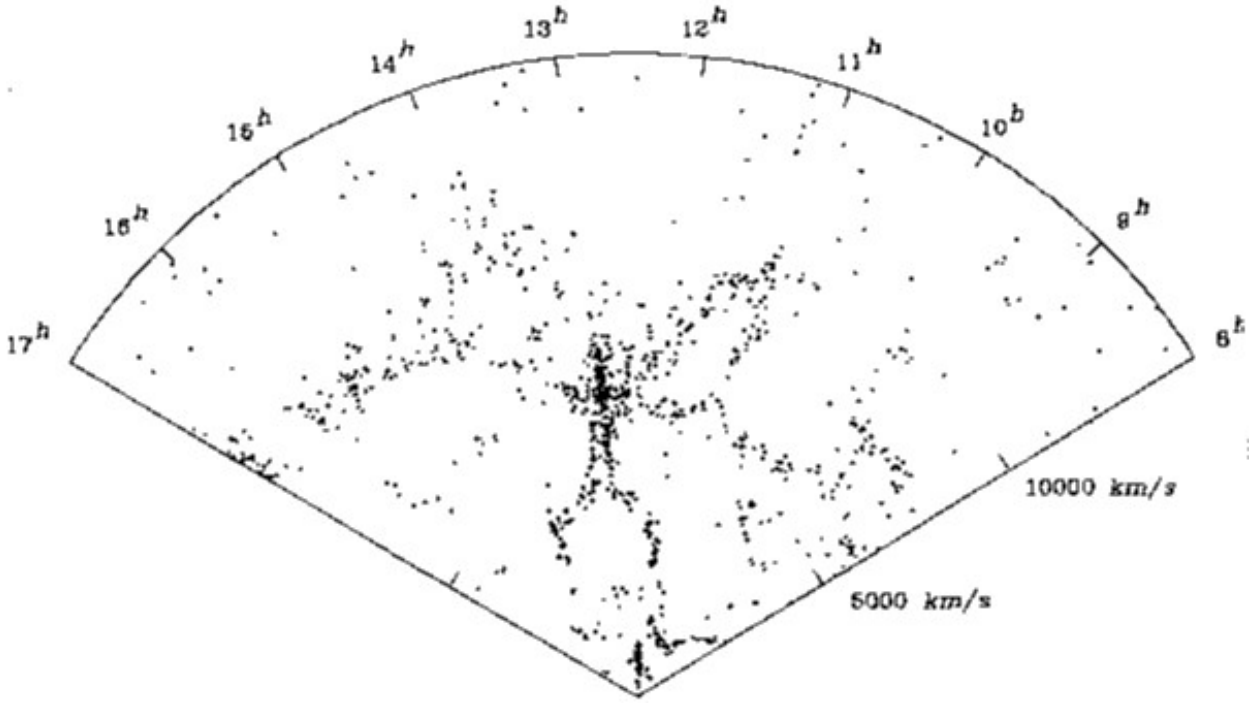

Figure: Illustration d'un des premiers grands relevés extragalactiques reproduisant la position 3D de milliers de galaxies. Cette "tranche d'univers" a été publiée initialement par V. de Lapparent et ses collaborateurs [**?**].

Sonder les grandes structures de l'Univers avec les galaxies

Le moyen le plus direct pour sonder les grandes structures de l'univers est encore de faire des relevés extragalactiques profonds et simplement de compter les galaxies présentes dans différentes régions de l'espace. Cette méthode permet au moins d'apprécier la manière dont se répartit la matière aux grandes échelles et historiquement ces premiers relevés ont joué un grand rôle dans la construction des modèles cosmologiques. Les premiers relevés systématiques ont été entrepris à la fin des années 70 et dans les années 80. Mentionnons en particulier le relevé CfA (voir figure 22).

Cela étant on se doute bien qu'une telle approche souffre de limitations importantes : en ne détectant que la lumière on s'expose à de multiples biais observationnels. Rien ne dit en effet que la quantité de lumière reçue d'une région donnée donne une bonne estimation de la quantité de matière qu'elle contient ; et quand bien même une relation étroite existerait entre l'une et l'autre, cette relation a toutes les chances d'évoluer sur des temps cosmologiques.

Comment décrire le biais ?

La description phénoménologique la plus simple qu'on puisse en faire, et qui est de fait souvent utilisée dans la littérature, est de supposer que les contrastes de densité mesurés sont proportionnels entre eux,

$$\delta_g(\mathbf{x}) = b\,\delta(\mathbf{x}). \tag{125}$$

Une des conséquences directes de cette hypothèse est que les spectres des deux champs sont proportionnels, $P_g(k) = b^2\,P(k)$.

Est-ce une hypothèse justifiée ?
Comment étendre cette relation aux petites échelles ?
Biais locaux ou non-locaux ?

Quelques résultats généraux

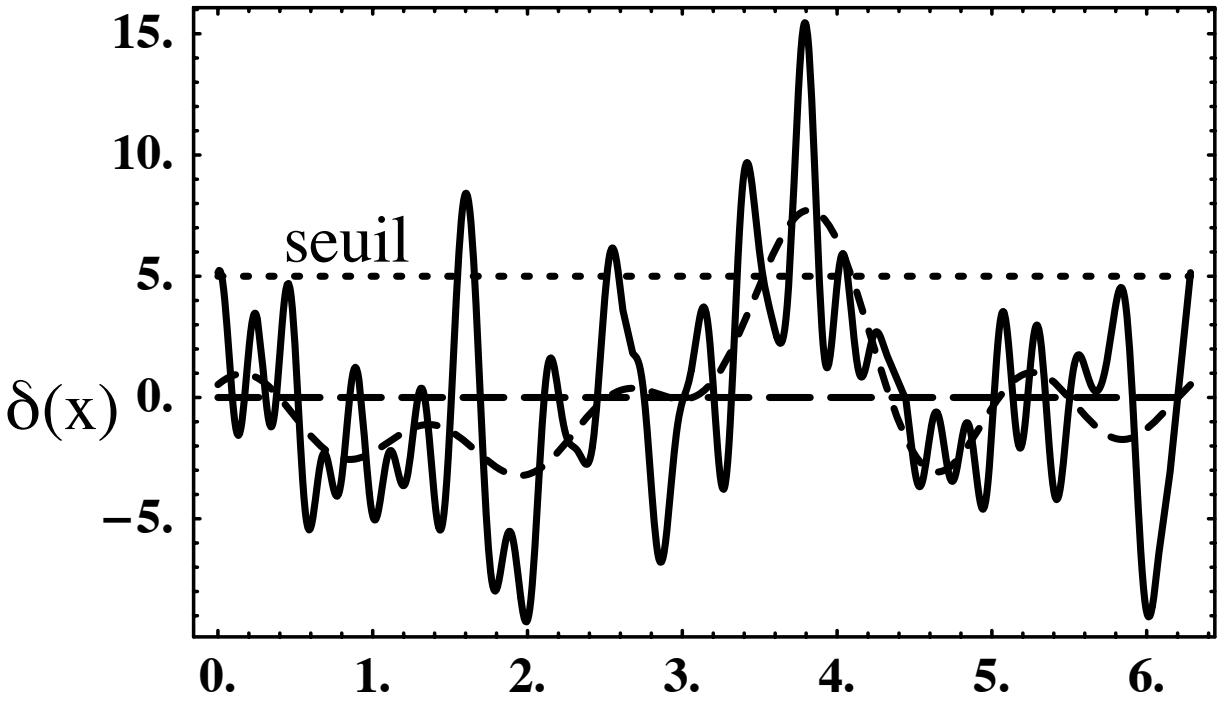

Figure: Modèle de biais de N. Kaiser : Les galaxies ne sont pas supposées être distribuées comme une représentation Poissonienne du champ de densité sous-jacent mais sur les extrema du champ où la densité excède un certain seuil. La figure illustre le fait que cette condition de seuil est plus facilement remplie dans les régions les plus denses conduisant à un effet de biais.

Galaxy bias

La première approche théorique visant à décrire le phénomène de biais a été mise en avant par N. Kaiser [**?**], qui a montré que les propriétés des maxima d'un champ gaussiens, plus fortement corrélés que le champ lui-même, pouvaient ainsi rendre compte des observations faites sur les amas de galaxies. Ces résultats ont été étendus en particulier dans [**?**] où il est montré que les pics rares sont corrélés de telle façon que,

$$\left\langle \delta_{\rm pic}^2 \right\rangle = b_{\rm pic}^2 \left\langle \delta^2 \right\rangle \tag{126}$$

où $\delta_{\rm pic}$ est le contraste de densité dans la densité de pics et où le paramètre de biais est donné par,

$$b_{\rm pic}(\nu) = \frac{\nu}{\sigma}, \tag{127}$$

σ étant la variance du champ de matière à l'échelle du pic et ν le contraste de densité servant à définir le pic en unité de σ.

Galaxy bias

Cette image a le mérite d'être simple. Elle ne rend pas forcément pleinement compte des observations faites dans les simulations numériques où il n'y a pas toujours une correspondance exacte entre pics du champ de densité initial et halos de matière noire. Une manière beaucoup plus phénoménologique d'aborder le problème est de supposer qu'il existe, au moins à une échelle suffisamment grande, une relation éventuellement nonlinéaire entre le contraste de densité des galaxies et le contraste de densité du champ de matière filtré à cette échelle, au même endroit. Autrement dit, on suppose qu'on peut écrire,

$$\hat{\delta_g}(\mathbf{x}) = \mathcal{F}[\hat{\delta}(\mathbf{x})], \qquad \hat{A}(\mathbf{x}) \equiv \int_{|\mathbf{x}'|<R} \mathrm{d}^3\mathbf{x}' A(\mathbf{x}-\mathbf{x}') W(\mathbf{x}') \quad (128)$$

où W est un filtre.

Galaxy bias

Pour de grandes valeurs de R, où $\hat{\delta} \ll 1$, rien n'empêche a priori de développer perturbativement $\mathcal{F}$ en série de Taylor permettant de reconstruire la hiérarchie des corrélation des galaxies [**?**]. Ainsi,

$$\hat{\delta_g} = \sum_{k=0}^{\infty} \frac{b_k}{k!} \hat{\delta}^k, \tag{129}$$

où b_1 correspondrait au facteur de biais linéaire standard. Dans une limite de grande échelle, une telle transformée locale préserve les propriétés hiérarchiques de la distribution de masse, mais en affecte les valeurs.

[9] Remarquons d'ailleurs que la prescription choisie englobe les modèles de biais basés sur des effets de seuil (comme celui proposé dans [**?**]) où on a par exemple la prescription $\delta_g = 1$ si $\delta > \nu\sigma$; $\delta_g = 0$ sinon.

Galaxy bias

Dans la mesure où les transformées de Fourier peuvent être vues aussi comme des opérations de filtrage, des résultats similaires à ceux écrits précédemment s'appliquent pour les grandes longueurs d'onde. Le spectre de puissance des galaxies doit donc s'écrire,

$$P_g(k) = b_1^2 \, P(k), \tag{130}$$

tandis que le bispectre réduit prend la forme,

$$Q_g(\mathbf{k}_1, \mathbf{k}_2, \mathbf{k}_3) = \frac{1}{b_1} Q(\mathbf{k}_1, \mathbf{k}_2, \mathbf{k}_3) + \frac{b_2}{b_1^2}. \tag{131}$$

However bias is not necessarily local

see review paper of Desjacques et al., soon to come ?

$$b_\delta(\tau)\delta(\boldsymbol{x},\tau) \to \int d^3\boldsymbol{y}\, F_\delta(\boldsymbol{y},\tau)\delta(\boldsymbol{x}+\boldsymbol{y},\tau)\,,$$

Consequences are that biasing is not only a function of the local matter density. There are now non-local operators,

$$b_\delta(\tau)\delta(\boldsymbol{x},\tau) \to \left[\int d^3\boldsymbol{y}\, F_\delta(\boldsymbol{y},\tau)\right]\delta(\boldsymbol{x},\tau) + \left[\frac{1}{6}\int d^3\boldsymbol{y}\,\boldsymbol{y}^2\, F_\delta(\boldsymbol{y},\tau)\right]\nabla_x^2\delta(\boldsymbol{x},\tau) + \cdots$$
$$= b_\delta(\tau)\delta(\boldsymbol{x},\tau) + b_{\nabla^2\delta}(\tau)R_*^2\nabla_x^2\delta(\boldsymbol{x},\tau) + \cdots\,,$$

- ***Should be extended to non-linear operators (imposing ext. Galilean invariance)***
- ***Very similar to EFT free parameters !***

Catalogues tri-dimentionnels : espace des redshifts

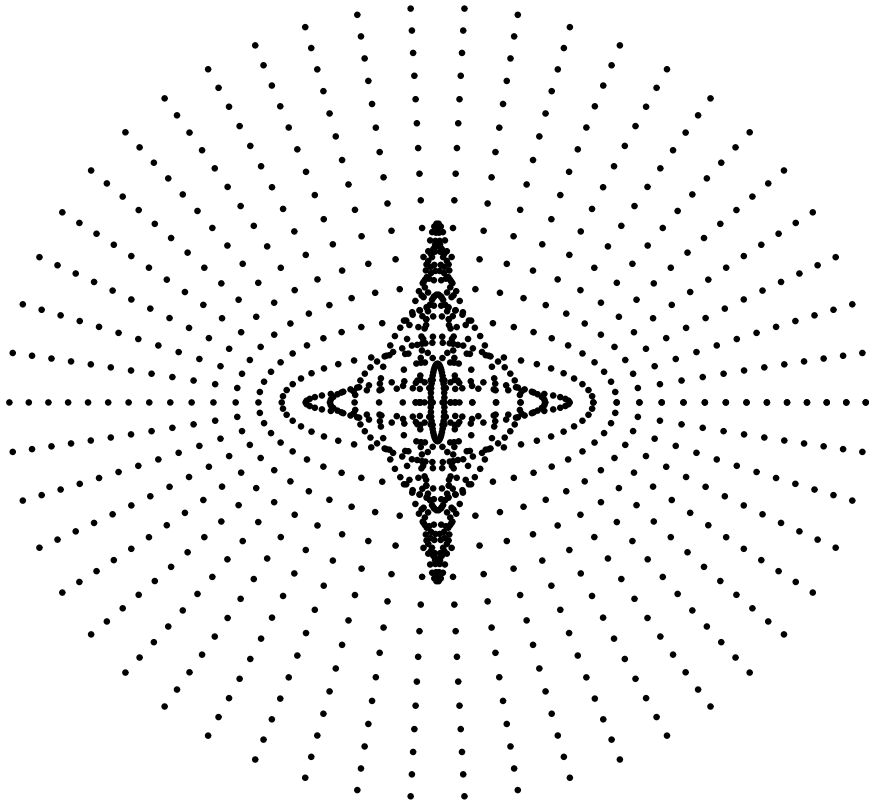

Figure: Illustration de l'apparition de caustiques en espace des redshifts. On voit apparaître au centre une région multiflots pour cette perturbation à symétrie sphérique non-critique en espace réel.

Catalogues tri-dimentionnels : espace des redshifts

Les observations en espace des redshifts mélangent donc les positions réelles et certaines composantes de la vitesse particulière des objets. L'objet des calculs qui suivent est d'explorer les propriétés statistiques d'un tel ensemble de points. Pour mener ces calculs on va d'ailleurs faire une approximation habituelle, celle des plans parallèles, ou des petits angles. Cela revient à dire que localement la direction $\hat{\mathbf{n}}$ reste inchangée. Elle est identique à une direction $\hat{z}$ fixe. Dans une telle approximation l'univers reste statiquement homogène - mais pas isotrope. Il reste qu'une décomposition en modes de Fourier reste toujours possible. On va donc s'intéresser au comportement du spectre de puissance dans cette représentation et naturellement celui-ci sera différent pour des modes dans la direction $\hat{z}$ et pour des modes dans les directions orthogonales.

Catalogues tri-dimentionnels : espace des redshifts

De la relation (133) on peut construire la densité dans l'espace des redshifts. Remarquons tout de suite que la relation (133) peut avoir plus d'une solution en $\mathbf{x}$ pour une position en espace des redshift donnée. Pour une solution donnée, la densité découle de ce changement de variable et de la conservation de la densité de particules, e.g.,

$$(1+\delta_z)\mathrm{d}^3\mathbf{x}_\mathrm{z} = (1+\delta)\mathrm{d}^3\mathbf{x}\ . \tag{134}$$

En utilisant le fait que $\mathrm{d}^3\mathbf{x}_\mathrm{z} = J(\mathbf{x})\mathrm{d}^3\mathbf{x}$, où,

$$J(\mathbf{x}) = |1 + \frac{1}{a\,H}\frac{\partial}{\partial z}\mathbf{u}_z(\mathbf{x})|, \tag{135}$$

est le jacobien exact du moins dans l'approximation des plans-parallèles, il vient,

$$1+\delta_z(\mathbf{x}_\mathrm{z}) = \sum_i \frac{1}{J(\mathbf{x}_i)}(1+\delta(\mathbf{x}_i)). \tag{136}$$

où la somme sur i porte sur chacune des solutions de (133).

Catalogues tri-dimentionnels : espace des redshifts

L'existence de solutions multiples dans la relation $\mathbf{x} - \mathbf{x}_z$ vient des effets de vitesse particulière et de la possibilité pour le jacobien de s'annuler. Il est à noter que le régime multiflot en espace des redshifts est beaucoup plus étendu qu'en espace réel dans la direction radiale ; c'est une des limitations principales des investigations analytiques qu'on peut mener dans cet espace. A l'extérieur des caustiques, donc à l'extérieur des régimes multiflots, l'expression du contraste de densité en espace de Fourier découle de l'équation (136),

$$\delta_z(\mathbf{k}) = \int \frac{\mathrm{d}^3\mathbf{x}}{(2\pi)^{3/2}} e^{-\mathrm{i}\mathbf{k}\cdot\mathbf{x}} e^{\mathrm{i}k_z \mathbf{u}_z(\mathbf{x})/(a\,H)} \left[\delta(\mathbf{x}) - \frac{1}{a\,H}\frac{\partial}{\partial z}\mathbf{u}_z(\mathbf{x})\right] . \tag{137}$$

Le spectre de puissance en espace des redshifts

Les calculs en espace des redshifts procèdent de la même façon qu'en espace réel. A l'ordre dominant il vient [**?**],

$$P_z(\mathbf{k}) = P(k)\,(1 + f\mu^2)^2. \tag{144}$$

Cette expression est valable pour des traceurs reproduisant le champ de densité. Introduisons la possibilité que les galaxies puissent être un traceur biaisé du champ de densité. Ici on suppose simplement que le contraste de densité linéaire de champ de galaxies δ_g est proportionnel au contraste de densité linéaire de masse,

$$\delta_g(\mathbf{k}) = b\delta(\mathbf{k}), \tag{145}$$

tout en ayant des flots de déplacement à grande échelle reproduisant ceux de la matière[11].

[11] L'idée sous-jacente est simple : l'accélération d'un objet est indépendante de sa masse.

Le spectre de puissance en espace des redshifts

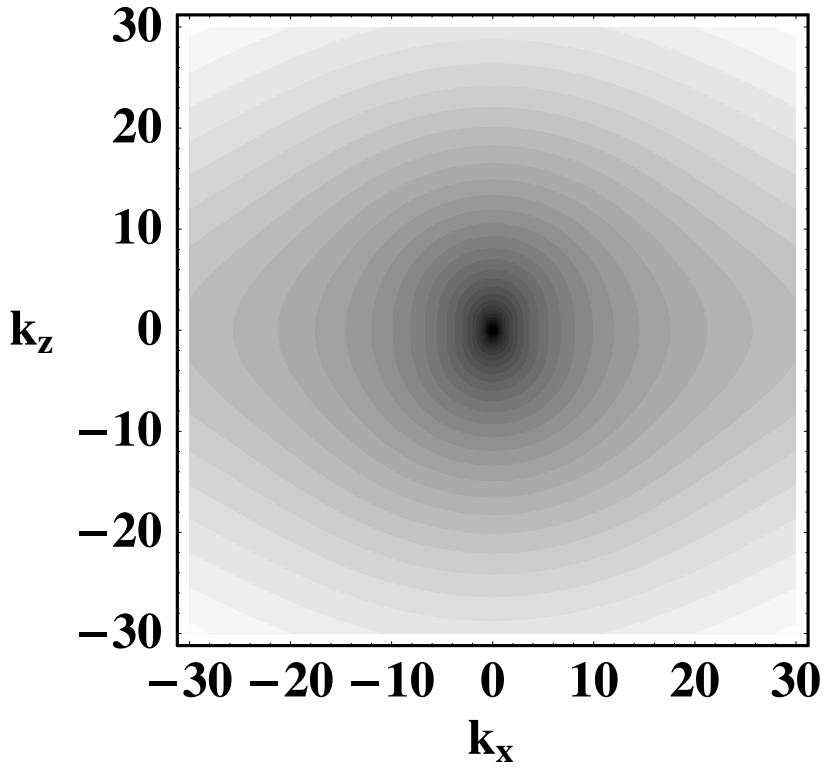

Figure: Dépendance géométrique du spectre de puissance en espace des redshifts pour le modèle cosmologique concordant en fonction de **k** (en unité de h/Mpc). L'axe vertical correspond à la direction le long de la ligne de visée ; l'axe horizontal à une direction transverse. Les lignes de contour sont régulièrement espacées en échelle logarithmique. La dispersion de vitesse sur la ligne de visée adoptée correspond à $\sigma_v = 0.05 h^{-1}$Mpc.

Le spectre de puissance en espace des redshifts

Alors en espace réel le spectre de puissance est simplement,

$$P_g(k) = b^2\, P(k). \tag{146}$$

En espace des redshifts il vient,

$$P_z(\mathbf{k}) = P_g(k)\ (1+\beta\mu^2)^2, \tag{147}$$

où $\beta \equiv f/b \approx \Omega_m^{0.6}/b$. Remarquons que le spectre de puissance a une dépendance angulaire spécifique qui peut s'exprimer au travers d'une décomposition multipolaire,

$$P_z(\mathbf{k}) = \sum_{l=0}^{\infty} a_l(\beta)\, P_l\,(\mu) P_g(k), \tag{148}$$

avec les coefficients a_l non nuls suivant,

$$a_0 = 1 + \frac{2}{3}\beta + \frac{1}{5}\beta^2, \quad a_2 = \frac{4}{3}\beta + \frac{4}{7}\beta^2, \quad a_4 = \frac{8}{35}\beta^2. \tag{149}$$

La relation (147) est un outil largement utilisé non seulement pour mesurer le spectre de puissance $P_g(k)$ mais aussi pour mesurer β.

Le spectre de puissance en espace des redshifts

Il est à noter que cette expression est malheureusement valable uniquement pour les grandes échelles, c'est à dire quand $k \to 0$. En pratique les effets de petites échelles restent très importants. Et en effet les dispersions de vitesses intrinsèques dans les puits de potentiel modifient significativement la forme du spectre. On retrouve ici les effets des régimes multi-flots dans les propriétés de l'espace des redshifts. Ces effets sont évidemment difficiles à décrire rigoureusement. On peut cependant s'appuyer sur une description phénoménologique de la dispersion de vitesse le long de la ligne de visée, σ_v. Si on admet que celle-ci agit comme un simple filtre Lorentzian/Gaussian dans cette direction alors le spectre de puissance prend finalement la forme suivante,

$$
\begin{aligned}
P_s(\mathbf{k}) &= P_g(k)\,\frac{(1+\beta\mu^2)^2}{\left[1+(k\mu f\sigma_v)^2/2\right]^2}\ (\textit{Lorentzian}) \\
P_s(\mathbf{k}) &= P_g(k)\,(1+\beta\mu^2)^2 \exp\left[-(k\mu f\sigma_v)^2\right]\ (\textit{Gaussian}).
\end{aligned}
$$

Catalogues tri-dimentionnels : espace des redshifts

L'expression formelle de ce mode de Fourier, exprimée en fonction des modes de Fourier du champ de densité réel et du champ de divergence est alors,

$$\delta_z(\mathbf{k}) = (2\pi)^{3/2} \sum_{n=1}^{\infty} \int \frac{\mathrm{d}^3\mathbf{k}_1}{(2\pi)^{3/2}} \cdots \frac{\mathrm{d}^3\mathbf{k}_n}{(2\pi)^{3/2}} \, \delta_{\mathrm{Dirac}}(\mathbf{k} - \Sigma_i \mathbf{k}_i)$$
$$\times \Big[\delta(\mathbf{k}_1) - \mu_1^2 \theta(\mathbf{k}_1)\Big] \frac{(-\mu k)^{n-1}}{(n-1)!} \frac{\mu_2}{k_2} \theta(\mathbf{k}_2) \ldots \frac{\mu_n}{k_n} \theta(\mathbf{k}_n), \quad (138)$$

où on rappelle que $\theta = 1/(a\,H)\nabla.\mathbf{u}$ (et où $\theta(\mathbf{k})$ sont ses modes de Fourier), $\mu_i \equiv \mathbf{k}_i \cdot \hat{z}/k_i$ est le cosinus de l'angle entre $\mathbf{k}_i$ et la direction de la ligne de visée (avec une définition similaire pour μ). Si l'on s'en tient à une théorie linéaire où l'on a $\theta = -f\delta$, on retrouve le résultat de N. Kaiser [**?**]

$$\delta_z(\mathbf{k}) = \delta(\mathbf{k})(1 + f\mu^2). \quad (139)$$

Catalogues tri-dimentionnels : espace des redshifts

Il reste que l'équation (138) peut être utilisée pour obtenir les propriétés de la densité en espace des redshifts au delà de la théorie linéaire. Ainsi Formellement on peut écrire les termes d'un développement perturbatif de la densité en espace des redshifts de la forme

$$\delta_z(\mathbf{x}) = \sum_n \delta_z^{(n)}(\mathbf{x}) \tag{140}$$

$$\begin{aligned} \delta_z^{(n)}(\mathbf{k},t) &= \int \frac{\mathrm{d}^3\mathbf{k}_1}{(2\pi)^{3/2}} \cdots \int \frac{\mathrm{d}^3\mathbf{k}_n}{(2\pi)^{3/2}} e^{\mathrm{i}\mathbf{x}_z\cdot\Sigma_i\mathbf{k}_i} \\ &\times Z_n(\mathbf{k}_1,\ldots,\mathbf{k}_n) D_1^n(t)\,\delta_1(\mathbf{k}_1)\cdots\delta_1(\mathbf{k}_n), \end{aligned} \tag{141}$$

où $D_1(t)$ facteur de croissance de la théorie linéaire et où on suppose que la dépendance en temps du terme d'ordre n est $D_n \propto D_1^n$, (résultat exact en espace Einstein-de Sitter et qui est une excellente approximation en général).

Catalogues tri-dimentionnels : espace des redshifts

Les noyaux Z_n se déduisent alors des noyaux obtenus en théorie quasilinéaire pour le champ de densité et de divergence,

$$Z_1(\mathbf{k}) = (1 + f\mu^2), \tag{142}$$

$$Z_2(\mathbf{k}_1, \mathbf{k}_2) = F_2(\mathbf{k}_1, \mathbf{k}_2) + f\mu^2 G_2(\mathbf{k}_1, \mathbf{k}_2) + \frac{f\mu k}{2}\left[\frac{\mu_1}{k_1}(1 + f\mu_2^2) + \frac{\mu_2}{k_2}(1 + f\mu_1^2)\right], \tag{143}$$

où on a $\mu \equiv \mathbf{k} \cdot \hat{z}/k$, avec $\mathbf{k} \equiv \mathbf{k}_1 + \ldots + \mathbf{k}_n$, et $\mu_i \equiv \mathbf{k}_i \cdot \hat{z}/k_i$. Les fonctions F_2 et G_2 sont les noyaux[10] pour le second ordre pour le champ de densité et de divergence. Ces résultats peuvent bien sûr être étendus à de plus grands ordres. Nous avons maintenant tous les éléments pour aborder le calcul du spectre ou du bispectre en espace des redshifts.

[10] Ainsi définis ces noyaux dépendent très peu des paramètres cosmologiques.

z-space power spectrum: Taruya et al. formula

$$P^{(\mathrm{S})}(k,\mu) = D_{\mathrm{FoG}}[k\mu\, f\, \sigma_{\mathrm{v}}] \Big\{ P_{\delta\delta}(k) + 2\, f\, \mu^2\, P_{\delta\theta}(k) + f^2\, \mu^4\, P_{\theta\theta}(k) + A(k,\mu) + B(k,\mu) \Big\}. \tag{18}$$

with corrective term :

$$A(k,\mu) = (k\mu\, f) \int \frac{d^3\boldsymbol{p}}{(2\pi)^3}\, \frac{p_z}{p^2} \times \{ B_\sigma(\boldsymbol{p}, \boldsymbol{k}-\boldsymbol{p}, -\boldsymbol{k}) - B_\sigma(\boldsymbol{p}, \boldsymbol{k}, -\boldsymbol{k}-\boldsymbol{p}) \}\,, \tag{19}$$

$$B(k,\mu) = (k\mu\, f)^2 \int \frac{d^3\boldsymbol{p}}{(2\pi)^3} F(\boldsymbol{p}) F(\boldsymbol{k}-\boldsymbol{p})\ ; \tag{20}$$

$$F(\boldsymbol{p}) = \frac{p_z}{p^2} \left\{ P_{\delta\theta}(p) + f\, \frac{p_z^2}{p^2}\, P_{\theta\theta}(p) \right\},$$

where the function B_σ is the cross bispectra defined by

$$\left\langle \theta(\boldsymbol{k}_1) \left\{ \delta(\boldsymbol{k}_2) + f\, \frac{k_{2z}^2}{k_2^2} \theta(\boldsymbol{k}_2) \right\} \left\{ \delta(\boldsymbol{k}_3) + f\, \frac{k_{3z}^2}{k_3^2} \theta(\boldsymbol{k}_3) \right\} \right\rangle = (2\pi)^3 \delta_D(\boldsymbol{k}_1 + \boldsymbol{k}_2 + \boldsymbol{k}_3)\, B_\sigma(\boldsymbol{k}_1, \boldsymbol{k}_2, \boldsymbol{k}_3). \tag{21}$$

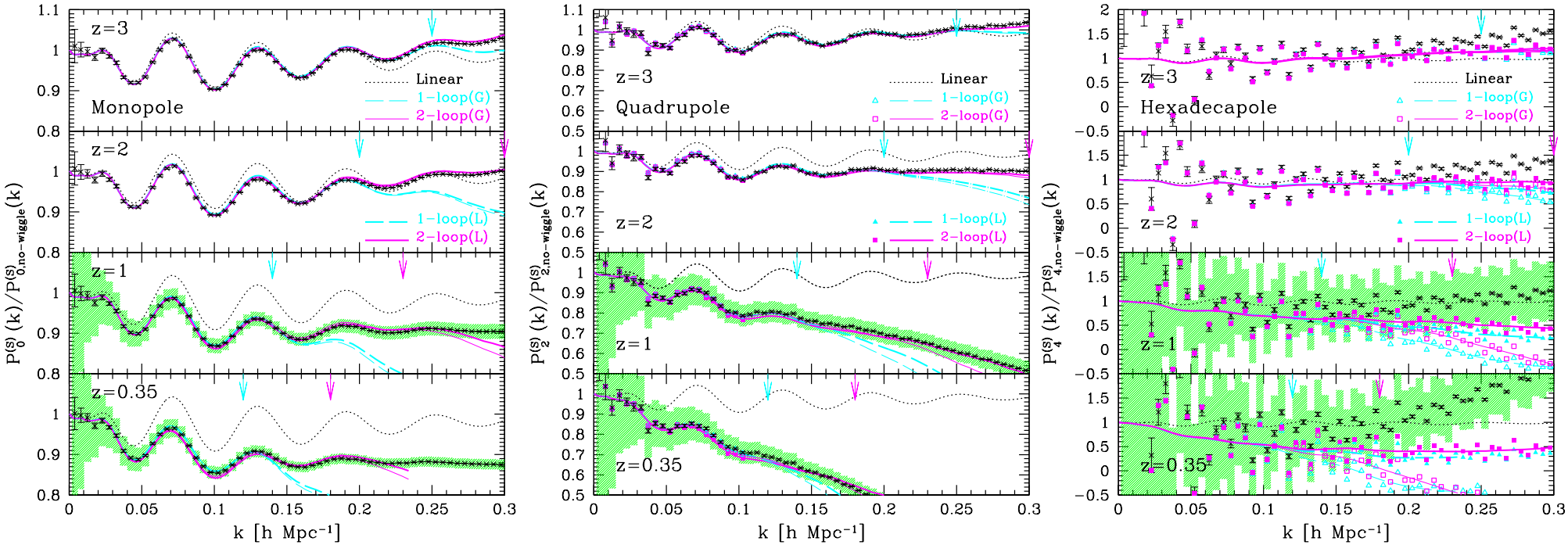

FIG. 2: Ratio of power spectra to the smoothed reference spectra in redshift space, $P_\ell^{(\mathrm{S})}(k)/P_{\ell,\text{no-wiggle}}^{(\mathrm{S})}(k)$. Left, middle, and right panels respectively show the monopole ($\ell = 0$), quadrupole ($\ell = 2$) and hexadecapole ($\ell = 4$) contributions to the redshift-space power spectrum. N-body results are taken from the `wmap5` simulations of Ref. [45]. The reference spectrum $P_{\ell,\text{no-wiggle}}^{(\mathrm{S})}$ is computed with the no-wiggle approximation of the linear transfer function [49], taking account of the linear theory of the Kaiser effect. Long-dashed and solid lines respectively indicate the results based on the RegPT calculations at one- and two-loop orders, adopting the Gaussian (thin) and Lorentzian (thick) form of the damping functions. Triangles and squares in middle and right panels are also obtained from the same calculation at one- and two-loop orders, but taking account of the effect of finite grid-size for the power spectrum measurement in N-body simulations (see text and Appendix B in detail). For comparison, the 1-σ statistical errors of the hypothetical survey with volumes $V = 5\,h^{-3}\,\mathrm{Gpc}^3$ and number density $n = 5 \times 10^{-4}\,h^3\,\mathrm{Mpc}^{-3}$ are estimated from Eq. (35), and are depicted as green shaded regions around the N-body results at $z = 0.35$ and 1.

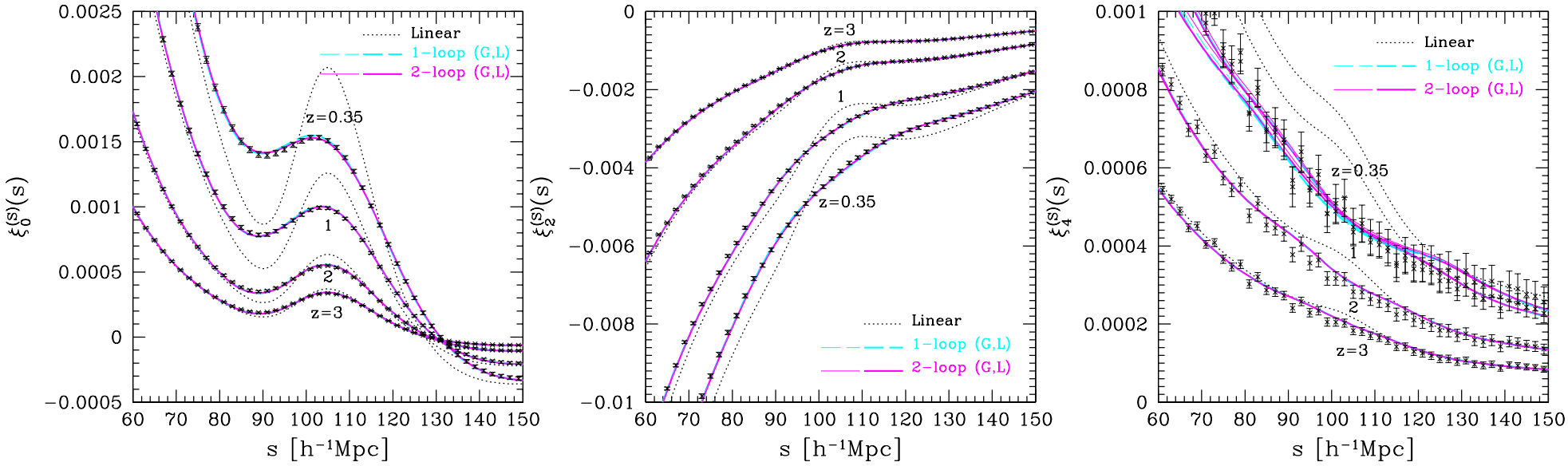

FIG. 4: Redshift-space correlation functions around the baryon acoustic peak. Monopole ($\ell = 0$), quadrupole ($\ell = 2$), and hexadecapole ($\ell = 4$) moments of the redshift-space correlation function are respectively shown in left, middle and right panels. Dotted lines are the linear theory predictions, while the dashed and solid lines respectively represent the results based on the RSD model using the RegPT up to the one- and two-loop orders, adopting the Gaussian (thin) and Lorentzian (thick) damping function.

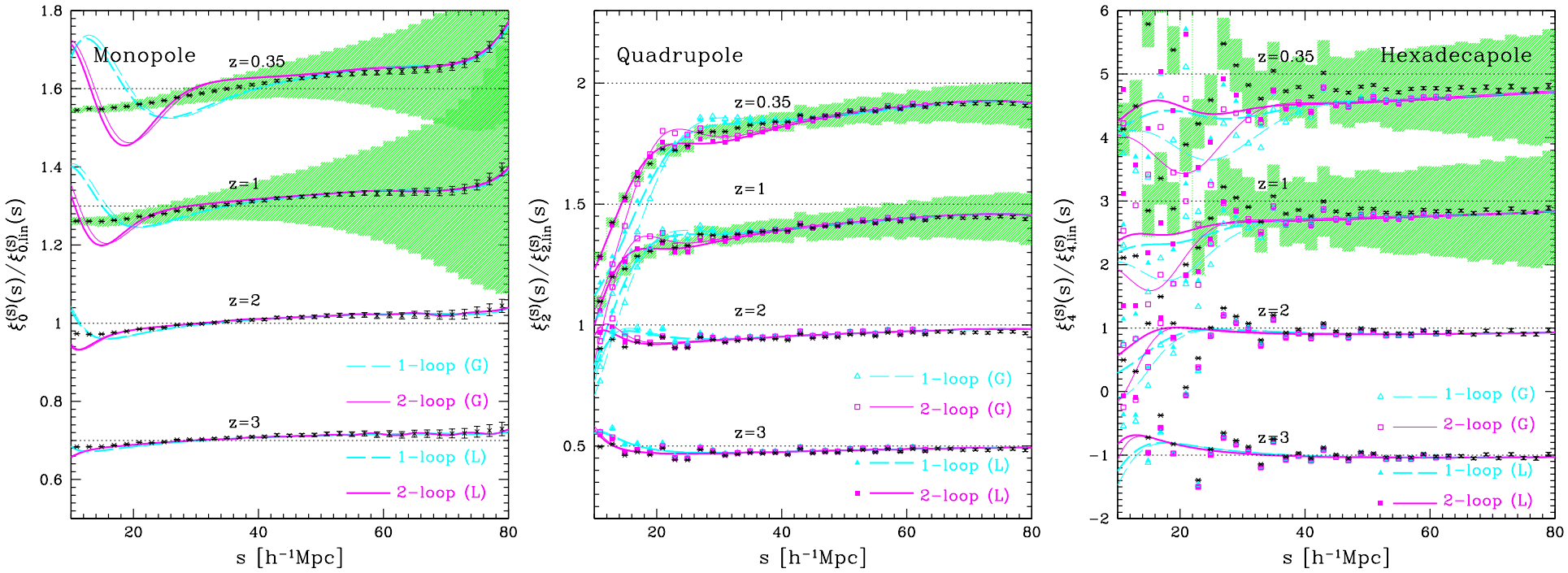

FIG. 5: Redshift-space correlation functions at small scales. Plotted results are the ratio of correlation function to the linear theory predictions taking account of the linear Kaiser factor, i.e., $\xi_\ell^{(\mathrm{S})}(s)/\xi_{\ell,\mathrm{lin}}^{(\mathrm{S})}(s)$. For clarity, we artificially shift the results at each redshift by a constant value (indicated by the horizontal dotted line). Symbols and line types are the same as those in Fig. 2. The green shaded regions at $z = 0.35$ and 1 indicate the expected 1-σ error of the hypothetical galaxy survey with the volume $V = 5\,h^{-3}\,\mathrm{Gpc}^3$ and number density $n = 5 \times 10^{-4}\,h^3\,\mathrm{Mpc}^{-3}$.

z-space bispectra

Given the second-order PT kernel in redshift-space, the leading-order (tree-level) galaxy bispectrum in redshift-space reads [313, 669, 562]

$$B_s(\mathbf{k}_1, \mathbf{k}_2, \mathbf{k}_3) = 2Z_2(\mathbf{k}_1, \mathbf{k}_2)\, Z_1(\mathbf{k}_1)\, Z_1(\mathbf{k}_2)\, P(k_1)\, P(k_2) + \text{cyc.}, \tag{620}$$

which can be normalized by the power spectrum monopole to give the reduced bispectrum in redshift space, Q_s,

$$Q_s(\mathbf{k}_1, \mathbf{k}_2, \mathbf{k}_3) \equiv \frac{B_s(\mathbf{k}_1, \mathbf{k}_2, \mathbf{k}_3)}{a_0^2\, (P_g(k_1)\, P_g(k_2) + \text{cyc.})}, \tag{621}$$

Decomposing into Legendre polynomials, $B_{s\,\text{eq}}(\mu) = \sum_{\ell=0}^{\infty} B_{s\,\text{eq}}^{(\ell)}\, P_\ell(\mu)$, the redshift-space reduced bispectrum for equilateral configurations reads [562]

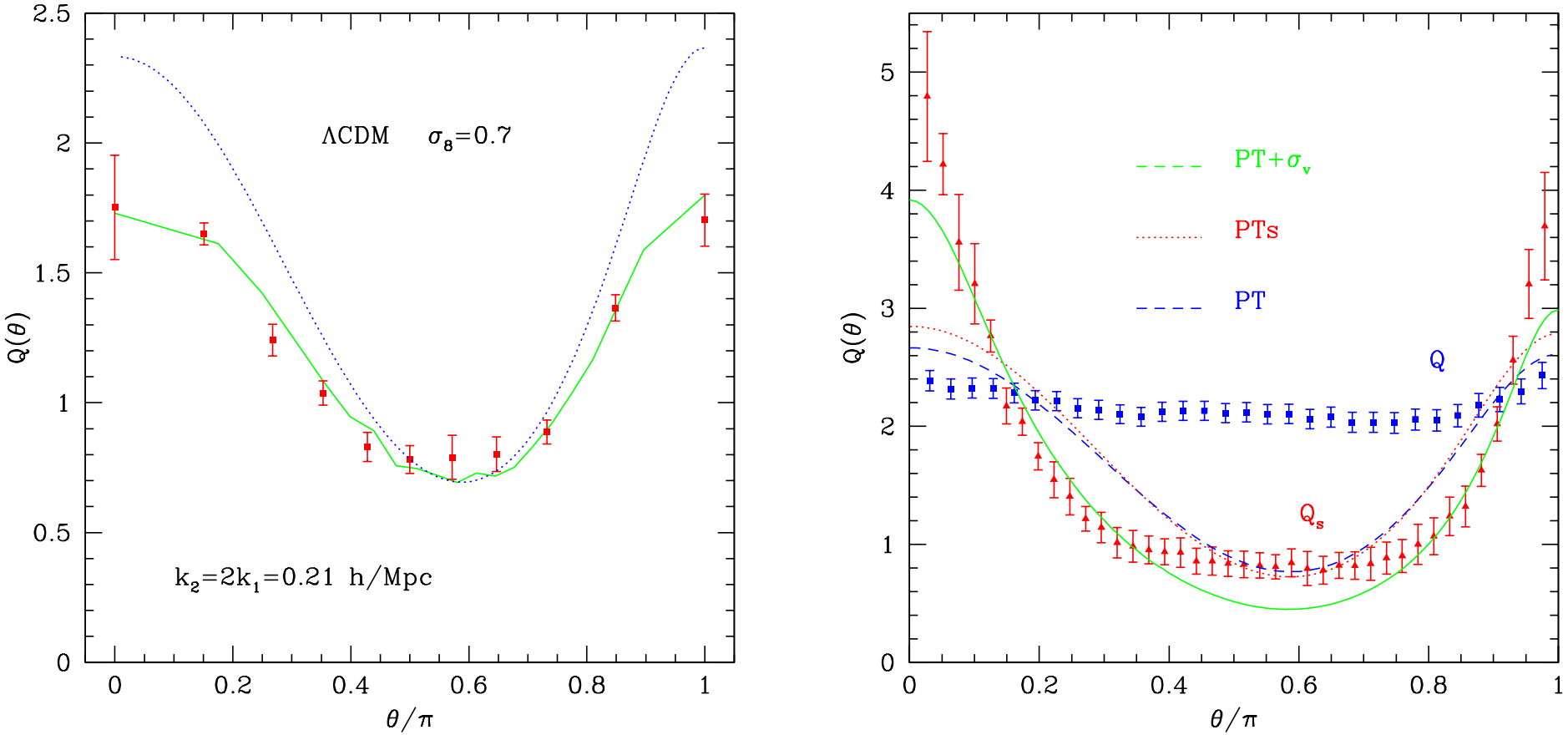

Figure 48: The left panel shows the bispectrum in redshift space for configurations with $k_2 = 2k_1$ as shown as a function of the angle θ between $\mathbf{k}_1$ and $\mathbf{k}_2$. The dotted line shows the predictions of second-order Eulerian PT, whereas the solid lines correspond to 2LPT. Error bars correspond to the average between 4 realizations. The right panel shows the bispectrum in redshift space for configurations with $k_2 = 2k_1 = 1.04$ h/Mpc, i.e. in the non-linear regime. Square symbols denote Q in real space, whereas triangles denote the redshift-space bispectrum. Also shown are the predictions of PT in real space (dashed lines), PT in redshift space (PTs, dotted line) and the phenomenological model with $\sigma_v = 5.5$, (PT+σ_v, continuous line).

A concluding slide

The missing ingredients:

- *massive neutrinos (should be OK as they account for only a small fraction of the energy density; can also be incorporated in the same framework).*
- *dark energy fields: very model dependent, see Martin's talk*
- *covariances :* $\langle \hat{P}_{l_1}(k_1)\ \hat{P}_{l_2}(k_2) \rangle$ *is now expected to be a non-diagonal matrix.*
- *Note that one should also compute similar quantities for higher order observables such as bispectra (or other observables)*
- *construction of a theory of the theoretical error !*

Information content of WL power spectrum

- The ‘’information’’ content of WL power spectrum is (significantly) smaller than the Gaussian expectation (Sato et al., ’09)
- Where is the information gone ?

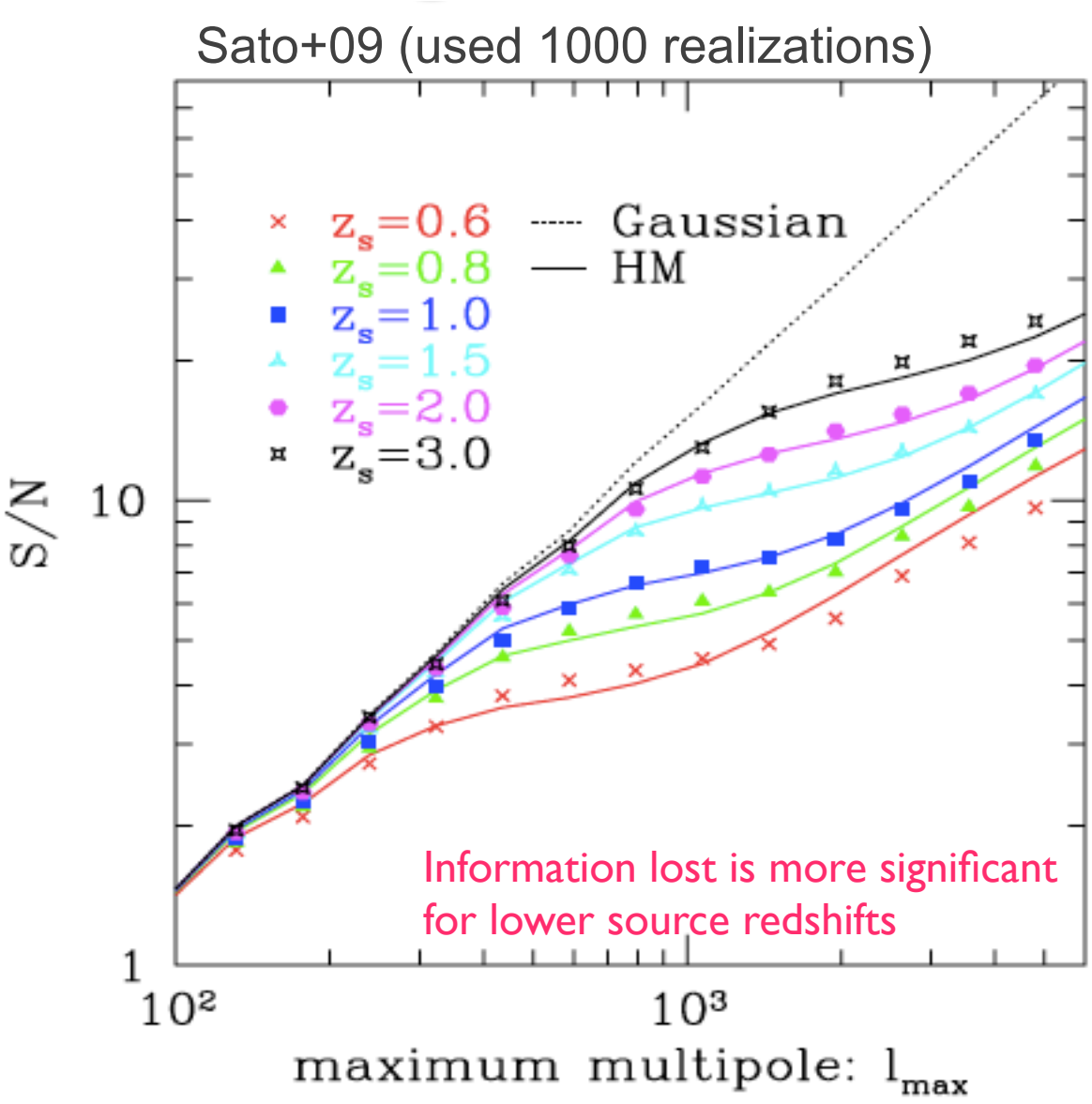

Information content of WL power spectrum and bispectrum

(Kayo, Takada & Jain 2012)